

THE STABILITY OF FRAMES

M. R. HORNE

Sc.D., M.I.C.E., A.M.I.Struct.E.

Professor of Civil Engineering, University of Manchester

and

W. MERCHANT

M.A., S.M., D.Sc., M.I.Struct.E., M.I.C.E., A.M.I.Mech.E.

Professor of Structural Engineering, University of Manchester

PERGAMON PRESS

OXFORD · LONDON · EDINBURGH · NEW YORK
PARIS · FRANKFURT

Pergamon Press Ltd., Headington Hill Hall, Oxford
4 & 5 Fitzroy Square, London W.1

Pergamon Press (Scotland) Ltd., 2 & 3 Teviot Place, Edinburgh 1

Pergamon Press Inc., 122 East 55th Street, New York 22, N.Y.

Pergamon Press GmbH, Kaiserstrasse 75, Frankfurt-am-Main

Federal Publications Ltd., Times House, River Valley Rd., Singapore

Samcax Book Services Ltd., Queensway, P.O. Box 2720, Nairobi, Kenya

Copyright © 1965 Pergamon Press Ltd.

First Edition 1965

Library of Congress Catalog Card No. 65-19833

Set in 10 on 12 pt. Times New Roman

Printed in Great Britain by

The Pitman Press, Bath

This book is sold subject to the condition
that it shall not, by way of trade, be lent,
re-sold, hired out, or otherwise disposed
of without the publisher's consent,
in any form of binding or cover
other than that in which
it is published.

Preface

THE authors have set out, in this volume, to give a clear picture of phenomena affecting the stability, both in the elastic and in the partially plastic range, of plane, rigid-jointed, triangulated and non-triangulated frames. Necessarily, much has been omitted. Thus, there is no mention of energy methods in the derivation of critical loads. The authors believe that, although energy methods are of prime importance in dealing with the stability of isolated members and of plate elements within members, the behaviour of plane frames can be adequately presented without the use of such methods, and that there are certain advantages in so doing in an elementary treatment.

The method of presentation is through examples designed to illustrate the physical principles involved rather than to present in detail a multiplicity of analytical methods; it is considered that, once a reader familiar with linear elastic analysis has understood the principles of non-linear behaviour, he will rapidly develop, for any particular problem, a suitable method of analysis. The examples treated in the text may be solved by hand with the help of a desk calculator. It is recommended that readers intending to carry out stability calculations should make use of the examples given at the ends of the chapters, these being either algebraic or, if numerical, again solvable by hand. Extensive calculations of the stability of frames are likely to be programmed for automatic digital computer, and reference to another book in this series (R. K. Livesley, *Matrix Methods of Structural Analysis*) may be made for help with such aspects.

Chapter 1 introduces the essential features of stability in elastic and elastic-plastic structures by reference to single members bending about one axis. Stability functions for prismatic elastic members are derived in Chapter 2, tables of these functions being

given at the end of the book (more extensive tables by Livesley and Chandler (Ref. 17) are available elsewhere). Chapter 3 deals with the elastic stability of triangulated frames, and Chapter 4 with non-triangulated frames. The behaviour of both triangulated and non-triangulated frames beyond the elastic limit is discussed in Chapter 5.

The authors acknowledge the assistance of various members of the staffs of the Department of Structural Engineering in the Faculty of Technology, and of the Department of Civil Engineering in the Faculty of Science, both in the University of Manchester, for reading and criticising the manuscript. Thanks are due to Dr. N. J. Gardner and Mr. M. J. Davies for their assistance in programming, for automatic digital computer, the tables of stability functions on pages 157ff. The authors acknowledge permission from the University Presses of Cambridge and Manchester to reproduce examination questions taken from Degree papers.

CHAPTER 1

The Stability and Failure of Individual Members

1.1 Introduction

It is common, in dealing with rigid-jointed frames, to calculate deflexions and bending moments by a *linear analysis*. When this is done, the *equations of equilibrium* are established by considering the geometry of the structure in its undeformed state. This may

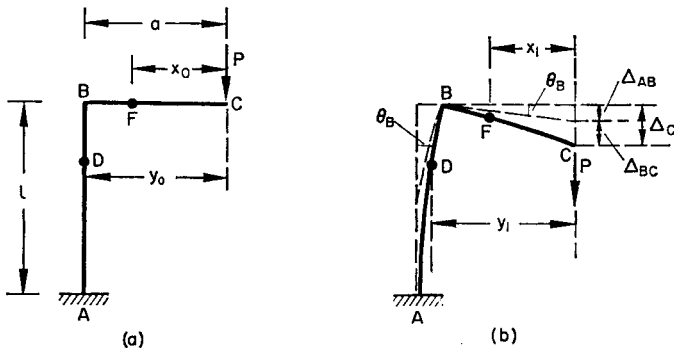


FIG. 1.1

be illustrated by reference to the simple structure ABC in Fig. 1.1(a). The vertical column AB is fixed to a rigid foundation at A , and supports the cantilever BC through a rigid joint at B . If a vertical load P acts at C , the bending moment at any point D in the column is calculated as $P y_0 = P a$, while the bending moment at any point F in the cantilever is $P x_0$. The total vertical deflection Δ_C at C (Fig. 1.1(b)) may be obtained as $\Delta_C = \Delta_{BC} + \Delta_{AB}$

where Δ_{BC} is the deflexion produced by BC acting as a cantilever while Δ_{AB} is the additional deflexion induced at C by the rotation θ_B of the joint B . If EI denotes the uniform flexural rigidity of AB and BC , then $\Delta_{BC} = \frac{Pa^3}{3EI}$ and $\Delta_{AB} = \frac{Pa^2l}{EI}$, whence

$$\Delta_C = \frac{Pa^2}{3EI}(a + 3l) \quad (1.1)$$

The deflexion Δ_C is thus proportional to the applied load P , giving the straight line Ob in Fig. 1.2(a) as the load-deflexion

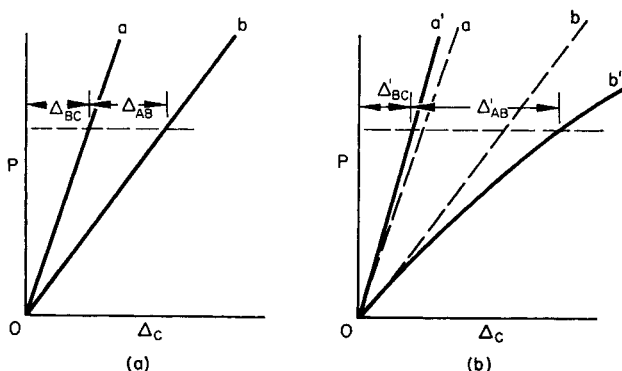


FIG. 1.2

relation. In this treatment, it has been assumed that deflexions due to shear deformation and direct axial compression may be ignored. If these are allowed for, the deflexions are slightly increased, but are still linearly related to the applied load.

It is evident that, in a more refined analysis, one should calculate the bending moments in the actual deformed state of the structure, Fig. 1.1(b). The bending moment at D becomes Py_1 , while that at F becomes Px_1 . When this is done, the deflexion components, now denoted by Δ_{AB}' and Δ_{BC}' , are no longer directly proportional to the applied load P , and the load-deflexion relation becomes curved as shown by Ob' in Fig. 1.2(b).

The difference between the approximately and accurately calculated cantilever deflexions Δ_{BC} and Δ_{BC}' is likely to be small, provided the deflexions are small compared with the dimensions a and l . The difference between x_0 and x_1 is of order of magnitude $a(1 - \cos \theta)$ (that is, of order $a\theta^2$ or $l\theta^2$ if a and l are of like order), where θ is a typical value of the angle of slope of the cantilever. On the other hand, the difference between y_0 and y_1 is of order $l\theta$, and may cause a significant difference between Δ_{AB} and Δ_{AB}' . The linear analysis is thus in the first instance likely to be in error on account of the incorrect calculation of the bending moments in column AB , and generally in any structure it is the flexure of the axially loaded members that is the prime cause of non-linearity. The stability of frames is concerned with this non-linear behaviour, and the first step must be to consider the influence of axial loads in single members. The study of an isolated member under axial load develops ideas which have direct application to complete frames, and these ideas are explored in the present chapter.

It is assumed throughout that the member is undergoing flexure about one principal axis only, and that bending about the other principal axis (i.e. out of the plane of the paper) does not occur. This may imply that restraints must be present preventing such deformations, this being particularly so if the bending which is allowed is about the major principal axis.

1.2 Axially Loaded Member with Terminal Couples

The initially straight strut AB in Fig. 1.3(a) is subjected to an axial thrust P applied at the centroids of the end sections, together with equal and opposite terminal couples M . As a result of this loading the strut takes up the deflected form ACB in Fig. 1.3(b), the deflexion at D , distance x from A , being denoted by y relative to the straight line OB forming the X -axis. The bending moment in the strut at D is thus $(M + Py)$. If the strut has a uniform flexural rigidity EI about axes parallel to the terminal

couples, and if the deflexions are sufficiently small for $(dy/dx)^2$ to be neglected in comparison with unity, the differential equation governing the deflected form becomes

$$EI \frac{d^2y}{dx^2} = -(M + Py) \quad (1.2)$$

The solution is

$$y = A \sin \alpha x + B \cos \alpha x - \frac{M}{P} \quad (1.3)$$

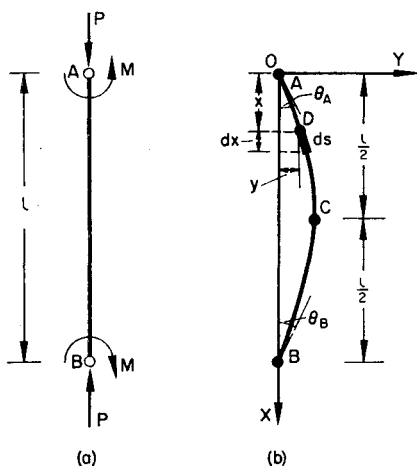


FIG. 1.3

where $\alpha^2 = P/EI$. The constants of integration A and B are derived from the boundary conditions that the deflexion y is zero at the ends $x = 0$ and $x = l$ of the member. Hence

$$0 = B - \frac{M}{P},$$

$$0 = A \sin \alpha l + B \cos \alpha l - \frac{M}{P},$$

giving $B = M/P$ and $A = (M/P) \tan \alpha l/2$. The deflexion y given by equation (1.3) thus becomes

$$y = \frac{M}{P} \left\{ \tan \frac{\alpha l}{2} \sin \alpha x + \cos \alpha x - 1 \right\} \quad (1.4)$$

The maximum deflexion occurs at C ($x = l/2$), and has the value

$$y_c = \frac{M}{P} \left(\sec \frac{\alpha l}{2} - 1 \right) \quad (1.5)$$

The relation between y_c and P is shown for four different values of M in Fig. 1.4. The values of y_c , P and M are expressed non-dimensionally in terms of suitable functions of the length l of the strut and its flexural rigidity EI . For any value of M , the deflexion becomes indefinitely large as

$$\sec \frac{\alpha l}{2} \rightarrow \infty, \text{ i.e. as } \frac{\alpha l}{2} \rightarrow \frac{\pi}{2} \text{ or } P \rightarrow \pi^2 \frac{EI}{l^2}$$

Hence the load $\pi^2 EI/l^2$, denoted by P_E , is the elastic failure load of the strut, and is independent of the applied bending moment M .

An alternative presentation of the results is shown in Fig. 1.5. The *stiffness* k of the member with respect to end moments may be defined as the ratio of the applied moments M to terminal rotations $\theta_A = \theta_B$. It follows from equation (1.4) that

$$\left(\frac{dy}{dx} \right)_{x=0} = \theta_A = \frac{M}{P} \alpha \tan \frac{\alpha l}{2},$$

whence

$$k = \frac{M}{\theta_A} = \frac{\frac{\pi}{2} \sqrt{\frac{P}{P_E}}}{\tan \frac{\pi}{2} \sqrt{\frac{P}{P_E}}} k_0 \quad (1.6)$$

where $k_0 = 2EI/l$, the stiffness of the strut when $P = 0$. The variation of k/k_0 with P/P_E is shown in Fig. 1.5, from which it

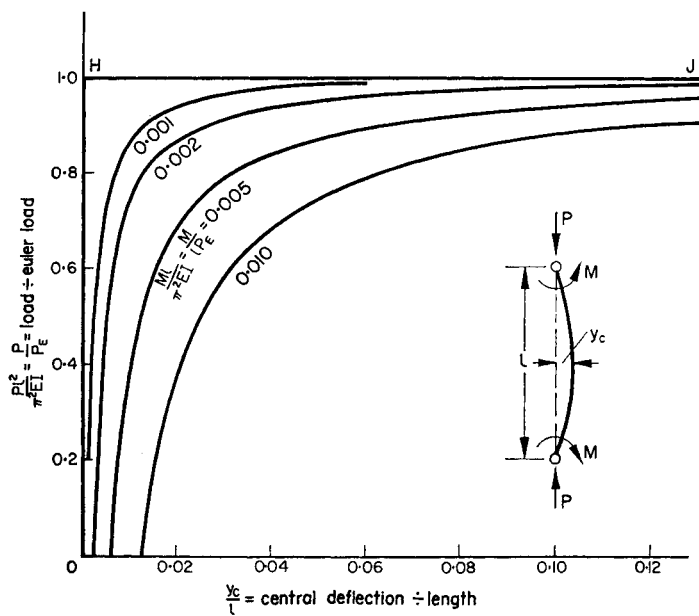


FIG. 1.4

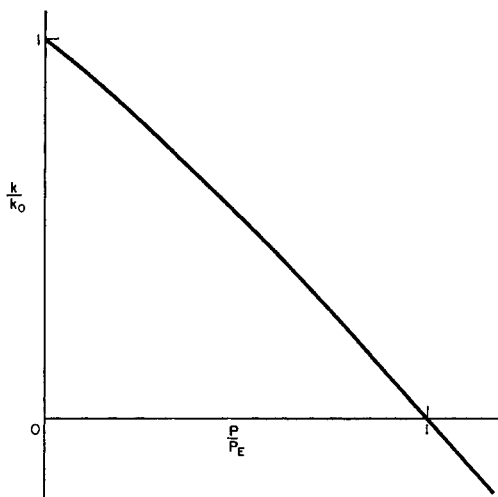


FIG. 1.5

is seen that there is an almost linear reduction in stiffness of the member as the axial load is increased from zero to the elastic failure load ($P = P_E$). The elastic failure load may in fact be interpreted as that axial load at which the stiffness becomes zero. It is important to note that the stiffness depends only on the axial load (equation (1.6)), and is independent of the magnitude of the terminal bending moment M .

It should be noted that there is no mathematical reason for rejecting the above analysis for values of P greater than P_E . The stiffness k then becomes negative (Fig. 1.5), and this provides a clue to the physical significance of assuming $P > P_E$. Negative stiffness implies that an increase in end rotation is accompanied by an increase in the *restraining* moment, so that the strut must be connected at its ends to other members capable of supplying such restraint. It is only thus that any member will support an axial compressive load greater than its failure load as a pin-ended strut. The concept of negative stiffness arises frequently in the treatment of the stability of frames.

1.3 Member under Axial Load Only

The behaviour of a member subjected to axial load only may conveniently be obtained by allowing M to approach zero in the solution obtained above. The curves in Fig. 1.4 then approach the limit represented by OHJ , indicating that no deformation occurs until $P = P_E$ or $\alpha = \pi/l$, at which load deflexions of indefinite magnitude occur, with the form

$$y = A \sin \pi x/l \quad (1.7)$$

The load $P = P_E = \pi^2 EI/l^2$ (the "Euler load") now achieves the significance attributed to it by Euler, who first obtained the load in 1759 in the form $P_E = \pi^2 S/l^2$ where S was defined as the flexural rigidity. The Euler load is that load at which a deflected form becomes statically admissible and may, with a more general connotation, be referred to as the *first elastic*

critical load of a strut with pinned ends. It may alternately be derived directly from equation (1.3) by putting $M = 0$. The condition $y = 0$ at $x = 0$ then gives $B = 0$, while $y = 0$ at $x = l$ gives

$$0 = A \sin \alpha l$$

This is satisfied by putting $A = 0$ (i.e. zero deflexions) or $\alpha l = n\pi$ where n is an integer, whence, since $\alpha^2 = P/EI = \pi^2 P/l^2 P_E$, it follows that

$$\frac{P}{P_E} = n^2$$

There thus exists a series of "elastic critical loads" $P_{C1} = P_E$, $P_{C2} = 4P_E$, $P_{C3} = 9P_E$, etc., with corresponding deflected forms (the "critical modes") $y = A_1 \sin \pi x/l$, $y = A_2 \sin 2\pi x/l$, $y = A_3 \sin 3\pi x/l$, etc. Since absolute axial loading is a limiting ideal condition, any real strut will deform according to a curve which lies below *HJ* in Fig. 1.4, and so only the first critical load P_E has practical significance. The higher critical loads and critical modes are, however, of interest when analysing the behaviour of struts under various loading conditions, as explained later in the chapter.

1.4 The Effect of Various End Conditions

The elastic critical load may be obtained for columns with end conditions other than those of a pin-ended strut by solving the differential equation and obtaining the constants of integration by reference to the boundary conditions. A readier solution is, however, obtained by observing that the solution of the differential equation can always be represented as part of the continuous sine wave $y = A \sin \alpha x$ referred to suitable axes. The axial thrust $P_C = \alpha^2 EI$ which makes the sinusoidal deformation of the member possible is then the elastic critical load for the given end conditions. The distance between points of contraflexure, l' , known as the *effective length*, is given by $\alpha l' = \pi$, whence

$P_C = \pi^2 EI / (l')^2$. By expressing l' as a proportion of the actual length l of the member, the critical load is derived as a function of the known properties of the member. Four cases for differing end conditions are represented in Fig. 1.6(a) to (d).

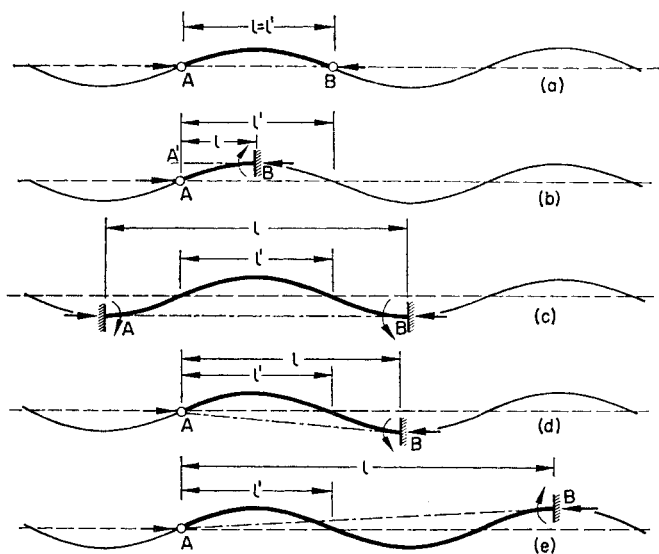


FIG. 1.6

In the first case, that of a pin-ended strut, the effective length is equal to the actual length, i.e. $l' = l$, whence $P_C = \pi^2 EI / l^2 = P_E$.

Figure 1.6(b) represents a member fixed in position and direction at B and completely free at A . The load at A acts parallel to the original longitudinal axis $A'B$ of the member. Here we have $l' = 2l$ and $P_C = \pi^2 EI / (2l)^2 = P_E / 4$.

Figure 1.6(c) represents a member constrained in position and direction at both ends, except that the ends are allowed to approach each other along AB . Hence $l' = l/2$ and $P_C = \pi^2 EI / (l/2)^2 = 4P_E$.

In Fig. 1.6(d), a straight line has been drawn from the point of contraflexure at A to touch the sine curve at B . The column AB is then restrained in position and direction at B , while end A is unrestrained in direction (zero bending moment) but constrained to move along AB . In this case, the reference axis for the sine wave is not parallel to the original longitudinal axis AB of the member. The value of l is obtained from a simple trigonometric equation, the solution of which gives $l' \approx 0.7l$ and $P_C \approx 2.05P_E$.

It is evident that the above solutions for the various end conditions are not unique. Thus the end conditions of Fig. 1.6(d) are also satisfied by taking a greater length of the continuous sine curve, as shown in Fig. 1.6(e). This critical mode corresponds to a higher critical load, and as in the case of a pin-ended strut, there will exist an infinite series of critical modes and corresponding critical loads.

1.5 The Effect of Large Deformations

The differential equation

$$\frac{d^2y}{dx^2} + \frac{P}{EI}y = 0 \quad (1.8)$$

governing the behaviour of an axially loaded pin-ended strut applies only when dy/dx is small. When this is not so, the correct expression for curvature $(d^2y/dx^2)/\{1 + (dy/dx)^2\}^{3/2}$ must be used in place of the approximation d^2y/dx^2 . Hence equation (1.8) has to be modified to

$$\frac{d^2y}{dx^2} + \frac{P}{EI} \{1 + (dy/dx)^2\}^{3/2} y = 0 \quad (1.9)$$

The solution of this equation involves the use of elliptic integrals and will not be given here.^{(1)*} The curved shape taken up by the strut (assuming indefinite elastic behaviour) is known as the *elastica*, and successive forms for increasing values of P are shown

* For references, see p. 155.

in Fig. 1.7. The relation between P and central lateral deflexion y_c is given by OHK in Fig. 1.8, the curve HK being tangential at H to the solution HJ given by the approximate theory. A relation between P and y_c which is accurate to within 1 percent in terms of P up to $y_c/l = 0.25$ is

$$\frac{y_c}{l} = \frac{2\sqrt{2}}{\pi} \sqrt{\left(\frac{P}{P_E} - 1\right)} \quad (1.10)$$

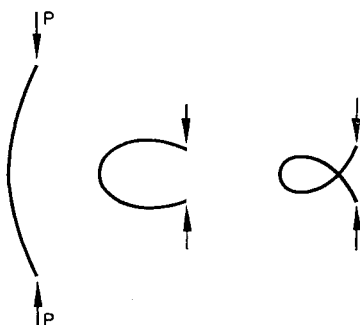


FIG. 1.7

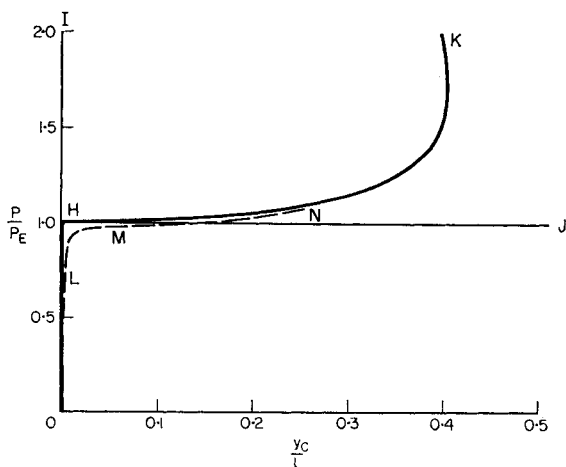


FIG. 1.8

When $y_c/l = 1/20$, P is only 0.3 percent above P_E , and when $y_c/l = 1/10$, P still only exceeds P_E by 1.2 percent. Hence, although the more accurate analysis shows that the elastic deflexions do not in fact increase indefinitely at $P=P_E$, large deflexions can occur with a negligible increase in load. The properties of the elastica are thus of no great practical importance. Moreover, at large deflexions the elastic limit of the material will in practical structures be exceeded, and the present analysis becomes in any case irrelevant.

1.6 Axial Deformations

Axial deformations have two components, namely direct axial compression and longitudinal shortening due to flexure.

Direct axial compression Δ_D is proportional to the axial load, and is of magnitude $\Delta_D = Pl/EA$ where A is the cross-sectional area and E is the elastic modulus. This requires no further treatment.

The flexural shortening of a member is due to the difference between the developed length OCB (Fig. 1.3(b)) and the effective length OB . Ignoring shortening due to direct axial compression, the developed length OCB is equal to the original straight length l , while OB should be represented as less than l . In Fig. 1.3, this difference has been ignored since it does not affect significantly the calculation of lateral deflexions. The difference between OCB and OB is $\int_A^B ds - \int_A^B dx \approx \frac{1}{2} \int_0^l (dy/dx)^2 dx$, hence when $M = 0$ and consequently $y = y_c \sin \pi x/l$, the shortening due to flexure Δ_F becomes $\Delta_F = (\pi^2/4)y_c^2/l^2$. Substituting the expression for y_c given in equation (1.10), the total axial compression after buckling, $\Delta = \Delta_D + \Delta_F$, is obtained in terms of the axial load P in the form

$$\frac{\Delta}{l} = \frac{P}{EA} + 2 \left(\frac{P}{P_E} - 1 \right) \quad (1.11)$$

In Fig. 1.9, equation (1.11) gives the straight line HQ , which is tangential at H to the correct curve HK , obtained from elliptic integrals. There is thus an important difference between the axial load versus deformation relations for a strut as between lateral and longitudinal displacements. While at the Euler load P_E the load-deflexion relation is parallel to the deflexion axis

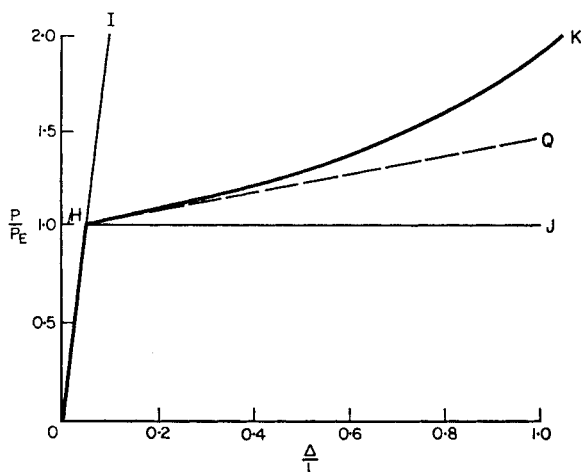


FIG. 1.9

for small lateral deflexions (HJ in Fig. 1.4), the development of longitudinal displacement requires an increase in the axial load. This result has a bearing on the significance of elastic critical loads in triangulated structures (Chapter 3).

1.7 The Bifurcation of Equilibrium States

A strut loaded axially above the Euler load P_E has more than one possible state of *equilibrium*. If it buckles, it follows the relationship HK (Figs. 1.8 and 1.9), and unless it has equal flexural rigidity about all axes, there will at any given axial load $P > P_E$ be two buckled states, one either side of the initial

longitudinal axis. Both these states of equilibrium will be stable, which means that a slight disturbing force applied to the strut and then removed will leave the strut in the same state as before the application of the force. If the potential energy of the applied load plus the strain energy in the strut together constitute the total potential energy of the system, then for a structure to be in stable equilibrium, the total potential energy must be at a stationary minimum with respect to any small arbitrary displacement.

Instead of the strut buckling when it reaches the Euler load, it would theoretically be possible for it to remain straight, following the load-deflexion relations HI in Figs. 1.8 and 1.9. Such a state would be one of *unstable equilibrium*, since a slight disturbance would cause the strut to buckle. When $P > P_E$ with the strut perfectly straight, the total potential energy of the system is at a stationary maximum.

The point H at which divergent equilibrium states become possible is called a *point of bifurcation*. For a pin-ended strut, points of bifurcation occur in the unbuckled state at axial loads of $P = P_E, 4P_E, 9P_E$, etc. It may be noted that, in any practical strut, sufficient disturbances in the form of incidental lateral loads, eccentricities of axial load or imperfections prevent the attainment of unstable states of equilibrium, and the load-deflexion curve for perfectly elastic behaviour follows, for example, the dotted curve OMN in Fig. 1.8. It is of interest that such behaviour represents a stable equilibrium state at each stage of loading, despite the fact that in the region of the Euler load, a small increase of load may be accompanied by a large increase of deformation.

1.8 Effect of Shear Deformation on Critical Loads

In the preceding analysis, no account has been taken of the effect of shear deformation. When a pin-ended strut buckles laterally, Fig. 1.10(a), the applied loads P_E will have components transverse to the bent longitudinal axis, thus introducing into

the member shear forces F as shown. These forces F will in turn produce additional deformation due to shear (Fig. 1.10(b)), and when these deformations are allowed for in the analysis,

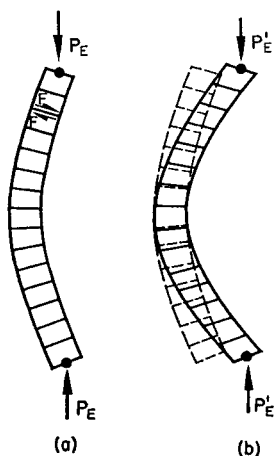


FIG. 1.10

the critical load is reduced below the Euler load P_E . It is found that, for practical purposes, the effect is unimportant, amounting to a reduction of a fraction of 1 percent.⁽²⁾

1.9 General Treatment of Lateral Loads

It is now possible to deal more generally with axially loaded members subjected to transverse loads. The bending moments produced by such loads in the absence of axial loading may be referred to as *primary moments*. In the case already considered, in which a strut was subjected to terminal couples M (Fig. 1.3), the primary moments consisted of a uniform bending moment M throughout the length of the member. In the more general case, we express the primary bending moments, denoted by M_0 , as some function of the distance x from one end of the member,

viz. $M_0 = F(x)$. Thus, for a uniformly distributed lateral load w per unit length (Fig. 1.11(a)), the primary moments are given by

$$M_0 = -\frac{wx(l-x)}{2} \quad (1.12)$$

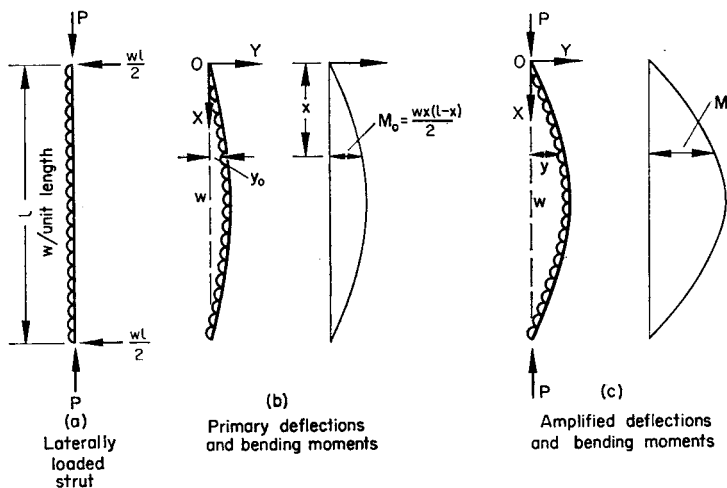


FIG. 1.11

The critical modes of deformation for the strut when subjected to axial load only are $y_{C1} = A_1 \sin \pi x/l$, $y_{C2} = A_2 \sin 2\pi x/l$, etc., where A_1 , A_2 , etc., are arbitrary constants, and are conveniently put equal to unity. The bending moments induced are respectively $EI y_{C1}'' = -(\pi^2/l^2) \sin \pi x/l$, $EI y_{C2}'' = -(4\pi^2/l^2)EI \sin 2\pi x/l$, etc. It is possible to express the primary moments M_0 as a half-range Fourier series in terms of the critical bending moments $EI y_{C1}''$, $EI y_{C2}''$ etc., so that

$$M_0 = EI\{a_1 y_{C1}'' + a_2 y_{C2}'' + \dots + a_n y_{Cn}'' \dots\}, \quad (1.13)$$

or, substituting for y_{C1}'' , y_{C2}'' , etc.,

$$M_0 = -\frac{\pi^2}{l^2} EI \left\{ a_1 \sin \frac{\pi x}{l} + 4a_2 \sin \frac{2\pi x}{l} + \dots + n^2 a_n \sin \frac{n\pi x}{l} \dots \right\} \quad (1.14)$$

The n th coefficient a_n is obtained by multiplying both sides of equation (1.14) by $\sin n\pi x/l$ and integrating over the range $x = 0$ to $x = l$. Since $\int_0^l \sin m\pi x/l \cdot \sin n\pi x/l \cdot dx$ has value zero when $m \neq n$ and has value $l/2$ when $m = n$, it follows that

$$a_n = \frac{2}{\pi^2 n^2} \frac{l}{EI} \int_0^l M_0 \sin \frac{n\pi x}{l} \cdot dx. \quad (1.15)$$

Since $d^2y/dx^2 = M_0/EI$, equation (1.14) is readily integrated to give the deflexions induced by the primary moments. Since $y = 0$ when $x = 0$ and $x = l$, the constants of integration vanish and the primary deflexions y_0 become

$$y_0 = a_1 \sin \frac{\pi x}{l} + a_2 \sin \frac{2\pi x}{l} + \dots + a_n \sin \frac{n\pi x}{l} \dots \quad (1.16)$$

Taking the example represented in Fig. 1.11, the bending moments M_0 may be expressed as

$$M_0 = -\frac{4}{\pi^3} w l^2 \left\{ \sin \frac{\pi x}{l} + \frac{1}{27} \sin \frac{3\pi x}{l} + \dots + \frac{1}{n^3} \sin \frac{n\pi x}{l} \dots \right\} \quad (1.17)$$

where only odd values of n are taken. The primary deflexions become

$$y_0 = \frac{4}{\pi^5} \frac{w l^4}{EI} \left\{ \sin \frac{\pi x}{l} + \frac{1}{243} \sin \frac{3\pi x}{l} + \dots + \frac{1}{n^5} \sin \frac{n\pi x}{l} \dots \right\}. \quad (1.18)$$

We now consider, for the general case of lateral loading, the effect on the equation of flexure of an axial load P . The total bending moment at any section is $(M_0 - Py)$, whence substituting for M_0 from equation (1.14),

$$\begin{aligned} \frac{d^2y}{dx^2} + \frac{P}{EI} y = -\frac{\pi^2}{l^2} \left\{ a_1 \sin \frac{\pi x}{l} + 4a_2 \sin \frac{2\pi x}{l} \right. \\ \left. + \dots + n^2 a_n \sin \frac{n\pi x}{l} \dots \right\}. \end{aligned} \quad (1.19)$$

The solution of this equation is

$$y = A \sin \alpha x + B \cos \alpha x - \frac{\pi^2}{l^2} \left[\frac{a_1}{\frac{P}{EI} - \frac{\pi^2}{l^2}} \sin \frac{\pi x}{l} + \frac{4a_2}{\frac{P}{EI} - \frac{4\pi^2}{l^2}} \sin \frac{2\pi x}{l} + \dots + \frac{n^2 a_n}{\frac{P}{EI} - \frac{n^2 \pi^2}{l^2}} \sin \frac{n\pi x}{l} + \dots \right], \quad (1.20)$$

where, as before, $\alpha^2 = P/EI$. At any value of P less than $P_E = \pi^2 EI/l^2$, $\alpha l < \pi$, and so the end conditions $y = 0$ when $x = 0$ and $x = l$ require $A = B = 0$. Equation (1.20) may then be rewritten

$$y = \frac{a_1}{1 - \frac{P}{P_E}} \sin \frac{\pi x}{l} + \frac{a_2}{1 - \frac{P}{4P_E}} \sin \frac{2\pi x}{l} + \dots + \frac{a_n}{1 - \frac{P}{n^2 P_E}} \sin \frac{n\pi x}{l} \dots \quad (1.21)$$

The bending moment M at any section is given by EIy'' , whence

$$M = -\frac{\pi^2}{l^2} EI \left[\frac{a_1}{1 - \frac{P}{P_E}} \sin \frac{\pi x}{l} + \frac{4a_2}{1 - \frac{P}{4P_E}} \sin \frac{2\pi x}{l} + \dots + \frac{n^2 a_n}{1 - \frac{P}{n^2 P_E}} \sin \frac{n\pi x}{l} \dots \right]. \quad (1.22)$$

Comparisons between equations (1.21) and (1.16) and between equations (1.22) and (1.14) show that the axial load has the effect of amplifying the deflexions and bending moments induced in the absence of axial load. The factors $1/\{1 - (P/n^2 P_E)\}$ by which the components in the Fourier analysis are multiplied by

the presence of axial load are called the *amplification factors*. The amplification factor for the n th component is actually $1/\{1 - (P/P_{Cn})\}$ where $P_{Cn}(= n^2 P_E)$ is the n th critical load, corresponding to the n th mode in the buckling of the member under axial load only. As $P \rightarrow P_{C1}$ (i.e. in this case, as $P \rightarrow P_E$) the deflexions and bending moments become very large. Hence the lowest critical load is that at which, for any form of lateral ("primary") loading, the deflexions tend to large values, and the behaviour depicted in Fig. 1.4 is of general application.

It is to be noted that, as the first critical load is approached, the terms other than the first in the Fourier analysis becoming less and less important. Thus, for a uniform lateral load when $P = 0$, the actual deflexion at the mid-point (equation (1.18)) is $(5/384)wl^4/EI = 0.013021wl^4/EI$, while the first term alone gives $(4/\pi^5)wl^4/EI = 0.013071wl^4/EI$, an error of 0.39 percent. When $P = 0.9P_E$, the actual central deflexion is $0.13065wl^4/EI$ (equation (1.21)), while the first term alone gives $0.13071wl^4/EI$, an error of no more than 0.04 percent. Using the first term only in equations (1.17) and (1.22), the error in the central bending moment is 3.20 per cent when $P = 0$ and 0.34 percent when $P = 0.9P_E$.

The results which have been obtained for a pin-ended strut may be applied in an analogous manner to columns with various end conditions. Instead of using a Fourier sine series, the primary bending moments and deflexions may be expressed as a series in terms of the critical modes $y_{C1}, y_{C2}, \dots, y_{Cn}, \dots$, etc. The primary moments are then given by equation (1.13), while the primary deflexions y_0 become

$$y_0 = a_1 y_{C1} + a_2 y_{C2} + \dots + a_n y_{Cn} \dots \quad (1.23)$$

In the presence of an axial load P , these deflexions become amplified to

$$y = \frac{a_1}{1 - \frac{P}{P_{C1}}} y_{C1} + \frac{a_2}{1 - \frac{P}{P_{C2}}} y_{C2} + \dots + \frac{a_n}{1 - \frac{P}{P_{Cn}}} y_{Cn} \dots \quad (1.24)$$

where P_{Cn} denotes the n th critical load of the columns for the given end conditions. Similarly, the bending moments become

$$M = EI \left[\frac{a_1}{1 - \frac{P}{P_{C1}}} y_{C1}'' + \frac{a_2}{1 - \frac{P}{P_{C2}}} y_{C2}'' + \dots + \frac{a_n}{1 - \frac{P}{P_{Cn}}} y_{Cn}'' \dots \right]. \quad (1.25)$$

Equations (1.13), (1.23), (1.24) and (1.25) are applicable not only when the flexural rigidity EI is uniform, but also when it varies with x , the distance along the member. When the member is of variable section, the critical modes no longer form part of a continuous sine wave. Both for uniform and non-uniform members, the calculation of the coefficients $a_1, a_2, \dots, a_n, \dots$ is facilitated by certain *orthogonal relations* which may be shown to exist between the critical modes.⁽²⁾ These correspond to the orthogonal relations $\int_0^l \sin m\pi x/l \sin n\pi x/l \, dx = 0$ for $m \neq n$ in the Fourier series. Provided the ends of the columns are either completely free to move laterally, or completely fixed against lateral movement, and either completely fixed or completely free with respect to rotation, it may be shown that $\int_0^l EI y_{Cm}'' y_{Cn}'' \, dx = 0$ when $m \neq n$. All the end conditions considered in Fig. 1.6 fall into one of these categories. Hence, from equation (1.13),

$$a_n = \frac{\int_0^l M_0 y_{Cn}'' \, dx}{\int_0^l EI (y_{Cn}'')^2 \, dx}. \quad (1.26)$$

This general treatment is also applicable to frames.

In the whole of the above analysis, it has been assumed that deflexions are everywhere sufficiently small for d^2y/dx^2 to be regarded as a close approximation to the curvature. Strictly

speaking, the load-deflexion curves in the presence of lateral load do not approach asymptotically to the line $P = P_{C1}$ (the lowest critical load), but ultimately curl upwards, as shown for the case of a pin-ended strut by the dotted line LMN in Fig. 1.8. This upward trend only occurs, however, at gross deformations, and may for practical purposes be neglected.

1.10 The Effect of Initial Lack of Straightness

Suppose a pin-ended strut has an initial lack of straightness defined by deflexions y_0 . In just the same way as primary deflexions due to lateral loads may be expressed as a Fourier series, so also may initial deflexions. Hence we may regard equation (1.16) as expressing the initial lack of straightness of the member. If the deflexions of the strut change to y as the result of applying an axial load P , the change of curvature is $d^2(y - y_0)/dx^2$, and hence the equation of flexure (in the absence of lateral loading) becomes

$$\frac{d^2(y - y_0)}{dx^2} + \frac{P}{EI}y_0 = 0. \quad (1.27)$$

After substituting for y_0 from equation (1.16), integrating and using the boundary conditions $y = 0$ when $x = 0$ and $x = l$, the deflexions y are found to be given by equation (1.21). Hence initial imperfections are magnified according to amplification factors in exactly the same way as are deflexions and bending moments due to primary loading.

1.11 Experimental Determination of Critical Load

The presence of initial imperfections prevents the observation of the buckling load as that load at which deflexions suddenly appear. In practice, small deflexions occur as soon as any load is applied. Were the strut to remain indefinitely elastic, the elastic buckling load could be identified as the load at which really

large deflexions appeared, but inelastic behaviour usually sets in before this limit is approached at all closely. Southwell⁽¹⁾ has suggested a method whereby the elastic buckling load may be deduced from an observation of behaviour at loads below the buckling load.

Observations are made of the increase in central deflexion Δ as the axial load P is increased from zero. This deflexion is additional to some initial deflexion Δ_0 as the axial load P is increased from zero. The additional deflexion Δ_0 is difficult to measure accurately and is therefore regarded as unknown. We now investigate analytically the significance of the experimentally observed quantities.

The total central deflexion may be expressed as the sum of the terms from equation (1.24) corresponding to the mid-points of the strut. All terms except the first will change negligibly as P is increased, since P is always less than the first critical mode P_{C1} , and therefore very much less than the higher critical loads P_{C2} , P_{C3} , etc. Hence we write the total central deflexion $\Delta + \Delta_0$ in the form

$$\Delta + \Delta_0 = \frac{\Delta_1}{1 - \frac{P}{P_{C1}}} + \Delta_r \quad (1.28)$$

where Δ_1 is the first critical mode component of the central deflexion at no load, and Δ_r is the remaining component of the central deflexion corresponding to all the higher modes. Since when $P = 0$, $\Delta = 0$,

$$\Delta_0 = \Delta_1 + \Delta_r. \quad (1.29)$$

The elimination of the unknown initial deflexion Δ_0 between equations (1.28) and (1.29) gives

$$\Delta = \frac{\frac{P}{P_{C1}}}{1 - \frac{P}{P_{C1}}} \Delta_1. \quad (1.30)$$

Equation (1.30) may be rearranged in two alternative forms:

$$\frac{\Delta}{P} = \frac{\Delta}{P_{C1}} + \frac{\Delta_1}{P_{C1}}, \quad (1.31)$$

$$\frac{P}{\Delta} = \frac{P}{\Delta_1} - \frac{P_{C1}}{\Delta_1}. \quad (1.32)$$

In each case, the second term on the R.H.S. is constant. Equation (1.31) represents a linear relationship between Δ/P and Δ , while equation (1.32) represents a linear relationship between P/Δ and P .

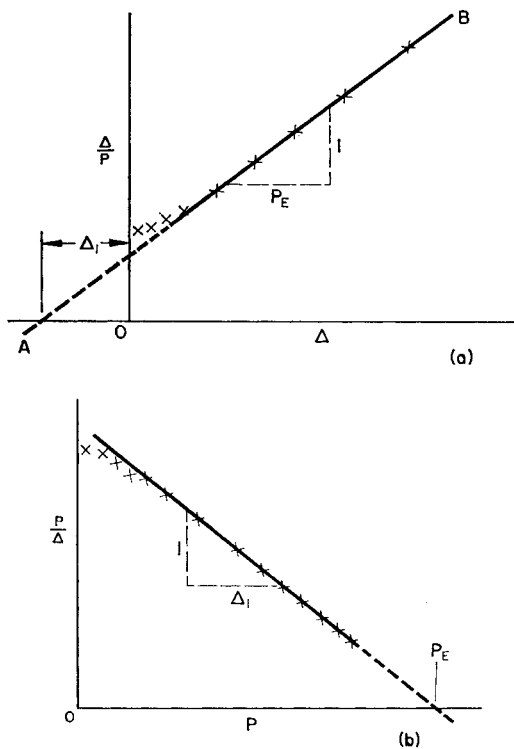


FIG. 1.12

The result of plotting experimentally observed values of Δ/P versus Δ is shown in Fig. 1.12(a). This is the original plot suggested by Southwell, and it follows from equation (1.31) that the inverse slope of the straight line through the experimental points gives the critical load P_{C1} , while the negative intercept with the deflexion axis gives Δ_1 , the first critical mode component of the initial deflexion Δ_0 . Some departure from a straight line commonly occurs for the points obtained at low P values, but the higher points are usually found to lie close to a straight line.

An alternative plot is of P/Δ against P , as shown in Fig. 1.12(b). Hence, it follows from equation (1.32) that the critical load P_{C1} is given by the intercept with the P -axis, while the inverse slope gives Δ_1 . This plot is more useful than the standard Southwell, since it gives a better realisation of the nearness to buckling reached in the experiment.

Similar methods may be used in the interpretation of observations on any complete structure subjected to loads in the elastic range. A close estimate of the first elastic critical load is obtained, provided the first critical mode of deformation has a dominant deflexion component corresponding to the deflexion used in the plot.

1.12 Inelastic Behaviour

Hitherto in this chapter it has been assumed that the material considered remains perfectly elastic. In real structures, the material has only a limited elastic range. In the case of mild steel, the material properties are represented closely by the stress-strain relations OAB (for direct tension) and $OA'B'$ (for direct compression) in Fig. 1.13, the maximum strains considered being of the order of 1 percent. The straight lines OA , OA' are of slope equal to the elastic modulus E . At the yield stress $\pm\sigma_y$ (virtually the same in tension and compression), a large amount of pure plastic deformation can occur without further increase of stress, although at strains of about ten times the strain at yield, strain-hardening occurs according to BC , $B'C'$. The

behaviour of mild steel structures beyond the elastic limit may, however, be assessed with sufficient accuracy by assuming that the material has an indefinitely long pure plastic range. Mild steel may thus be treated as “elastic-plastic”. If, after straining to some point D or D' in the plastic range, the stress is reduced, the stress-strain relation followed is DF or $D'F'$, with a slope equal to that of the elastic range OA , OA' . This is known as “unloading”.

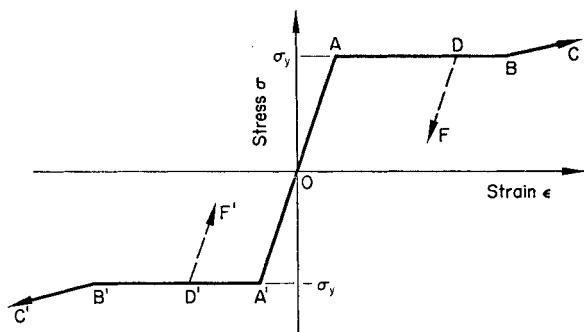


FIG. 1.13

A more general type of inelastic stress-strain relation is shown in Fig. 1.14, and is obtained for high tensile steel as well as light alloys, copper and many other materials. Behaviour is elastic up to the limit of proportionality at A or A' , after which there is a strain-hardening curve AB or $A'B'$. The slope of the tangent CD at any point C is called the *tangent modulus*, and is denoted by E_T . Hence $E_T = d\sigma/d\epsilon$, the ratio of increase of stress to increase of strain when the material is at the given stress. If the material is unloaded from point C , the stress-strain relation CF is of slope E , parallel to the elastic line OA , OA' .

The discussion of inelastic stability differs according to whether an elastic-plastic or an elastic-strain-hardening material is involved. Sections 1.13 to 1.16 below refer to struts of elastic-plastic material, while struts of strain-hardening material are discussed in Sections 1.17 to 1.19.

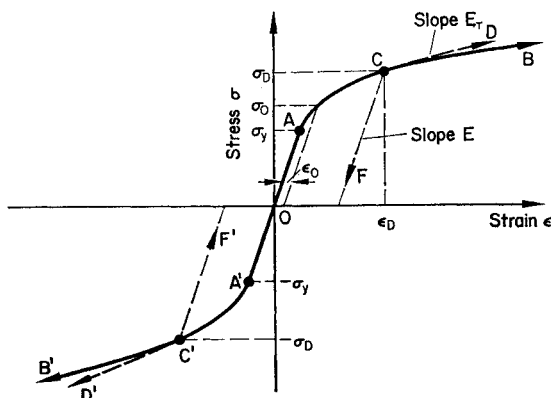


FIG. 1.14

1.13 Elastic-Plastic Struts with No Initial Imperfections

If an initially straight, axially loaded strut is sufficiently slender, the lowest elastic critical load will be reached before the material yields. If A is the cross-sectional area of such a pin-ended strut of length l , and σ_y is the yield stress, then the required condition is that $\sigma_y > P_E/A$. If the radius of gyration about the axis of bending is r , then since $P_E = \pi^2 EI/l^2$ and $I = Ar^2$, the limitation can be expressed as $l/r > \pi\sqrt{(E/\sigma_y)}$. In the case of mild steel with $E = 30 \times 10^6 \text{ lb/in}^2$ and $\sigma_y = 36,000 \text{ lb/in}^2$, this gives $l/r > 91$. Such a member will buckle laterally at the Euler load, but at some stage in the deformations, the material on the concave face will yield, causing a drop in the stiffness of the strut and consequently a decrease in load. The complete load-deflexion curve will take the form $OHJK$ in Fig. 1.15(a). The stress distribution across the member at a section near the mid-height of the strut is shown at various stages of deformation.

When $\sigma_y < P_E/A$, or $l/r < \pi\sqrt{(E/\sigma_y)}$, the material reaches the yield stress over the whole cross-section while the strut is still perfectly straight. The load at which this occurs is $A\sigma_y$, denoted

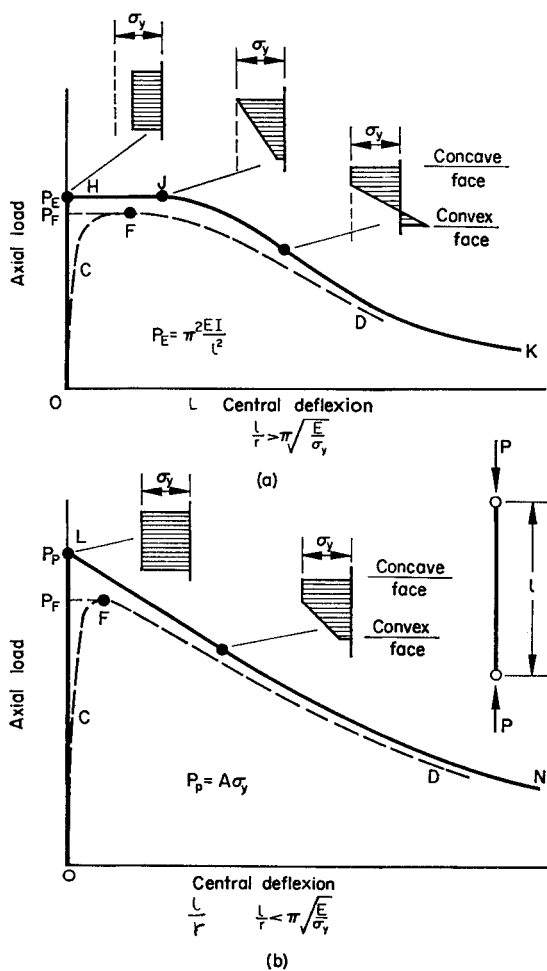


FIG. 1.15

by P_P , and referred to as the “squash” load, since it is the load at which a very short strut would squash in pure plastic compression throughout its length. In other than very short struts, a small lateral disturbance at the squash load causes more plastic deformation on one side, which then becomes concave, and the consequent bending moment induced by the axial load results in an unloading of the material on the convex face. The load therefore immediately decreases, and the load-deflexion curve LN in Fig. 1.15(b) is obtained.

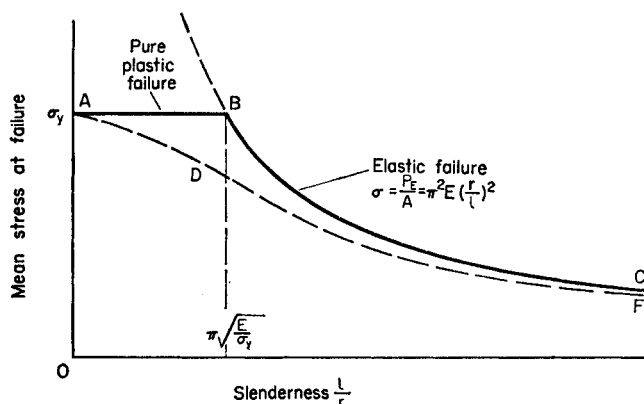


FIG. 1.16

The above behaviour is summarised by ABC in Fig. 1.16, which gives, as a function of the slenderness l/r , the theoretical mean stress at failure for a perfectly straight pin-ended strut loaded axially. Practical struts, although they may nominally be perfectly straight and axially loaded, will in fact contain some imperfections, and the longitudinal load may be applied with some eccentricity. Hence experimental points for mild steel all lie below ABC , except at very low values of l/r , when the incidence of strain-hardening may raise the mean stress at failure above σ_y . Before practical formulae for the loads of struts can be

discussed, it is therefore necessary to consider the effect of initial imperfections and eccentric loading.

1.14 Effect of Initial Imperfections

It was shown in the previous section that perfectly straight elastic-plastic struts have load-deflexion relations given by *OHJK* in Fig. 1.15(a) or *OLN* in Fig. 1.15(b). Struts with initial imperfections follow the behaviour indicated by the dotted curves

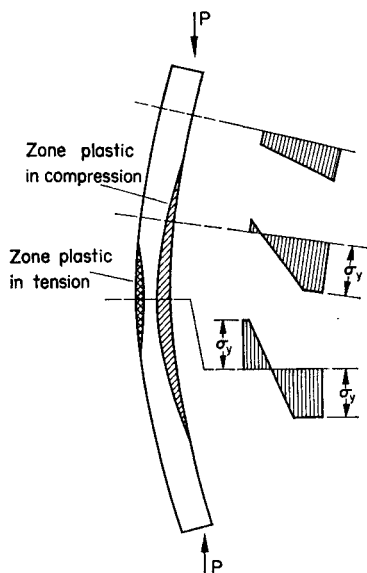


FIG. 1.17

OCFD, and a complete theoretical treatment is laborious. The load of greatest interest is the peak or failure load P_F . The behaviour of eccentrically loaded struts of certain cross-sectional shapes (solid rectangular and circular tubes) has been investigated,^(3,4,5) and the state of a typical strut when at the maximum load is represented in Fig. 1.17.

Since an accurate elastic-plastic treatment of strut behaviour is too complex for practical use, it is useful to study upper and lower limits between which the correct solution must lie. One upper limit is obtained by assuming that the material has indefinite elastic behaviour, so that, ignoring the effect of gross deformations, the failure load becomes the Euler load $P_E = \pi^2 EI/l^2$. This gives the line HJ in Fig. 1.18 as an upper bound to the load-deflexion curve. The effect of any imperfections is to produce

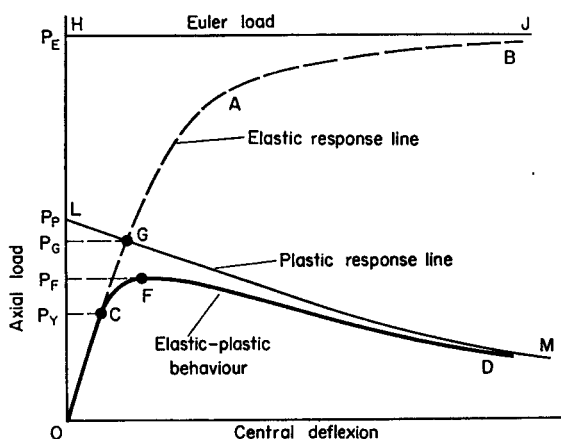


FIG. 1.18

some curve OAB lying below HJ . Another upper limit to the load-deflexion curve is obtained by ignoring entirely the elastic deformations, allowing only for the pure plastic-deformation that can take place at the yield stress in tension or compression. The material is then assumed to be *rigid-plastic*, with the stress-strain relations OAB , $OA'B'$ in Fig. 1.19(a). A collapsing strut JK (Fig. 1.19(b)) will develop a plastic hinge at some point C within its length, with plastic deformation occurring in compression on one side of the neutral axis and plastic deformation in tension on the other side. If a rectangular section strut of width b and depth d (Fig. 1.19(d)) has its neutral axis NA at a distance

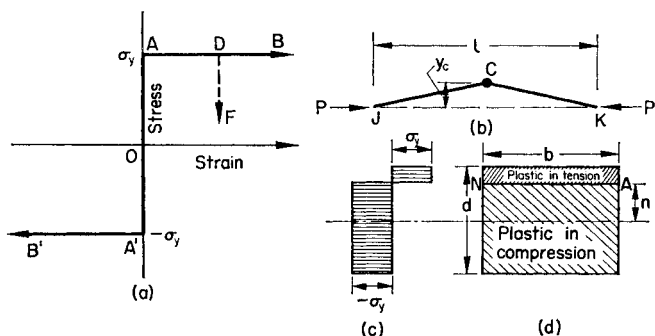


FIG. 1.19

n from the central axis, the plastic moment of resistance about the central axis is M_P' where

$$M_P' = \left\{ b \left(\frac{d}{2} + n \right) \sigma_y \right\} \left\{ \frac{1}{2} \left(\frac{d}{2} - n \right) \right\} + \left\{ b \left(\frac{d}{2} - n \right) \sigma_y \right\} \left\{ \frac{1}{2} \left(\frac{d}{2} + n \right) \right\},$$

$$\text{i.e.} \quad M_P' = b \left(\frac{d^2}{4} - n^2 \right) \sigma_y. \quad (1.33)$$

The resultant axial thrust is P where

$$P = b \left(\frac{d}{2} + n \right) \sigma_y - b \left(\frac{d}{2} - n \right) \sigma_y,$$

$$\text{i.e.} \quad P = 2bn\sigma_y. \quad (1.34)$$

The equilibrium of the strut, considering moments taken about the hinge, requires that

$$Py_c = M_P'.$$

Hence it follows that

$$y_c = \frac{d}{4} \left\{ \frac{bd\sigma_y}{P} - \frac{P}{bd\sigma_y} \right\}. \quad (1.35)$$

This equation gives the curve LM in Fig. 1.18, and is known as the *rigid-plastic line*. At zero deflexion, $P = P_P = bdf_y$, the squash load which, as already discussed, may be above or below the Euler load P_E . The curve LM lies above the load-deflexion curve for zero imperfections when allowance is made for elastic as well as plastic behaviour (LN in Fig. 1.15(b)), and above the load-deflexion curves for all actual struts (e.g. OFD in Fig. 1.18).

The lines HJ and LM in Fig. 1.18 are thus upper limits for the true load-deflexion relation. If the initial imperfections in the longitudinal shape of the strut are known, the resulting *elastic response line* OAB is also an upper limit. If OAB intersects LM at G , then OGM is the closest upper limit to the true elastic-plastic curve obtainable by simple analysis. Evidently, the intersection point G (axial load P_G) is obtained as an upper limit to the true collapse load P_F .

The only readily calculable lower limit available is the load P_Y at which yield is first reached in the most highly stressed fibres of the strut. This occurs at the point C (Fig. 1.18) at which the true elastic-plastic curve OFD diverges from the elastic response line OAB . Formulae for P_Y are readily obtained if a state of initial imperfection is assumed. Thus, if a uniform strut of length l has a shape in the unloaded state given by $y_0 = a_1 \sin \pi x/l$, then under an axial load P_Y the deflexions increase to $y = a_1 \sin \pi x/l / (1 - P_Y/P_E)$, and the maximum bending moment, which occurs at mid-height ($x = l/2$) is $P_E P_Y a_1 / (P_E - P_Y)$. If the distance to the extreme fibres on the concave side is c , the maximum fibre stress is equal to the yield stress σ_y when

$$\sigma_y = \frac{P_Y}{A} + \frac{P_E P_Y}{P_E - P_Y} \frac{a_1 c}{l}. \quad (1.36)$$

If r is the radius of gyration about the axis of bending, then $I = Ar^2$. Put $P_Y = Ap_Y$ and $P_E = Ap_E$, so that p_Y and p_E are the mean axial stresses at the load at first yield P_Y and at the Euler load P_E respectively. Moreover, let it be assumed that the initial imperfection a_1 is defined in terms of a non-dimensional coefficient

η such that $\eta = a_1 c / r^2$. Then equation (1.36) may be solved to give

$$p_Y = \frac{1}{2} \left\{ \sigma_y + (1 + \eta)p_E - \sqrt{[(\sigma_y + (1 + \eta)p_E)^2 - 4\sigma_y p_E]} \right\}. \quad (1.37)$$

In a similar manner, the load at first yield can be calculated for a strut loaded eccentrically, using equation (1.5). If a load P is applied with eccentricity a_1' , then the terminal moment M is given by $M = Pa_1'$. It follows from equation (1.5) that the central deflexion is $a_1' [\sec(\alpha l/2) - 1]$ where $\alpha^2 = P/EI$. It is then readily shown that the mean axial stress at first yield is given by the solution of the equation

$$\sigma_y = p_Y \left\{ 1 + \eta' \sec \frac{\pi}{2} \sqrt{\frac{p_Y}{p_E}} \right\} \quad (1.38)$$

where $\eta' = a_1' c / r^2$.

1.15 Practical Strut Formulae

Formulae for the failure loads of struts may be obtained either by using an empirically elevated lower limit or by applying an empirical reduction to an upper limit.

In the former category are the Perry–Robertson⁽⁶⁾ and Secant⁽⁷⁾ formulae. If a suitable *effective* imperfection or eccentricity, smaller than the actual imperfection or eccentricity, is assumed, the theoretical first yield load P_Y of the resulting imaginary strut may be made to coincide with the failure load of the actual strut. This is conveniently achieved by selecting a value for the dimensionless coefficient η in equation (1.37) or η' in equation (1.38) such that the best correlation exists between experimental failure loads and the load $P_Y = Ap_Y$. Equation (1.37) is then the Perry–Robertson formula, and equation (1.38) the Secant formula. Robertson found that a lower limit on the failure

loads of practical struts could be obtained by taking $\eta = 0.003/l$ in equation (1.37), whence $a_1/l = 0.003$ $r/c \approx 0.0015$ for most cross-sections. This is the basis for the design of struts in British Standard 449 (1958) for slenderness ratios exceeding 80. The Secant formula may be used as a basis for the design of mild steel struts, taking $\eta' = 0.25$.⁽⁷⁾ Both the Perry–Robertson and the Secant formulae give a curve of the general shape of ADF in Fig. 1.16, rising to σ_y as $l/r \rightarrow 0$ and approaching the Euler

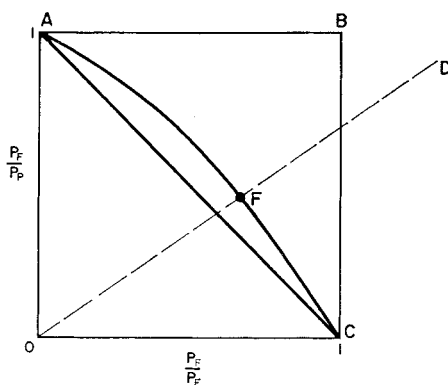


FIG. 1.20

curve BC as l/r becomes large. Despite their apparent basis on an accurately derived formula, it is important to realise that both the Perry–Robertson and the Secant formulae are empirical approximations to the failure load. The “effective” initial imperfection or eccentricity does not correspond to any observable value, and is an empirically chosen quantity.

Turning now to modifications of the upper limits, the failure load P_F (Fig. 1.18) is lower than either the Euler load P_E or the squash load P_P . Hence $P_F/P_E < 1$ and $P_F/P_P < 1$. This may be expressed by stating that the solution for any practical strut must lie within the area $OABC$ in Fig. 1.20. The tangent slope of any straight line OD through the origin is $P_E/P_P = (\pi^2 EI/l^2)/A\sigma_y =$

$\pi^2(r/l)^2 E/\sigma_y$, so that struts of any given material and slenderness will be represented by points on a fixed line OD . When l/r is very large, so that $P_E \ll P_P$ (i.e. OD lies close to OC), the strut fails by elastic instability, and $P_F/P_E \approx 1$. When l/r is very small so that $P_E \gg P_P$ (i.e. OD lies close to OA), the strut fails by squashing at the yield stress, whence $P_F/P_P \approx 1$. Hence A and C are the extreme points of a *failure locus AFC* for practical struts. While any number of curves could be drawn, the most useful locus turns out to be the straight line AC , which gives the following relationship between the failure load P_F , the Euler load P_E and the squash load P_P .

$$\frac{1}{P_F} = \frac{1}{P_E} + \frac{1}{P_P} \quad (1.39)$$

Putting $P_E = \pi^2 EA (r/l)^2$ and $P_P = A\sigma_y$, this gives

$$\frac{P_F}{A} = \frac{\sigma_y}{1 + \frac{\sigma_y}{\pi^2 E} \left(\frac{l}{r}\right)^2} \quad (1.40)$$

This is a particular case of an empirical formula suggested by Rankine in 1866.⁽⁸⁾ Its significance has been studied more generally by Merchant.⁽⁹⁾ In Rankine's formula, an arbitrary constant appears in place of $\sigma_y/\pi^2 E$, thus giving a straight line in Fig. 1.20 that passes through A but not through C . It is found that equation (1.40) gives a reasonable approximation to the failure loads of pin-ended struts throughout the full range of slenderness values, and is represented in Fig. 1.16 by the curve ADF . In its more general form, Rankine's formula gives a curve which is tangential to the squash line AB at A , but does not become asymptotic to the Euler curve BC for struts of high slenderness. On theoretical grounds, therefore, the particular form of Rankine's formula represented by equation (1.40) (and therefore by equation (1.39)) is to be preferred.

1.16 The Failure of Struts with Lateral Loads

As in the case of struts with initial imperfections, the calculation of failure loads for laterally loaded struts involves consideration of elastic-plastic behaviour, and is too complex for practical use. If an initially straight strut of length l carries an axial load P and a central lateral load kP (Fig. 1.21(a)), the elastic load-

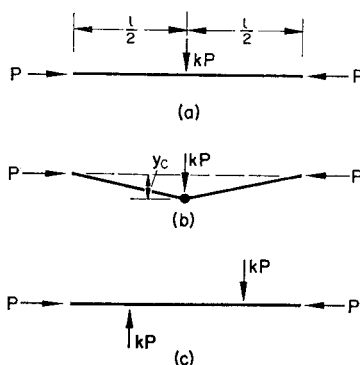


FIG. 1.21

deflexion curve is of the form OAB in Fig. 1.18, and rises asymptotically to the Euler load P_E , which is thus an upper limit. The rigid-plastic load P_P , also an upper limit, is given by

$$M_P' = \frac{kP_P l}{4}$$

where M_P' is the full plastic moment of resistance under an axial load P_P . The rigid-plastic line LM in Fig. 1.18 is given by

$$M_P' = \frac{kPl}{4} + Py_c$$

where y_c is the central deflexion (Fig. 1.21(b)). Finally, the load at first yield P_Y is readily calculated, and gives a lower bound.

Various semi-empirical methods of obtaining the failure load have been investigated, but the most consistently successful appears to be that based on equation (1.39), as investigated by Merchant.⁽⁹⁾ In applying this Rankine type formula, the Euler load P_E is that upper bound on the failure load which is obtained by assuming indefinite elastic behaviour. The other upper bound P_P (see above) has been obtained by ignoring elastic behaviour, but taking account of plasticity. These two upper limits, when used in equation (1.39), give an empirical estimate of the failure load P_F which depends both on elastic and on plastic behaviour. It has been shown theoretically (Horne⁽¹⁰⁾) that the "Rankine load" P_F as obtained from equation (1.39) is likely to be a reasonable approximation to the failure load in all cases where the deflected shape due to lateral loading only is closely similar in form to the buckled form of the strut for axial loading only. In cases where this is not so (as for example for the loading in Fig. 1.21(c)), the actual failure load is likely to be above the "Rankine load".

1.17 The Stability of Axially Loaded Members with Strain-hardening Stress Relations—Double Modulus Load

We discuss now a centrally loaded member composed of strain-hardening material (Fig. 1.14), sufficiently short for the elastic limit of stress $-\sigma_y$ to be reached over the entire cross-section before any buckling occurs. The question may be asked "Is it possible, when the stress in the member reaches some uniform value $-\sigma_D$, for the strut to buckle laterally with zero increase of load for small deformations?" In other words, we seek an axial load (to be denoted by P_D) at which behaviour analogous to the behaviour of an Euler strut can take place.

Consider an axially loaded member of rectangular cross-section $b \times d$ (Fig. 1.22(a)) which has remained straight until it reaches the load $P_D = bd\sigma_D$. The uniform stress $-\sigma_D$ ($ABCD$ in Fig. 1.22(c)) causes a uniform strain $-\varepsilon_D$ ($ABCD$ in Fig. 1.22(b)), corresponding to point C' on the stress-strain curve in

Fig. 1.14. Suppose the strut buckles so that the face FG becomes concave, the radius of curvature at some particular section being R . With the usual assumption that plane sections remain plane during buckling, the total strain becomes $AB'C'D$ in Fig. 1.22(b), zero *change* of strain occurring at a depth d_1 from the concave face and d_2 from the convex face. The extreme fibre strains are $\epsilon_1 = d_1/R$ and $\epsilon_2 = d_2/R$ as shown. On the concave

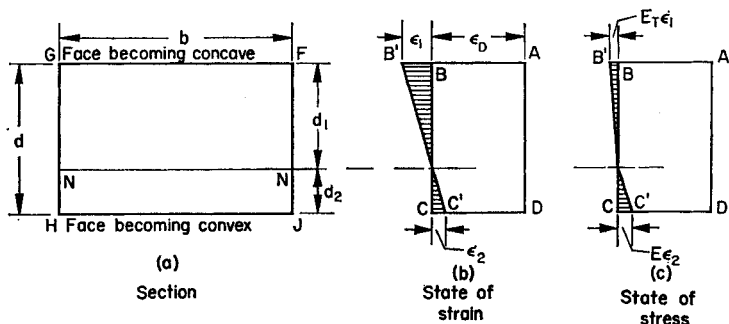


FIG. 1.22

face, the increase of stress is governed by the tangent modulus E_T (slope of $C'D'$ in Fig. 1.14), and so the change of extreme fibre stress becomes $E_T \epsilon_1$ (Fig. 1.22(c)). On the convex side, the material unloads and follows an elastic relationship between change of stress and change of strain ($C'F'$ in Fig. 1.14). Hence the change of extreme fibre stress on the convex face of the strut becomes $E \epsilon_2$ (Fig. 1.22(c)). The *changes* of stress throughout the cross-section are proportional to fibre distances from the axis NN (Fig. 1.22(a)) along which there is zero change of strain, and hence the changes of stress are as shown by the shaded triangles in Fig. 1.22(c). This change of stress corresponds to zero change of axial load, but gives a moment of resistance denoted by M . From the condition of zero change of axial load,

$$\frac{E_T \epsilon_1}{2} b d_1 - \frac{E \epsilon_2}{2} b d_2 = 0. \quad (1.41)$$

Since the change of stress represents a pure couple, moments may be taken about the axis NN , whence

$$\frac{E_T \varepsilon_1}{2} b d_1 \cdot \frac{2}{3} d_1 + \frac{E \varepsilon_2}{2} b d_2 \cdot \frac{2}{3} d_2 = M. \quad (1.42)$$

Moreover,

$$d_1 + d_2 = d. \quad (1.43)$$

Substituting $\varepsilon_1 = d_1/R$ and $\varepsilon_2 = d_2/R$, it follows from (1.41) that $d_1/d_2 = \sqrt{(E/E_T)}$. Hence from (1.43), $d_1 = \{\sqrt{E}/(\sqrt{E} + \sqrt{E_T})\}d$ and $d_2 = \{\sqrt{E_T}/(\sqrt{E} + \sqrt{E_T})\}d$, and equation (1.42) may be reduced to

$$M = \frac{b d^3}{3} \cdot \frac{E E_T}{(\sqrt{E} + \sqrt{E_T})^2} \cdot \frac{1}{R}. \quad (1.44)$$

The relationship between moment of resistance M and curvature $1/R$ may be compared with that for the member in the elastic range, namely

$$M = \frac{b d^3}{12} \cdot E \cdot \frac{1}{R}.$$

Hence the flexural rigidity has been modified due to inelastic behaviour by the reduction of the modulus from the elastic value E to a "reduced modulus" or "double modulus" E_D given by

$$E_D = \frac{4 E E_T}{(\sqrt{E} + \sqrt{E_T})^2}. \quad (1.45)$$

The solution for the buckling of the strut under the axial load P_D is obtained in exactly the same way as for an elastic strut at the Euler load, with the substitution of E_D for E in the equation of flexure (1.8). Hence it follows that

$$P_D = \pi^2 \frac{E_D I}{l^2} \quad (1.46)$$

where l is the length of the strut and $I = (1/12)bd^3$. Since the value of E_D depends on the tangent modulus E_T , and therefore on the mean stress $\sigma_D = P_D/bd$, equation (1.46) can only be solved for a given member by trial and error. The load P_D is the *reduced modulus* or *double modulus* load, and marks the point of bifurcation of equilibrium at A in the curve of load P

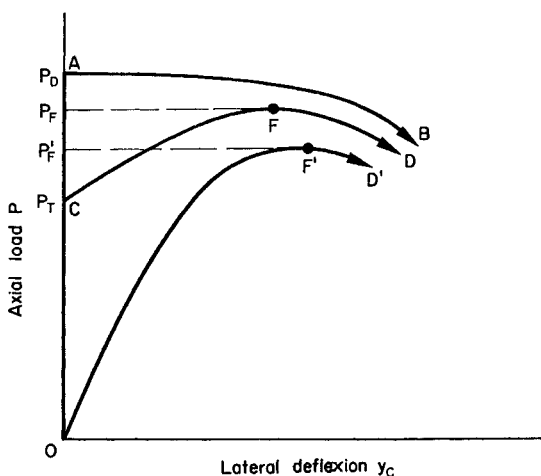


FIG. 1.23

versus lateral deflection shown by AB in Fig. 1.23. The changes of stress considered above are assumed to be small, and for larger changes of stress, the effective modulus decreases below E_D , causing a drop in the load-deflection curve AB .

It is important to note that the expression for the reduced modulus E_D depends on the shape of cross-section of the member. Thus, if an I-section is buckling in the plane of the web, and the area of the web can be assumed small compared with that of the flanges, it is readily shown that

$$E_D = \frac{2EE_T}{E + E_T}$$

The way in which E_T and E_D vary with stress for a typical light alloy is shown in Fig. 1.24. The double modulus buckling loads for rectangular section members of varying slenderness ratio

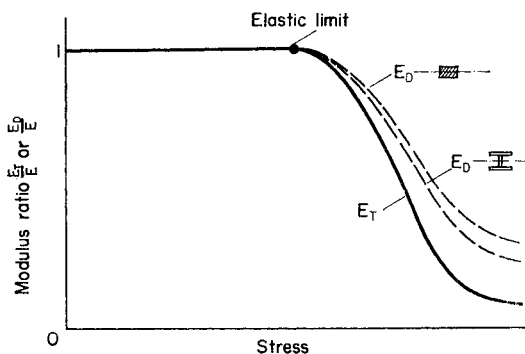


FIG. 1.24

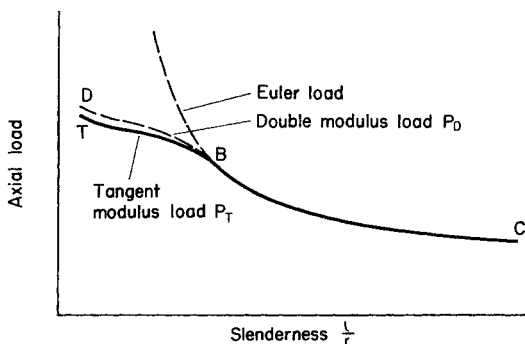


FIG. 1.25

are shown by curve DBC in Fig. 1.25. The part BC of the curve refers to slender members buckling in the elastic range, and is therefore part of the Euler curve.

The reduced modulus or double modulus load was first introduced by Engesser,⁽¹¹⁾ and was for a long time considered to

be the lowest load at which an initially straight axially loaded strut would deviate from a straight line. In 1947, Shanley⁽¹²⁾ showed the greater significance of the tangent modulus load, which had in fact been discussed and then discarded by Engesser.

1.18 The Tangent Modulus Load

The double modulus load, considered in the previous section, is based on the concept of buckling while the axial load remains constant. Shanley realised that the condition of zero rate of

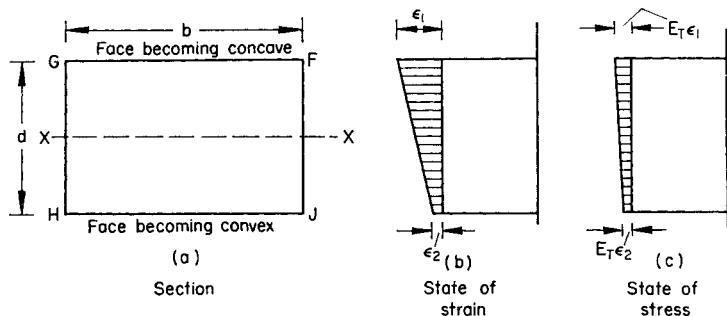


FIG. 1.26

increase of axial load during buckling is an unnecessary restriction, and that if this restriction is removed, bifurcation of equilibrium can occur at a load lower than P_D . Buckling is governed by the incremental flexural rigidity of the member, namely the ratio of increase of moment of resistance to increase of curvature. This has its least value when *all* the fibres in a cross-section undergo an increase of stress, following, for a small increase of strain, the tangent modulus relation $C'D'$ in Fig. 1.14. Considering again a strut of rectangular cross-section (Fig. 1.26(a)), the increases in strain and stress become as shown in Figs. 1.26(b) and (c) respectively. The changes of strain and stress on the convex face HJ may be zero or compressive, but not tensile. The relation between curvature and moment of resistance, measured about the central axis XX , is obtained by substituting E_T in place of

E in the usual elastic formula, whence the condition for buckling becomes

$$P_T = \pi^2 \frac{E_T I}{l^2}. \quad (1.47)$$

The load P_T is the *tangent modulus* load, and is that stage at which buckling just becomes possible as the load is further increased, as shown by the curve CFD in Fig. 1.23. It may be noted that, unlike equation (1.45), equation (1.47) applies to all shapes of cross-section. To follow the curve CD in detail involves a complicated step-by-step calculation, and for this reason the maximum or true failure load P_F is difficult to obtain theoretically. The load P_F is however known to lie between the tangent modulus load P_T and the double modulus load P_D . Typical tangent modulus loads are given by the curve TB in Fig. 1.25.

1.19 Non-axial Loading of Strain-hardening Struts

The behaviour of strain-hardening struts under non-axial loading is even more difficult to calculate than that of elastic-plastic struts. Qualitatively, it is easily seen that the load-deflexion curve $OF'D'$ (Fig. 1.23) will lie below the curve CFD for an axially loaded member, but the peak load P_F' has no specific relation to any of the loads P_T , P_F or P_D except that P_F and P_D furnish upper bounds. A common assumption is to identify P_F' for *nominally* axially loaded members (i.e. members with some initial imperfection and unintentional load eccentricity) with the tangent modulus load P_T for a similar ideal member. Experimentally, there is considerable evidence that the tangent modulus load provides a close estimate of the failure loads of nominally axially loaded members for a wide range of strain-hardening materials, and for this reason the tangent modulus load has an extensive use in design. It is, however, important to realise that the identification of the tangent modulus load with the failure load is an empirical rule to be justified experimentally.

An alternative basis for practical strut curves of strain-hardening material is to use equation (1.37) or (1.38), the yield stress σ_y

being replaced by a *proof stress*, that is, the stress for which the permanent strain ε_0 (Fig. 1.14) has a specified value (e.g. 0.1 percent proof stress, corresponding to $\varepsilon_0 = 1/1000$). As in the case of elastic-plastic members, the imperfection constant η or η' is settled empirically by reference to test results.

1.20 Load Factor, Stress Factor and Factor of Safety

A typical relation between applied load and maximum induced stress in a member subjected to longitudinal loads is shown by *OAB* in Fig. 1.27. As the combined loads (transverse and longi-

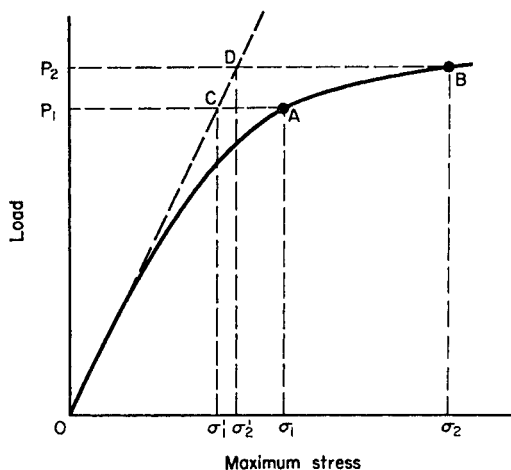


FIG. 1.27

tudinal) increase, the stresses induced by bending action increase more than proportionately on account of the increasing deformations. This behaviour is in contrast to the linear relation *OCD* between applied load and maximum induced stress obtained for a member subjected to transverse loads only.

Consider two load levels P_1 and P_2 . The load P_1 may correspond to the desired "working conditions" of the member, while load P_2 is either an accidental overload, or a load at which the behaviour

of the structure becomes dangerous or otherwise objectionable. The ratio P_2/P_1 is known as a *load factor*.

Instead of comparing the two states of the structure by reference to the applied loads, it would also be possible to compare the maximum induced stresses σ_1 and σ_2 or σ_1' and σ_2' . The ratio σ_2/σ_1 or σ_2'/σ_1' is then a *stress factor*. It is important to notice that, while for the member without axial load, $\sigma_2'/\sigma_1' = P_2/P_1$, i.e. stress factor = load factor, this is not true for the axially loaded member, for which $\sigma_2/\sigma_1 > P_2/P_1$. It is true in general that, when comparing two given states in a member which carries a compressive axial load, the load factor will be smaller than the stress factor, and this is the more noticeable the closer the load P_2 is to the Euler load P_E .

In order to establish a margin of safety in design, use may be made of either a load factor or a stress factor. While a load factor is usually a more satisfactory basis, it has been the more common to consider a stress ratio as providing the "factor of safety". The maximum working stress σ_1 is then defined as some proportion of a stress σ_2 , which may be a yield stress, a limit of proportionality or a proof stress. Since, in structures subject to instability, the margin of safety as measured by a load factor may be markedly and dangerously smaller than the "factor of safety" measured by a stress ratio, it is important that load factors, *not* stress factors, should be used in design.

Examples

1.1 An initially straight pin-ended strut of length l and flexural rigidity EI carries a compressive load P which acts at one end ($x = 0$) through the centroid, and at the other end at an eccentricity e . Show that the effect of the eccentricity on the undeformed strut is to introduce a bending moment M which may be represented by the Fourier series

$$M = \frac{2}{\pi} Pe \left\{ \sum_{n=1}^{\infty} (-1)^{n-1} \frac{1}{n} \sin \frac{n\pi x}{l} \right\}$$

Hence show that, under the axial load P , the additional deflexions of the strut may be represented by

$$y = \frac{2}{\pi} e \left\{ \sum_{n=1}^{\infty} (-1)^{n-1} \frac{1}{n} \frac{\sin \frac{n\pi x}{l}}{n^2 \frac{P_E}{P} - 1} \right\}$$

where $P_E = \pi^2 EI/l^2$.

1.2 The centre line of any initially straight compression member, of flexural rigidity EI and carrying an axial load P , may be represented by part of the sine curve $y = A \sin kx$ where $k^2 = P/EI$ (see Fig. 1.6). Use this fact to show that a strut AB of length l , with eccentricity e_A at end A and e_B at end B where $|e_A| > |e_B|$ will have the maximum bending moment at end A provided P is less than $(EI/l^2)\{\cos^{-1}(e_B/e_A)\}^2$.

1.3 A pin-ended strut has an area of cross-section of 10.3 in^2 , a radius of gyration about its minor axis of 2.03 in. , and is of length 12 ft. The extreme fibre distance for bending about the minor axis is 4.00 in. The strut is perfectly straight, but the axial load is applied at each end with an eccentricity of 0.5 in. on the same side of the centroidal axis. The strut has been designed to a load factor of 2.00 with respect to the attainment of a yield stress of 22.5 ton/in^2 in the most highly stressed fibres. Determine the maximum stress at working load. Take $E = 13,000 \text{ ton/in}^2$.

1.4 An elastic-plastic pin-ended strut of length l , with a rectangular cross-section $b \times d$ where $b > d$, has a centre line with an initial out-of-straightness given by $y = (\eta d/6) \sin \pi x/l$ (η is the non-dimensional imperfection coefficient of equation (1.37)). Show that the axial load P corresponding to point G in Fig. 1.18 is given by the solution of the equation

$$\eta = \frac{3}{2} \left(\frac{1}{n} - n \right) \left(1 - \frac{12}{\pi^2} \frac{\sigma_y l^2}{E d^3} n \right)$$

where σ_y is the yield stress and $n = P/bd\sigma_y$.

1.5 A pin-ended beam-column of rectangular cross-section carries an axial load P and a uniformly distributed transverse load of total value W where $W = \mu P$. The material is elastic-plastic with elastic modulus E and yield stress σ_y . If p denotes the mean axial stress and S the slenderness ratio about the axis of bending (i.e. length divided by relevant radius of gyration), use the magnification factor (see Section 1.9) to show that y_e , the lateral deflexion at mid-span, is given approximately by

$$y_e = \frac{5}{384} \frac{\frac{pS^2}{E} \mu L}{\left(1 - \frac{1}{\pi^2} \frac{pS^2}{E}\right)}.$$

Obtain also an equation for the plastic mechanism line (LM in Fig. 1.18), and hence show that the estimate of the failure load represented by point G is given very closely by the solution of the equation

$$\left\{1 - \left(\frac{p}{\sigma_y}\right)^2\right\} \left\{1 - \frac{1}{\pi^2} \frac{pS^2}{E}\right\} = \frac{\mu p S}{4\sqrt{3}\sigma_y}$$

1.6 A pin-ended strut of rectangular cross-section has a slenderness about its minor axis of 50. The stress-strain relationship for the material is similar in tension and compression. If σ is the stress in lb/in², then $|\epsilon| = 10^{-7} |\sigma|$ for $|\sigma| \leq 2 \times 10^4$ and $|\epsilon| = 10^{-7} |\sigma| + 0.5 \times 10^{-14} \times (|\sigma| - 2 \times 10^4)^3$ for $|\sigma| \geq 2 \times 10^4$. Using double modulus and tangent modulus loads, obtain upper and lower bounds for the mean axial stress at failure. Obtain also the Perry-Robertson failure stress (equation (1.37)), substituting the 0.1 percent proof stress in place of σ_y and taking the imperfection constant $\eta = 0.15$.

(Answers to questions 1.3 and 1.6 may be found on page 154).

Stability Functions

2.1 Introduction

The general features of structural behaviour in relation to elastic and plastic stability are described in Chapter 1. The development of methods of analysis for more extensive structures requires some convenient means of summarising the properties of individual members when subjected to bending moments in the presence of axial loads. While this is difficult to achieve for members loaded beyond the elastic limit, it is relatively easy in the elastic range, and the present chapter describes certain *stability functions* which are then employed in Chapters 3 and 4 as the basis for the analysis of stability in structures.

The analysis of elastic structures in which axial loads have negligible effect is facilitated by the application of the principle of superposition. Thus, suppose the member AB in Fig. 2.1(a) has a uniform flexural rigidity EI for bending in the plane of the diagram, and that the axial load $P = 0$. If, as shown, end B is kept fixed in position and direction while end A is rotated about a fixed point, the terminal moments M_{AB} and M_{BA} and the rotation θ_A are linearly related, viz.

$$M_{AB} = 4 \left(\frac{EI}{l} \right) \theta_A, \quad M_{BA} = \frac{1}{2} M_{AB}.$$

The ratio $M_{AB}/\theta_A = 4(EI/l)$ is the *stiffness* of the member AB for rotation at A , and is proportional to I/l . This rotational stiffness is used in the analysis of structures in the method of *moment distribution*. The ratio $M_{BA}/M_{AB} = \frac{1}{2}$ is also used in moment distribution as the carry-over factor.⁽¹³⁾ The rotation of

end B while A is kept fixed in position and direction (Fig. 1(b)) similarly gives

$$M_{BA} = 4 \left(\frac{EI}{l} \right) \theta_B, \quad M_{AB} = \frac{1}{2} M_{BA}.$$

Moment distribution consists of the step-by-step deformation of a structure by the superposition of operations such as those shown in Figs. 2.1(a) and (b), the operations being systematically

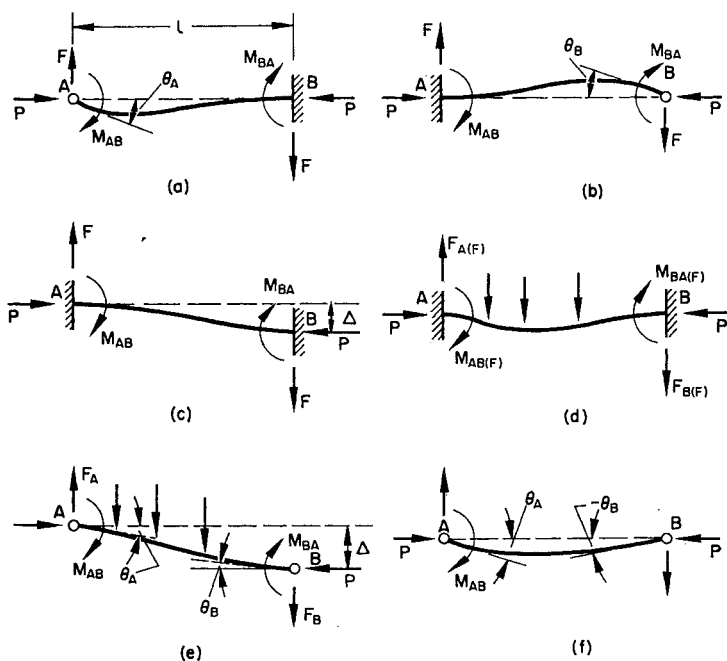


FIG. 2.1

directed towards a satisfaction of the equilibrium requirements. Superposition is justified by the linearity of the relationships between applied forces and deformation, i.e. by the constancy of the stiffnesses.

Another type of deformation used in moment distribution is the translation of one end of the member relative to the other through some distance Δ , see Fig. 2.1(c). The member retains its original direction at the ends A and B , thus inducing terminal moments M_{AB} and M_{BA} where

$$M_{AB} = M_{BA} = -6 \left(\frac{EI}{l} \right) \cdot \frac{\Delta}{l}.$$

The translating force F is given by

$$F = - \left[\frac{M_{AB} + M_{BA}}{l} \right] = 12 \left(\frac{EI}{l^3} \right) \cdot \Delta,$$

the quantity $12(EI/l^3)$ thus being the stiffness of the member with respect to translation.

The effect of transverse loads is introduced by considering the *fixed-end moments* $M_{AB(F)}$ and $M_{BA(F)}$ induced when both ends are kept fixed in position and direction, Fig. 2.1(d). The state of a laterally loaded member in which rotations have occurred at both ends together with a translation (Fig. 2.1(e)) is derived by superposition from the four separate operations in Figs. (a) to (d), giving the complete slope-deflexion equation for a member with no axial load in the form

$$M_{AB} = M_{AB(F)} + k \left[4\theta_A + 2\theta_B - \frac{6\Delta}{l} \right] \quad (2.1)$$

where $k = EI/l$.

2.2 The Effect of Axial Load on Member Stiffness

The introduction of an axial load P modifies the stiffness and fixed-end moments to an extent which depends on the value of the axial load. The principle of superposition can still be applied to a sequence of operations provided none of these operations alters the axial load in the member.

It is found convenient to express the axial load P as a proportion of P_E , the pin-ended Euler load for buckling in the plane of the applied loads and bending moments. Let $P/P_E = \rho$ and $EI/l = k$. Then since $P_E = \pi^2 EI/l^2$, P may be expressed in the form $P = \pi^2 \rho(k/l)$. For joint rotation at end A , Fig. 2.1(a),

$$M_{AB} = sk\theta_A, \quad M_{BA} = sck\theta_A,$$

$$M_{BA}/M_{AB} = c,$$

where s and c are functions of ρ only. Comparison with the solution for $P = 0$ shows that when $\rho = 0$, $s = 4$ and $c = 0.5$. For the translational operation in Fig. 2.1(c), it is then found that

$$M_{AB} = M_{BA} = -s(1+c)k \cdot \frac{\Delta}{l}.$$

The fixed-end moments $M_{AB(F)}$ and $M_{BA(F)}$ in Fig. 2.1(d) depend both on the distribution and intensity of the transverse loads and on the value of ρ , and may be denoted by $M'_{AB(F)}$ and $M'_{BA(F)}$. Superimposing the solutions for the elementary operations in Figs. 2.1(a) to (d), the general slope-deflexion equations for a laterally loaded member with axial load (Fig. 2.1(e)) become

$$M_{AB} = M'_{AB(F)} + k \left[s\theta_A + sc\theta_B - s(1+c) \cdot \frac{\Delta}{l} \right], \quad (2.2)$$

$$M_{BA} = M'_{BA(F)} + k \left[sc\theta_A + s\theta_B - s(1+c) \cdot \frac{\Delta}{l} \right]. \quad (2.3)$$

Stability functions of various types have been suggested by a number of authors, the first being due to Berry.⁽¹⁴⁾ Functions corresponding to s and c were first calculated by James⁽¹⁵⁾ and by Lundquist and Kroll.⁽¹⁶⁾ Livesley and Chandler⁽¹⁷⁾ retabulated s and c in terms of $\rho = P/P_E$, and their form of these functions

is used in the present treatment. The derivation of s and c functions will now be given.

2.3 The Functions s and c

The uniform member AB in Fig. 2.2 is, when unloaded, perfectly straight and of length l , with its longitudinal axis coincident with OX . The end B is fixed in position and direction, and in the presence of an axial load P , a terminal moment M_{AB} applied at A causes a rotation θ_A at A , and induces a restraining

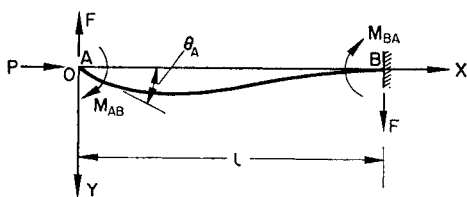


FIG. 2.2

moment M_{BA} at B . The uniform shear force F is obtained in terms of M_{AB} and M_{BA} by taking moments about one end, giving

$$F = -\frac{M_{AB} + M_{BA}}{l}.$$

If y denotes the deflexion perpendicular to OX of a point on the longitudinal axis distance x from end A , the equation of flexure becomes

$$EI \frac{d^2 y}{dx^2} = -Py - M_{AB} - Fx. \quad (2.4)$$

Substituting $P = \pi^2 \rho$ (k/l) and rearranging,

$$\frac{d^2 y}{dx^2} + \frac{\pi^2 \rho}{l^2} y = \frac{1}{kl} \left[(M_{AB} + M_{BA}) \frac{x}{l} - M_{AB} \right]. \quad (2.5)$$

The general solution of equation (2.5) is

$$y = A \sin \pi \sqrt{\rho} \frac{x}{l} + B \cos \pi \sqrt{\rho} \frac{x}{l} + \frac{l}{\pi^2 \rho k} \left[(M_{AB} + M_{BA}) \frac{x}{l} - M_{AB} \right]. \quad (2.6)$$

The constants of integration A and B may be derived from the two boundary conditions $y = 0$ when $x = 0$ and $y = 0$ when $x = l$, giving

$$A = -\frac{l}{4\alpha^2 k} \left[M_{AB} \cot 2\alpha + M_{BA} \operatorname{cosec} 2\alpha \right],$$

$$B = \frac{l}{4\alpha^2 k} M_{AB},$$

where $\alpha = (\pi/2)\sqrt{\rho}$. Substituting these values in equation (2.6) and differentiating with respect to x , it is found on rearrangement that

$$4\alpha^3 k \frac{dy}{dx} = M_{AB} \left(1 - 2\alpha \sin 2\alpha \frac{x}{l} - 2\alpha \cot 2\alpha \cos 2\alpha \frac{x}{l} \right) + M_{BA} \left(1 - 2\alpha \operatorname{cosec} 2\alpha \cos 2\alpha \frac{x}{l} \right). \quad (2.7)$$

The boundary condition $dy/dx = 0$ when $x = l$ leads to the evaluation of the carry-over factor c , namely

$$c = \frac{M_{BA}}{M_{AB}} = \frac{2\alpha - \sin 2\alpha}{\sin 2\alpha - 2\alpha \cos 2\alpha}.$$

Since $M_{AB} = sk\theta_A$ and $M_{BA} = csk\theta_A$, the value of s may now be obtained from equation (2.7), giving

$$s = \frac{(1 - 2\alpha \cot 2\alpha)\alpha}{\tan \alpha - \alpha}.$$

The variation of s and c with ρ is shown graphically in Fig. 2.3, and is tabulated in Tables A1 and A2 (pages 158 to 169). It is seen that as ρ increases from zero, s decreases from 4.0 to 0 at $\rho \approx 2.046$, thereafter becoming negative. The axial

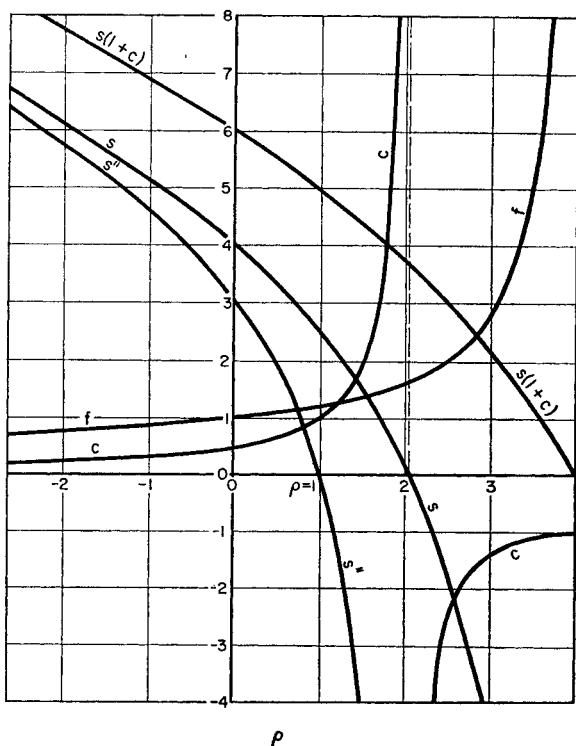


FIG. 2.3

load corresponding to $s = 0$ (given by the condition $2\alpha = \tan 2\alpha$) represents the critical load of a member AB direction fixed at B and pinned at A (Fig. 2.2), and it is evident that a member so loaded would have zero stiffness for rotation at A . At this same critical value of ρ , the carry-over factor c becomes infinitely

large, that is $M_{AB} = 0$ while M_{BA} is finite. At values of $\rho > 2.046$, the moment at A becomes a restraining moment, and this explains why the stiffness becomes negative.

It may be noted that the shear force F in Fig. 2.2 is given by

$$F = -\frac{M_{AB} + M_{BA}}{l} = -s(1 + c)\frac{k}{l}\theta_A.$$

In Tables A4 and A5 (pages 172 to 175) values of s and c are given for negative values of ρ , i.e. for axial tension. Increasing axial tension causes a continuous increase in stiffness s and a continuous decrease in carry-over factor c . The trigonometric functions are replaced by the corresponding hyperbolic functions. Thus if $\gamma = (\pi/2)\sqrt{(-\rho)}$,

$$s = \frac{(1 - 2\gamma \coth 2\gamma)\gamma}{\tanh \gamma - \gamma},$$

$$c = \frac{2\gamma - \sinh 2\gamma}{\sinh 2\gamma - 2\gamma \cosh 2\gamma}.$$

2.4 The Function s''

The stiffness of a member for rotation at one end is reduced when the remote end is free from rotational restraint. The deformation is represented in Fig. 2.1(f), and if $M_{AB} = s''k\theta_A$, the modified stiffness coefficient s'' may be obtained by a suitable superposition of the operations in Figs. 2.1(a) and (b). This may be represented in tabular form as follows.

TABLE 2.1

	M_{AB}	M_{BA}
Rotate θ_A Rotate θ_B	$sk\theta_A$ $sck\theta_B$	$sck\theta_A$ $sk\theta_B$
Rotate θ_A and θ_B	$sk(\theta_A + c\theta_B)$	$sk(c\theta_A + \theta_B)$

Since it is required to make $M_{BA} = 0$, the final column shows that $\theta_B = -c\theta_A$. Hence from the second column, $M_{AB} = s(1 - c^2)k\theta_A$ and thus $s'' = s(1 - c^2)$. The modified stiffness function s'' is shown graphically in Fig. 2.3, and is tabulated on pages 157-75.

As would be expected, $s'' = 0$ when $\rho = 1$, i.e. at the critical load for a pin-ended strut.

2.5 Sway Functions $s(1 + c)$ and m

The functions s , c and s'' are all associated with a joint rotation as the elementary operation. Another operation is that of sway, Fig. 2.4(a). The ends A and B are restrained against rotation, but one end is translated through a distance Δ (where Δ/l is small compared with unity) relative to the other. The angle $\Delta/l = \phi$ is the angle of translation. The sway operation may alternatively be regarded as the rotation of the ends A and B through angles of $-\phi$ (Fig. 2.4b), followed by a bodily rotation of $+\phi$, during which the terminal moments M_{AB} and M_{BA} remain unchanged. (Strictly speaking, the axial load P' in Fig. 2.4(b) differs from the axial load P in Fig. 2.4(a), but provided the angle of translation ϕ is small, the difference between P and P' may be neglected.) The table of operations for the calculation of the terminal moments is as follows.

TABLE 2.2

	M_{AB}	M_{BA}
Rotate $\theta_A = -\phi$	$-sk\phi$	$-sck\phi$
Rotate $\theta_B = -\phi$	$-sck\phi$	$-sk\phi$
	$-s(1 + c)k\phi$	$-s(1 + c)k\phi$

Hence $M_{AB} = M_{BA} = -s(1 + c)k\phi$.

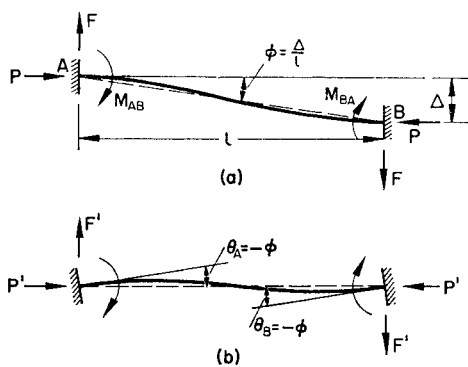


FIG. 2.4

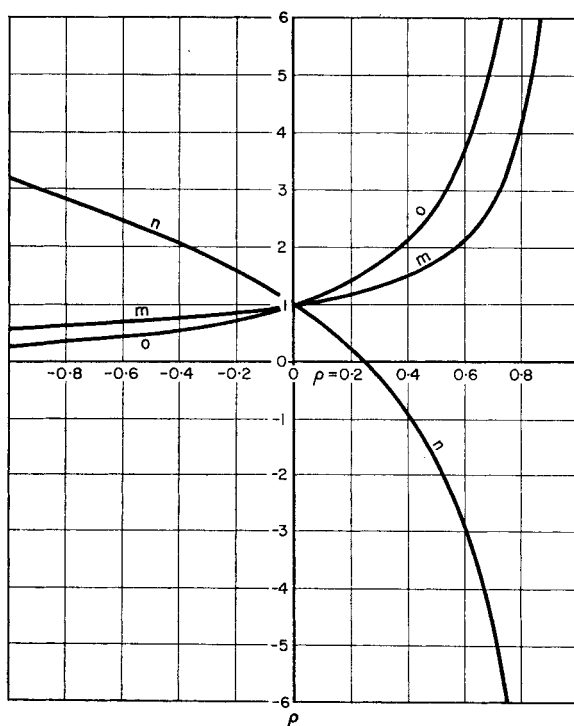


FIG. 2.5

In a translation such as that in Fig. 2.4(a), but with $P = 0$, the shear force F is given by $Fl = -(M_{AB} + M_{BA})$, whence $M_{AB} = M_{BA} = -Fl/2$. In the presence of axial load, this is modified to $M_{AB} = M_{BA} = -mFl/2$ where m is a function of ρ . Taking moments about one end of the member in Fig. 2.4(a), it follows that

$$Fl = -(M_{AB} + M_{BA}) - P\Delta.$$

Substituting $M_{AB} = M_{BA} = -mFl/2 = -s(1+c)k\phi$ and $P = \pi^2\rho k/l$, it is readily shown that

$$m = \frac{2s(1+c)}{2s(1+c) - \pi^2\rho}.$$

The shear force may also be calculated directly from the angle of translation ϕ , viz.

$$F = \frac{2s(1+c)}{m} \frac{k}{l} \phi = \frac{2s(1+c)}{m} \frac{k}{l^2} \Delta.$$

Hence the sway stiffness for both joints fixed against rotation is

$$\frac{2s(1+c)}{m} \frac{k}{l^2}.$$

The variation of m with ρ is shown graphically in Fig. 2.5.

2.6 No Shear Functions n and o

The joint translation depicted in Fig. 2.4(a) involves the introduction of a sway force F . It is found convenient in some analytical procedures to introduce a unit operation which avoids any change in shear force, and this is achieved by compounding a sway with the rotation of *one end only* of the member AB , as shown in Fig. 2.6. The terminal moments induced when end A rotates through θ_A are expressed in the form $M_{AB} = nk\theta_A$ and $M_{BA} = -ok\theta_A$, and the functions n and o so defined are dependent only on ρ and are called *no shear functions*. The following table of operations enables n and o to be expressed in terms of s , c and m .

TABLE 2.3

	M_{AB}	M_{BA}	F
Rotate θ_A	$sk\theta_A$	$sc k\theta_A$	$-s(1+c)\frac{k}{l}\theta_A$
Sway ϕ	$-s(1+c)k\phi$	$-s(1+c)k\phi$	$\frac{2s(1+c)}{m}\frac{k}{l}\phi$
	$nk\theta_A$	$-ok\theta_A$	0

It follows from the last column that $\phi = (m/2)\theta_A$, whence $n = s\{1 - m(1+c)/2\}$ and $o = s\{-c + m(1+c)/2\}$.

The variation of n and o with ρ is shown graphically in Fig. 2.5.

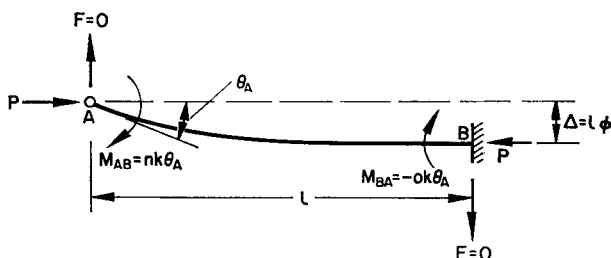


FIG. 2.6

The introduction of m , n and o functions, and their use in deriving the sway critical loads of rigid-jointed frames, is due to Merchant.⁽¹⁸⁾

2.7 Summary of Operations

A summary of the various elementary operations in terms of stability functions is given in Fig. 2.7. In addition to those already discussed, Fig. 2.7 gives at (d) the results for a joint translation in which one end is pinned and the other end is fixed in direction.

Also given in Fig. 2.7 are results for members with rigid gusset plates. These are discussed later in the chapter.

FIG. 2.7

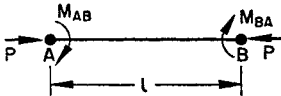
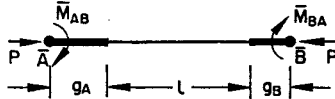
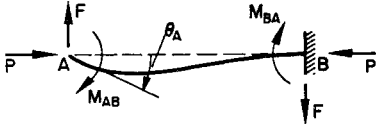
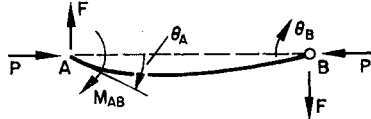
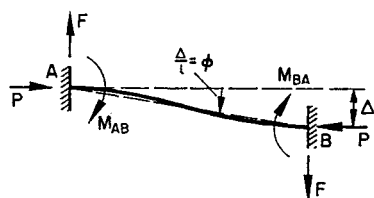
	UNIFORM MEMBER	UNIFORM MEMBER WITH GUSSETS
	 $k = \frac{EI}{l}, \rho = \frac{1}{\pi^2} \frac{Pl}{k}$	 $k = \frac{EI}{l}, \rho = \frac{1}{\pi^2} \frac{Pl}{k}$ $A = s(1 + c) - \frac{\pi^2}{2} \rho$
(a) END ROTATION. FAR END FIXED	 $M_{AB} = sk\theta_A,$ $M_{BA} = sck\theta_A = cM_{AB},$ $F = -s(1 + c) \frac{k}{l} \theta_A.$	$\bar{M}_{AB} = \bar{s}k\theta_A,$ $\bar{M}_{BA} = \bar{s}c k\theta_A,$ $F = -(\bar{s} + \bar{s}c) \frac{k}{l} \theta_A,$ $\bar{s} = s + 2 \frac{g_A}{l} \left(1 + \frac{g_A}{l}\right) A,$ $\bar{s}c = sc + 2 \frac{g_A}{l} \frac{g_B}{l} A + s(1 + c) \left(\frac{g_A}{l} + \frac{g_B}{l}\right)$ $\bar{s} + \bar{s}c = \left\{s(1 + c) + \frac{2g_A}{l} A\right\} \left\{1 + \frac{g_A}{l} + \frac{g_B}{l}\right\}$
(b) END ROTATION. FAR END PINNED	 $M_{AB} = s(1 - c^2)k\theta_A = s''k\theta_A,$ $F = -s(1 - c^2) \frac{k}{l} \theta_A = -s'' \frac{k}{l} \theta_A,$ $\theta_B = -c\theta_A.$	

FIG. 2.7 (continued)

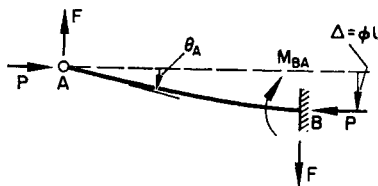
(c) JOINT TRANSLATION
(SWAY). BOTH ENDS
DIRECTION FIXED



$$\begin{aligned} M_{AB} &= M_{BA} = -s(1+c)k\phi \\ &= -m \frac{Fl}{2}, \\ F &= \frac{2s(1+c)k}{m} \frac{\Delta}{l} \phi. \end{aligned}$$

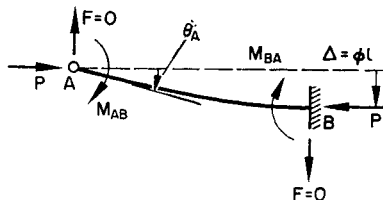
$$\begin{aligned} \bar{M}_{AB} &= -\bar{m}_A \frac{Fl}{2}, \\ \bar{M}_{BA} &= -\bar{m}_B \frac{Fl}{2}, \\ F &= \frac{2s(1+c)k}{m} \frac{\Delta}{l} \cdot \frac{\Delta}{l}, \\ \bar{m}_A &= m + 2 \frac{g_A}{l}, \\ \bar{m}_B &= m + 2 \frac{g_B}{l}. \end{aligned}$$

(d) JOINT TRANSLATION
(SWAY). ONE END PINNED



$$\begin{aligned} M_{BA} &= -s'k\phi \\ &= -\frac{s''}{s'' - \pi^2 \rho} Fl, \\ F &= (s'' - \pi^2 \rho) \frac{k}{l} \phi, \\ \theta_A &= (1+c)\phi \end{aligned}$$

(e) NO-SHEAR TRANSLATION



$$\begin{aligned} M_{AB} &= nk\theta_A, \\ M_{BA} &= -ok\theta_A, \\ \phi &= \frac{m}{2} \theta_A. \end{aligned}$$

$$\begin{aligned} \bar{M}_{AB} &= \bar{n}k\theta_A, \\ \bar{M}_{BA} &= -\bar{o}k\theta_A, \\ \frac{\Delta}{l} &= \frac{\bar{m}_A}{2} \theta_A, \\ \bar{n} &= n - \pi^2 \rho \frac{g_A}{l}, \\ \bar{o} &= o. \end{aligned}$$

2.8 Generalised Displacements

A generalised displacement (two end rotations plus a translation) may be established either in terms of s , c and m functions only, or in terms of n , o and m functions only. Using s , c , and m functions, the table of operations becomes:

TABLE 2.4

	M_{AB}	M_{BA}	F
Rotation at A θ_A	$sk\theta_A$	$sck\theta_A$	$-s(1+c)\frac{k}{l}\theta_A$
Rotation at B θ_B	$sck\theta_B$	$sk\theta_B$	$-s(1+c)\frac{k}{l}\theta_B$
Translation ϕ	$-s(1+c)k\phi$	$-s(1+c)k\phi$	$\frac{2s(1+c)}{m}\frac{k}{l}\phi$
Lateral load	$M'_{AB}(F)$	$M'_{BA}(F)$	$F'_{A(F)}, F'_{B(F)}$

For the sake of completeness, the components due to lateral loads within the length of a member have been added on the bottom line of the table.

Using n , o and m functions, the table of operations (excluding lateral loads) becomes:

TABLE 2.5

	M_{AB}	M_{BA}	ϕ
Rotation at A θ_A	$nk\theta_A$	$-ok\theta_A$	$\frac{m}{2}\theta_A$
Rotation at B θ_B	$-ok\theta_B$	$nk\theta_B$	$\frac{m}{2}\theta_B$
Applied shear force F	$-m\frac{Fl}{2}$	$-m\frac{Fl}{2}$	$\frac{m}{2s(1+c)}\frac{Fl}{k}$

In Table 2.4, the operations θ_A and θ_B introduce sway forces but are unaccompanied by sway deformation. In Table 2.5, the operations θ_A and θ_B are accompanied by sway deformation, but do not introduce any sway force. The functions n and o are more convenient to use than s and c functions when the equilibrium conditions for the structure preclude the introduction or alteration of the shear force in a member, as for example in the columns of a symmetrical single bay building frame in the absence of sway bracing.

2.9 Lateral Loads

As in structures where the effect of axial loads on flexure is ignored, lateral loads may be allowed for by the introduction of fixed-end moments. These are the moments incurred at the ends of the members by the given lateral loads when the ends are direction-fixed at zero slope. These fixed-end moments depend, not only on the distribution and intensity of the lateral loads, but also on the value of the axial loads as defined by the parameter $\rho = P/P_E$. Two cases will be considered—that of a load uniformly distributed throughout the length of the member, and that of a single point load applied anywhere within the span. The case for any number of point loads may be solved by superposition from the solution for a single point load.

2.10 Uniformly Distributed Load

The member AB , of length l and uniform flexural rigidity EI (Fig. 2.8), sustains an axial compressive load P and a uniformly distributed lateral load of intensity w per unit length. The ends A and B are fixed against rotation, the induced fixed-end moments being M_F at each end. The equation of flexure is

$$EI \frac{d^2y}{dx^2} = M_F - Py - \frac{wx(l-x)}{2}. \quad (2.8)$$

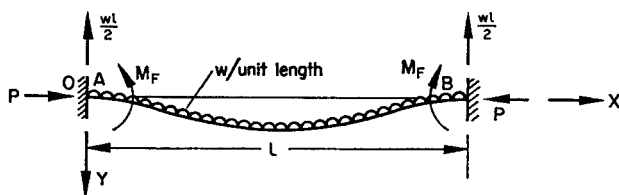


FIG. 2.8

Integrating the equation, and substituting $k = EI/l$, $P = \pi^2 \rho k/l$ and $\alpha = (\pi/2)\sqrt{\rho}$, it is found that

$$y = A \sin \frac{2\alpha x}{l} + B \cos \frac{2\alpha x}{l} + \frac{l}{4\alpha^2 k} \left[M_F - \frac{wl^2}{8\alpha^2} - \frac{w}{2} x(l-x) \right]. \quad (2.9)$$

Inserting the boundary conditions $y = 0$ and $dy/dx = 0$ when $x = 0$ gives

$$A = \frac{wl^3}{16\alpha^3 k},$$

$$B = \frac{wl^3}{32\alpha^4 k} \left[1 - \frac{8\alpha^2}{wl^2} M_F \right].$$

Using these values of A and B , and introducing the boundary condition $y = 0$ when $x = l$ in equation (2.9) gives finally

$$M_F = f \cdot \frac{wl^2}{12},$$

where

$$f = \frac{3}{\alpha^2} (1 - \alpha \cot \alpha).$$

The coefficient f , a function of α and hence of ρ , is the factor by which the fixed-end moment for zero axial load ($wl^2/12$) has to be multiplied to obtain the fixed-end moment when axial load is

present. The fixed-end moment coefficient f is shown graphically in Fig. 2.3, and values are tabulated on pages 157–75.

It is to be noted that, in the application of these results in equations (2.2) and (2.3) and in Table 2.4, $M'_{AB(F)} = -M_F$ and $M'_{BA(F)} = M_F$.

2.11 Concentrated Load

A concentrated load W acts transversely on a uniform member AB , of length l , the point of application of W being rl from end A and $(1-r)l$ from end B , as shown in Fig. 2.9(a). The

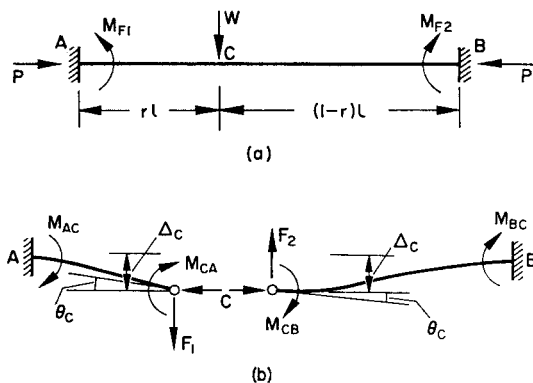


FIG. 2.9

fixed-end moments M_{F1} and M_{F2} are obtained by considering the behaviour of the two parts of the beam, AC and CB , as shown in Fig. 2.9(b). The deflection and rotation at C are denoted by Δ_c and θ_c respectively.

Let $\rho = P/P_E$ where P is the axial load in the member AB and P_E is the Euler load for AB considered as a pin-ended strut. If P_{E1} and P_{E2} are the Euler loads for AC and CB respectively when considered as separate members, then $P_{E1} = P_E/r^2$ and $P_{E2} = P_E/(1-r)^2$. If $\rho_1 = P/P_{E1}$ and $\rho_2 = P/P_{E2}$, then $\rho_1 = r^2\rho$

and $\rho_2 = (1 - r)^2 \rho$. The stability functions for AC and CB , obtained from ρ_1 and ρ_2 , will be denoted respectively by s_1, c_1, m_1 , etc., and s_2, c_2, m_2 , etc. It is also to be noted that if $k = EI/l$, then $k_1 = EI/rI = k/r$ and $k_2 = EI/(1 - r)I = k/(1 - r)$.

To obtain the deformed states of AC and CB depicted in Fig. 2.9(b), the initially straight members are subjected to a joint rotation at C of θ_c (as in Fig. 2.7(a)) followed by a joint translation of Δ_c (as in Fig. 2.7(c)). The bending moments M_{AC} , M_{CA} , M_{CB} and M_{BC} (clockwise positive, Fig. 2.9(b)) resulting from these two steps are shown in Table 2.6, the final values

TABLE 2.6

Operation	M_{AC}	M_{CA}	M_{CB}	M_{BC}
Rotate C (θ_c)	$c_1 s_1 \frac{k}{r} \theta_c$	$s_1 \frac{k}{r} \theta_c$	$s_2 \frac{k}{(1-r)} \theta_c$	$c_2 s_2 \frac{k}{(1-r)} \theta_c$
Translate C (Δ_c)	$-s_1(1 + c_1) \frac{k}{r^2} \frac{\Delta_c}{l}$	$-s_1(1 + c_1) \frac{k}{r^2} \frac{\Delta_c}{l}$	$s_2(1 + c_2) \frac{k}{(1-r)^2} \frac{\Delta_c}{l}$	$s_2(1 + c_2) \frac{k}{(1-r)^2} \frac{\Delta_c}{l}$

being obtained by addition of the two rows. Since for equilibrium at C , $M_{CA} + M_{CB} = 0$, it follows that

$$\left[\frac{s_1}{r} + \frac{s_2}{1-r} \right] \theta_c = \left[\frac{s_1(1 + c_1)}{r^2} - \frac{s_2(1 + c_2)}{(1-r)^2} \right] \frac{\Delta_c}{l}. \quad (2.10)$$

Since $M_{F1} = -M_{AC}$, it follows from Table 2.6 that

$$M_{F1} = s_1(1 + c_1) \frac{k}{r^2} \frac{\Delta_c}{l} - s_1 c_1 \frac{k}{r} \theta_c. \quad (2.11)$$

Using the last column of Table 2.4, the shear forces F_1 and F_2 either side of the applied load W may be derived (see Fig. 2.9(b)),

$$F_1 = 2s_1(1 + c_1) \left[\frac{1}{rm_1} \frac{\Delta_c}{l} - \frac{\theta_c}{2} \right] \frac{k}{r^2 l}, \quad (2.12)$$

$$F_2 = -2s_2(1 + c_2) \left[\frac{1}{(1-r)m_2} \frac{\Delta_c}{l} + \frac{\theta_c}{2} \right] \frac{k}{(1-r)^2 l}. \quad (2.13)$$

By vertical equilibrium at C ,

$$W = F_1 - F_2. \quad (2.14)$$

The elimination of θ_c , Δ_c , F_1 and F_2 between equations (2.10) to (2.14) gives an expression for the fixed-end moment M_{F1} in the form

$$\frac{M_{F1}}{Wl} = \left[\frac{(1 + c_1)A - c_1 r B}{2AC - B^2} \right] \frac{s_1}{r^2} \quad (2.15)$$

where

$$A = \frac{s_1}{r} + \frac{s_2}{1 - r},$$

$$B = \frac{s_1(1 + c_1)}{r^2} - \frac{s_2(1 + c_2)}{(1 - r)^2},$$

$$C = \frac{s_1(1 + c_1)}{r^3 m_1} + \frac{s_2(1 + c_2)}{(1 - r)^3 m_2}.$$

Values of M_F/Wl are shown graphically in Fig. 2.10 for values of ρ between -20 and $+2$ and of r between 0 and 1.0 . By entering the chart with r and $(1 - r)$, the fixed-end moments at both ends of a member due to a load placed anywhere along its length may be derived. As mentioned before, the fixed-end moments due to a series of concentrated loads may be obtained by superposition. In applying equations (2.2) and (2.3) and Table 2.4, due account must be taken of signs in substituting for $M'_{AB(F)}$ and $M'_{BA(F)}$. The shear forces $F'_{A(F)}$ and $F'_{B(F)}$ for the fixed-end moment condition are best derived directly from the fixed-end moments themselves by considering the equilibrium of the loaded member (Fig. 2.1(d)).

2.12 Effect of Gusset Plates

It is usually convenient to work to frame centre lines, so that the ends of members dealt with in a structural analysis actually lie within the boundaries of the joints. Although the joints

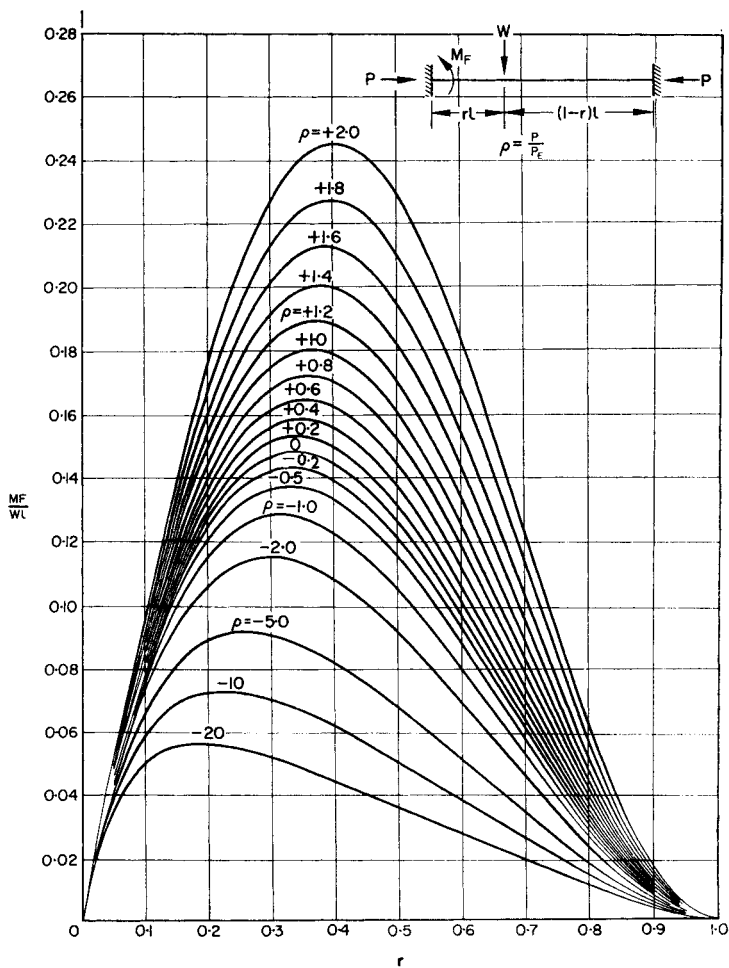


FIG. 2.10

cannot be absolutely rigid, it is more accurate to assume complete rigidity than to assume an effective rigidity equal to that of the rest of the member. Complete flexural rigidity over given lengths at the ends of members may be allowed for in the calculations by introducing modified values of the various stability functions as follows.

The member $\bar{A}\bar{B}$ (Fig. 2.11(a)) is completely rigid over the end lengths $\bar{A}A = g_A$ and $\bar{B}B = g_B$, the central length $AB = l$

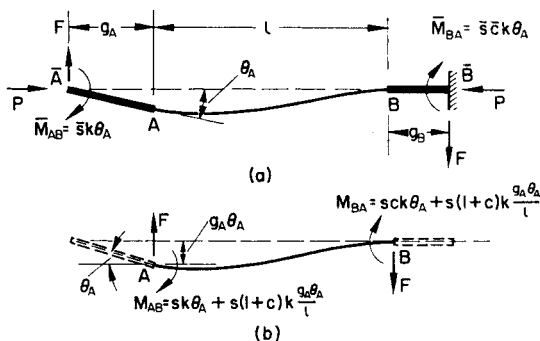


FIG. 2.11

having uniform flexural rigidity EI . The terminal bending moments \bar{M}_{AB} , \bar{M}_{BA} induced by a rotation θ_A at \bar{A} are expressed in terms of modified stability functions \bar{s} and \bar{c} where $\bar{M}_{AB} = \bar{s}k\theta_A$ and $\bar{M}_{BA} = \bar{s}\bar{c}k\theta_A$, k being based on the length l (i.e. $k = EI/l$). The moments at A and B (M_{AB} and M_{BA} respectively) may be derived from the standard stability functions s and c , as shown in Fig. 2.11(b). The appropriate value of ρ is based on the length l , i.e. $\rho = P/P_E$ where $P_E = \pi^2 EI/l^2$. Taking moments about \bar{A} for $\bar{A}A$, \bar{B} for $\bar{B}B$ and about \bar{A} for the whole member, the following three equations are obtained,

$$\bar{s}k\theta_A = sk\theta_A + s(1+c)k \frac{g_A \theta_A}{l} - Fg_A - Pg_A \theta_A, \quad (2.16)$$

$$\bar{s}\bar{c}k\theta_A = sc k\theta_A + s(1+c)k\frac{g_A\theta_A}{l} - Fg_B, \quad (2.17)$$

$$\bar{s}k\theta_A + \bar{s}\bar{c}k\theta_A = -F(l + g_A + g_B). \quad (2.18)$$

Eliminating F ,

$$\bar{s} = s + \frac{2g_A}{l} \left(1 + \frac{g_A}{l}\right) A, \quad (2.19)$$

$$\bar{s}\bar{c} = sc + s(1+c) \left[\frac{g_A}{l} + \frac{g_B}{l}\right] + 2\frac{g_A}{l} \frac{g_B}{l} A, \quad (2.20)$$

$$\bar{s}(1+\bar{c}) = \left[s(1+c) + \frac{2g_A}{l} A\right] \left[1 + \frac{g_A}{l} + \frac{g_B}{l}\right]. \quad (2.21)$$

where $A = s(1+c) - (\pi^2/2)\rho$. The quantity A may be regarded as a new function of ρ , and has been tabulated by Livesley and Chandler,⁽¹⁷⁾ to whom this treatment of gusset plates is due. Alternatively A may be calculated from the values of $s(1+c)$ given in Tables A.1 to A.5.

The modified sway functions \bar{m}_A and \bar{m}_B give the terminal moments $\bar{M}_{AB} = -\bar{m}_A Fl/2$ and $\bar{M}_{BA} = -\bar{m}_B Fl/2$ induced by a shear force F (Fig. 2.12(a)), and from Fig. 2.12(b),

$$\bar{M}_{AB} = -\bar{m}_A \frac{Fl}{2} = -m \frac{Fl}{2} - Fg_A,$$

$$\text{i.e.} \quad \bar{m}_A = m + \frac{2g_A}{l}. \quad (2.22)$$

$$\text{Similarly} \quad \bar{m}_B = m + \frac{2g_B}{l}. \quad (2.23)$$

The no-shear coefficients \bar{n}_A and \bar{o}_A (Fig. 2.13) define the terminal moments $\bar{M}_{AB} = \bar{n}_A k\theta_A$ and $\bar{M}_{BA} = -\bar{o}_A k\theta_A$ induced by a no-shear rotation θ_A at A .

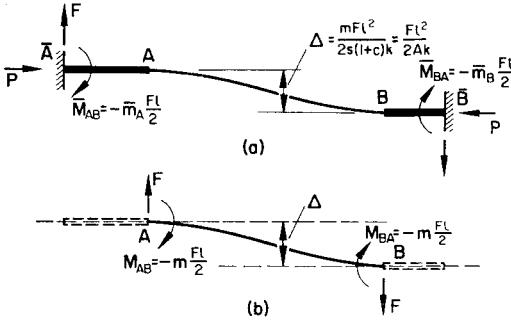


FIG. 2.12

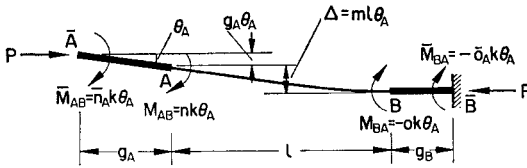


FIG. 2.13

Hence

$$\bar{M}_{AB} = \bar{n}_A k \theta_A = n k \theta_A - P g_A \theta_A,$$

$$\bar{M}_{BA} = -\bar{o}_A k \theta_A = -o k \theta_A.$$

Hence

$$\bar{n}_A = n - \pi^2 \rho \frac{g_A}{l}, \quad (2.24)$$

$$\bar{o}_A = o. \quad (2.25)$$

The total sway Δ is given by

$$\Delta = \frac{m}{2} l \theta_A + g_A \theta_A = \frac{\bar{m}_A}{2} l \theta_A. \quad (2.26)$$

Similarly, for a no-shear rotation θ_B at B,

$$\bar{M}_{BA} = \bar{n}_B k \theta_B \quad \text{and} \quad \bar{M}_{AB} = -\bar{o}_B k \theta_B$$

where

$$\bar{n}_B = n - \pi^2 \rho \frac{g_B}{l} \text{ and } \bar{o}_B = o.$$

A summary of modifications to stiffness functions to allow for gusset plates is given in Fig. 2.7.

2.13 Limitations on the Use of Stability Functions

In this chapter, attention has been confined to the elastic flexural behaviour of a prismatic member bending in one plane only. It is assumed that the centroid and the shear centre of any

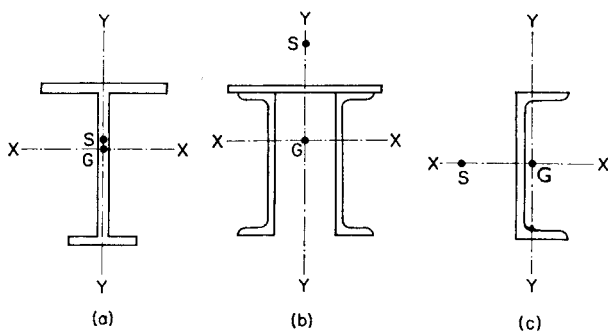


FIG. 2.14

cross-section both occur in that plane. This condition is satisfied for plane frames with loads acting in the plane of the frame only, the members all having axes of symmetry within that plane. Thus suppose each of the members with the successive cross-sections shown in Figs. 2.14(a), (b) and (c) has one principal axis YY in the plane of the frame containing the member. For flexure in the plane of the frame, bending will in each case take place about the other principal axis XX . The centroid of a cross-section is denoted by G , and the shear centre by S , these being almost coincident for the section in Fig. 2.14(a). The behaviour

of the members in Figs. 2.14(a) and (b) for bending about axis XX will be fully described in the elastic range by the functions derived in this chapter. The same cannot be said of the channel section in Fig. 2.14(c), since the shear centre S does not occur with the centroid G in the plane YY . The stability functions may only be applied to such a member if it is so constrained continuously along its length that twisting about the longitudinal axis is everywhere prevented.

It should also be noted that stability functions are only valid for small angles of slope relative to a straight line joining the ends of a member, i.e. for values of dy/dx small compared with unity. This means that they are inapplicable to a structure in which the deformations are of an order comparable with the dimensions of the structure.

2.14 Applications of Stability Functions

If it can be assumed that the axial loads in the members of a structure are known within sufficiently close limits without the necessity of performing a complete flexural analysis, the stability functions enable the setting up of a set of linear equations which express the equilibrium requirements in terms of the displacements and rotations of the joints. The analysis may then proceed exactly as for a structure in which the effects of axial loads or bending moments are neglected, and any of the standard methods of analysis may be applied. In particular, the methods of matrix analysis may be used, and the reader is referred to the treatment by Livesley.⁽¹⁹⁾ Matrix methods lead directly to computer solutions, and offer thereby an escape from the enormous labour encountered in the solution of stability problems by hand. While this procedure is attractive and will frequently be the ultimate goal, it is unwise to resort to it without first gaining some knowledge of the qualitative phenomena involved. The explanation of these phenomena is the main purpose of this volume. Chapter 3 describes the application of stability functions to triangulated frames, while Chapter 4 deals with non-triangulated frames. The

behaviour of frames beyond the elastic limit is discussed in Chapter 5.

Examples

2.1 The uniform member AB in Fig. 2.15 is subjected to an axial load P , terminal moments M_{AB} and M_{BA} and a shear force F . Show that

$$(a) \quad \theta_A - \frac{\Delta}{l} = \frac{M_{AB} - cM_{BA}}{s''k}$$

$$(b) \quad \theta_A = \frac{nM_{AB} + oM_{BA}}{(n^2 - o^2)k} + \frac{mFl}{2(n - o)k}$$

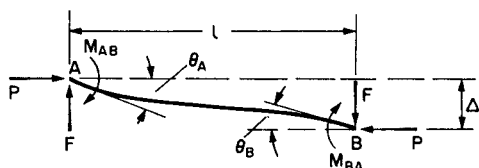


FIG. 2.15

2.2 The members AB , BC are rigidly joined at B , and sustain axial loads $P_{AB} = (\pi^2 k_{AB}/l_{AB})\rho_{AB}$ in AB and $P_{BC} = (\pi^2 k_{BC}/l_{BC})\rho_{BC}$ in BC . If the deformations indicated in Fig. 2.16 cause

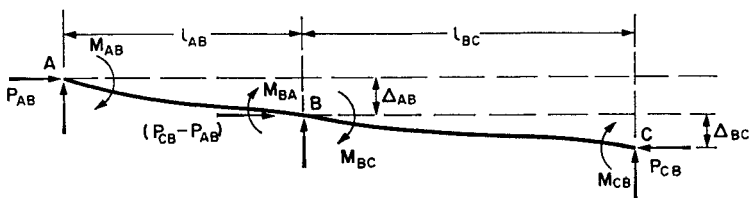


FIG. 2.16

moments at A , B and C as shown, show that these moments are related by the equation:

$$\frac{M_{BA} - c_{AB}M_{AB}}{s''_{AB}k_{AB}} - \frac{M_{BC} - c_{BC}M_{CB}}{s''_{BC}k_{BC}} + \frac{\Delta_{AB}}{l_{AB}} - \frac{\Delta_{BC}}{l_{BC}} = 0$$

[*Note.* This corresponds to the “four-moment equation” of Bleich. A possible method of analysing continuous frames is to apply this equation repeatedly to adjacent members, each application representing the satisfaction of the compatibility condition for the rotations of the members at the joint.

It may also be noted that transverse loads acting between joints may be allowed for by replacing the moments M_{AB} , M_{BA} , etc., by $(M_{AB} - M_{AB(F)})$, $(M_{BA} - M_{BA(F)})$, etc., where $M_{AB(F)}$, $M_{BA(F)}$, etc., are the appropriate fixed-end moments in the presence of the given axial loads.]

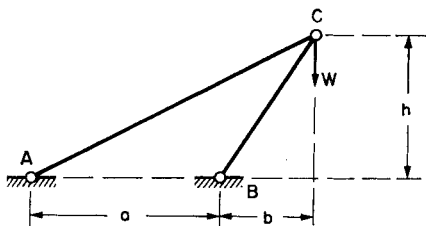


FIG. 2.17

2.3 The vertical load W (Fig. 2.17) is supported by the tie AC and the strut BC , both members being pin-ended. If failure occurs by the buckling of the strut BC , the dimensions a and b being fixed while h is undefined, show that W is a maximum when $h = b/\sqrt{2}$. If the flexural rigidity of BC is EI , show that the maximum value of W is

$$\frac{2\pi^2}{3\sqrt{3}} \frac{a}{(a+b)b^2} EI.$$

If $a = b = \sqrt{2}h$, and AC has the same flexural rigidity as BC , show that the effect of making joint C rigid is to increase the value of W at which buckling occurs by approximately 50 percent.

2.4 A uniform member AB , of length l and flexural rigidity $EI = kl$, carries an axial load P and is joined at A to members which provide a restraining moment of $q_A k \theta_A$ when A is rotated through θ_A . Show that the rotational stiffness at B is $q_B k$

where
$$\frac{q_B}{s} = 1 - \frac{c^2}{1 + (q_A/s)}$$

A uniform member of length $8l$ is fixed in direction at each end and is restrained against lateral movement at the ends and at intervals of l within its length. Use the above result to show that buckling occurs under an axial load P given by $c = \sqrt{(4 - 2\sqrt{2})}$ where c is the stability function corresponding to $\rho = Pl^2/\pi^2 EI$.

2.5 The end A of a member AB is held by another member which provides a restraining moment of $Q_A \theta_A$ when end A is rotated through an angle θ_A . Show that, in the presence of axial load, the “no-shear” rotational stiffness at end B , after allowing equilibrium to be established at A , is Q_B where

$$\frac{Q_B}{nk} = 1 - \frac{(o/n)^2}{1 + (Q_A/nk)}$$

A continuous vertical cantilever $ABCD$, where $AB = BC = CD = l$, is held rigidly at A and carries equal vertical loads W at B , C and D . The flexural rigidities are uniformly $3EI$ over AB , $2EI$ over BC and EI over CD . Show that buckling will occur when $o/n = \sqrt{(5/3)}$ where the stability functions n and o correspond to $\rho = Wl^2/\pi^2 EI$.

2.6 A pin-ended strut AD consists of a central section BC , of length $2l$, and flexural rigidity EI_1 , and two equal end sections AB and CD , each of length l_2 and flexural rigidity EI_2 . Show that buckling occurs under an axial load P given by

$$\left(\frac{o_2}{n_2}\right)^2 = 1 + \frac{n_1 k_1}{n_2 k_2}$$

where $k_1 = EI_1/l_1$, $k_2 = EI_2/l_2$ and stability functions o_1 , n_1 and o_2 , n_2 correspond to $\rho_1 = Pl_1^2/\pi^2 EI_1$ and $\rho_2 = Pl_2^2/\pi^2 EI_2$ respectively.

2.7 A pin-ended strut of constant cross-section is restrained at mid-height against lateral deflexion by a spring as shown in Fig. 2.18. If the spring stiffness is λ , i.e. $Q = \lambda\delta$, show that for λ small the critical load of the strut in the plane of the restraint is increased to

$$P_E \left\{ 1 + \frac{\lambda L^3}{48EI} \right\} \text{ approximately.}$$

(Manchester, Honours B.Sc. Tech., Part II 1956.)

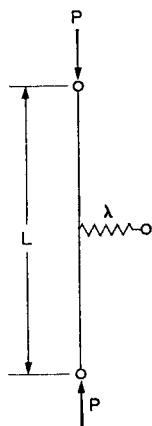


FIG. 2.18

(It may be assumed that the relation between stiffness and axial load for the strut with respect to a central disturbing force is very nearly linear.)

2.8 A composite strut consists of two portions AB and BC as in Fig. 2.19. The length of BC is λ times that of AB and the

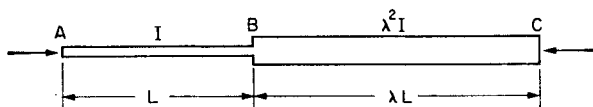


FIG. 2.19

moment of inertia of BC is λ^2 times that of AB . Show that if the composite strut is tested with pin ends at A and C its lowest critical load does not depend on λ and hence is equal to one-quarter of the Euler load of the portion AB .

(Manchester, Honours B.Sc. Tech., Part II 1958.)

Triangulated Frames

3.1 Introduction

The principles of structural analysis are the same for all frames, whether or not axial loads in members are sufficient to affect their stiffness, and amount to the simultaneous satisfaction of the conditions of equilibrium and compatibility. With the assistance of stability functions, analysis is straightforward provided the axial loads in the members are known, and for this reason structures in which axial loads are exactly or very nearly proportional to the applied loads are the most easily dealt with.

Pin-jointed, statically determinate frames present no problem, since axial loads are directly proportional to the applied loads. The inception of buckling is controlled by the readily ascertained critical members. For finite deformations after buckling, since a pin-ended Euler strut has finite stiffness with respect to axial compression (Fig. 1.9), the structure as a whole may become stable or unstable, depending on the particular geometry. This subject has been discussed by Britvec,⁽²⁰⁾ but is not of much practical significance since it concerns gross deformations which are not usually acceptable in practice. Redundant, pin-jointed, triangulated frames present greater difficulty. Initially, the axial load distribution is controlled by the ordinary elastic stiffness of the member, but after the inception of buckling, the stiffness of the compression members is modified to the value given by the slope of the curve HQ in Fig. 1.9 (cf. equation (1.11)). Since in any practical frame, the compression members will cease to behave elastically, certainly after the early stages of buckling if not before, problems involving the post-buckling behaviour of

such triangulated frames cannot be discussed at all usefully in terms of elastic theory.

Rigid-jointed-triangulated frames which would be statically determinate in the absence of the rigid joints (i.e. frames that are statically determinate in their primary stresses) are the most fruitful for discussion, both on account of their practical importance, and because of the light thereby shed on the phenomenon of "secondary stresses". To a close approximation, the axial loads in such a frame are proportional to the applied loads, but since the bending stiffnesses of the members will vary as these axial loads change, the entire pattern of secondary moments must depend on the load parameter. We illustrate this with a particular example.

Rigid-jointed triangulated frames which are redundant in their primary stresses form a special class as their axial force pattern depends on their axial stiffnesses which in turn depend on the amount of deflexion of the members. The class has certain similarities to laterally loaded portal frames discussed in Chapter 4, but will not be treated further in this book.

3.2 Secondary Stresses

Consider the frame shown in Fig. 3.1. AB and BC are prismatic members with constant flexural rigidity EI rigidly jointed at B and with fixed ends at A and C .

If there were pin-joints at A , B and C the frame would be statically determinate and all the load would be transferred from B to A and C by direct axial loads in the members. Owing to the rigidity of the joints at A , B and C some load can be transferred by bending of the members. Although this is usually an extremely small portion of the load it can cause important bending stresses. It is conventional to assume that this secondary transfer of load does not alter the axial forces in the members which can therefore be calculated for the frame with pin-joints at A , B and C .

Thus from the triangle of forces at B

$$P_{AB} = W/2 \text{ and } P_{BC} = \sqrt{3} \cdot W/2$$

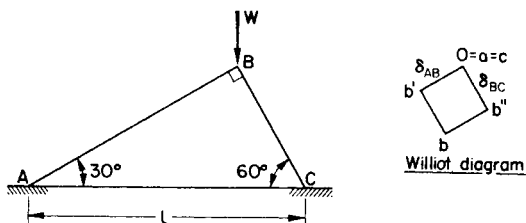


FIG. 3.1

The corresponding shortenings of AB and BC are

$$\delta_{AB} = \frac{\sqrt{3}}{4} \frac{Wl}{AE} = \delta \quad \text{and} \quad \delta_{BC} = \frac{\sqrt{3}}{4} \frac{Wl}{AE} = \delta$$

and the deflexion of B can be found as shown in the Williot diagram in Fig. 3.1. We imagine the frame moved to this position with the joint B prevented from rotating. This requires moments as shown in the table below. The moments due to an arbitrary rotation of B are also shown.

	A		B		C
Sway	$-\frac{4}{3} s_1(1 + c_1) \frac{EI\delta}{l^2}$		$+\frac{4}{3} s_1(1 + c_1) \frac{EI\delta}{l^2}$		$+\frac{4}{3} s_2(1 + c_2) \frac{EI\delta}{l^2}$
Rot B	$s_1 c_1 \frac{2EI}{\sqrt{3}l} \theta$	$s_1 \frac{2EI}{\sqrt{3}l} \theta$	$s_2 \frac{2EI}{l} \theta$	$s_2 c_2 \frac{2EI}{l} \theta$	

For equilibrium $M_{BA} + M_{BC} = 0$ and so

$$\frac{2EI}{l} \theta \left(\frac{s_1}{\sqrt{3}} + s_2 \right) = \frac{4EI\delta}{l^2} \left[\frac{s_1(1 + c_1)}{3} - s_2(1 + c_2) \right]$$

Substituting for δ ,

$$\left(\frac{s_1}{\sqrt{3}} + s_2 \right) \theta = \frac{\sqrt{3}}{2} \cdot \frac{W}{AE} \left[\frac{s_1(1 + c_1)}{3} - s_2(1 + c_2) \right]$$

Then

Graphs of θ/λ and $IM_{BC}/2EI\lambda$ against ρ_1 , are shown in Fig. 3.2 and also a graph of $M_{BC}/(M_{BC})_0$ where $(M_{BC})_0$ is the moment that would be obtained if there were no stability effects, i.e. $(M_{BC})_0$ varies linearly with ρ_1 , and is tangential to M_{BC} for small values of ρ_1 . The consequence of taking stability into account is that M_{BC} does not increase linearly with P and even changes sign as P increases. This is quite a normal consequence of stability and shows how little value a linear elastic analysis may have in predicting bending moments at high values of axial loads. M_{BC}

is zero at $\rho_1 = 2.26$; below this value BC is bending AB , above this value BC is restraining AB from bending and there is reversal of the sign of M_{BC} . θ , however, continues to increase steadily until a vertical asymptote at $s_1 + \sqrt{3} \cdot s_2 = 0$, i.e. ρ_1

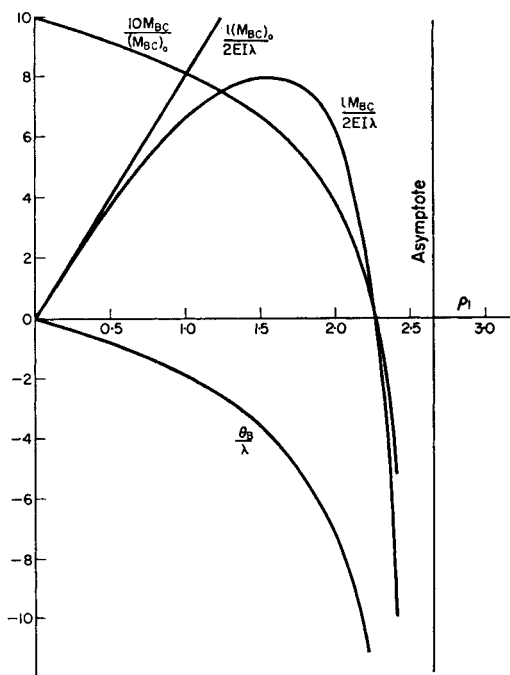


FIG. 3.2

$= 2.62$. Such a value of the load at which deflexions become very large is known as a "critical load". It corresponds to the "Euler load" for pin-ended struts.

For this type of frame it would usually be accepted without question for a linear elastic analysis that the axial forces are as given by simple resolution at B . This procedure neglects the shear forces in AB and BC by comparison with the axial forces. The shear forces are proportional to λW and for a normal value

of λ are less than 1 percent of W . This justifies this procedure for the linear elastic analysis. For the stability analysis the members become more flexible as W increases and this causes the effect to be even less significant.

3.3 Internal Stresses

The same example can be used to show the effects of stability on internal stresses due to lack of fit. Suppose that AB and BC are built in first at A and C and that on coming to make the joint at B it is discovered that there is an error in the angle of BC at B of ϕ . BC can be distorted to make the joint by applying a moment $(2EIs_2/l)\phi$ and on making the joint and releasing the restraint the joint will rotate through ψ , where

$$\frac{2EI}{\sqrt{3} \cdot l} (s_1 + \sqrt{3} \cdot s_2) \psi = \frac{2EI}{l} s_2 \phi$$

$$\text{Finally } M_{BA} = \frac{2EI}{\sqrt{3} \cdot l} s_1 \psi = \frac{2EI}{l} \frac{s_1 s_2}{s_1 + \sqrt{3} \cdot s_2} \phi$$

The moment at B due to lack of fit then also depends on the load and a graph of $lM_{BA}/2EI\phi$ against ρ_1 is shown in Fig. 3.3.

We note that, as in the case of secondary stresses, the sign of M_{BA} can change as the load increases and that the lack of fit moments have the same vertical asymptote as the secondary stress moments.

In linear elastic structures a change in moment due to a change in load can be calculated, but owing to the effects of lacks of fit this is from an unknown initial condition.

We have now demonstrated that when stability effects are taken into account then even changes of moment or deflexion cannot be calculated owing to the fact that the internal stresses and deflexions themselves change due to stability effects. In these circumstances the "critical loads" already mentioned remain the only invariant of the framework that can be calculated.

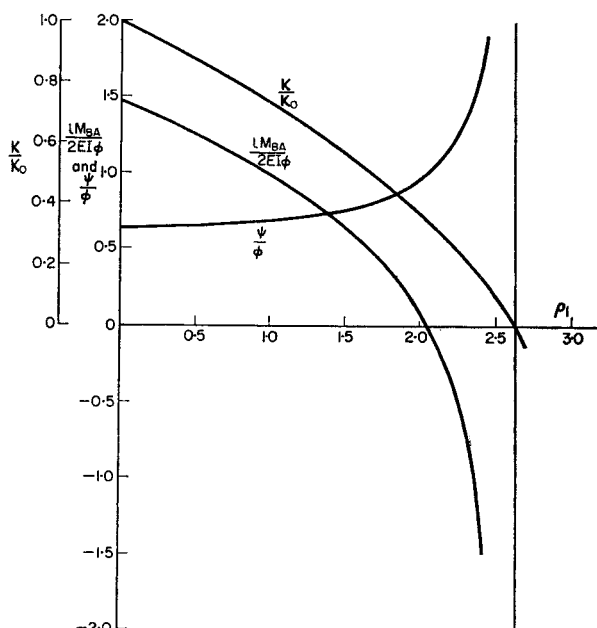


FIG. 3.3

3.4 Critical Loads

In Chapter 1 it was shown that for a pin-ended strut there is a series of critical loads $P_{C1}, P_{C2}, P_{C3}, \dots$, associated with a series of buckling modes y_1, y_2, y_3, \dots , such that for any initial distortion

$$y_0 = a_1 y_1 + a_2 y_2 + a_3 y_3 + \dots,$$

each component is magnified independently

$$\text{i.e.} \quad y = \frac{a_1 y_1}{1 - P/P_{C1}} + \frac{a_2 y_2}{1 - P/P_{C2}} + \frac{a_3 y_3}{1 - P/P_{C3}} + \dots$$

In the region of the first critical load the corresponding magnifier

$$\frac{1}{1 - P/P_{C1}}$$

dominates and we may write

$$y = \frac{a_1 y_1}{1 - P/P_{C1}} + b$$

which leads to the Southwell plot. It has been shown that similar results hold for complete frames^(21,22,23) where the axial loads are proportional to the load parameter and as an example we give in Fig. 3.4 the Southwell plots for the two cases we have

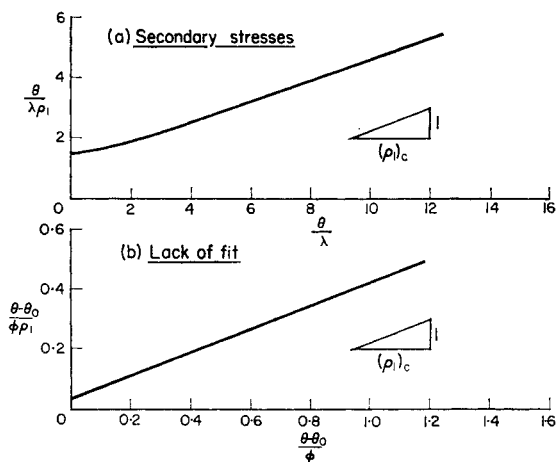


FIG. 3.4

calculated. The critical loads as given by the inverse slopes of the straight part of the graphs are both in good agreement with the calculated value of $\rho_1 = 2.62$.

The deflexions δ due to a disturbing force Q may also be thought of as arising from an initial imperfection

$$\frac{\delta_0}{Q} = a_1 y_1 + a_2 y_2 + a_3 y_3 + \dots$$

and
$$\frac{\delta}{Q} = \frac{a_1 y_1}{1 - P/P_{C1}} + \frac{a_2 y_2}{1 - P/P_{C2}} + \dots$$

The stiffness “ K ” corresponding to the disturbing force is defined by the equation $Q = K\delta$ where δ is the deflexion corresponding to Q .

Hence
$$\frac{1}{K} = \frac{b_1}{1 - P/P_{C1}} + \frac{b_2}{1 - P/P_{C2}} + \dots$$

A plot of K/K_0 , where K_0 is the value of K when $P = 0$, against the load parameter P provides a good technique for determining the critical load. Providing the disturbing force excites any component of the first buckling mode K , vanishes at $P = P_{C1}$. A linear plot is obtained if $0 = b_2 = b_3 = \dots$ and in general the best predictions are obtained by using disturbing forces which excite as large a component as possible of the first buckling mode. For our example let us use as disturbing force a moment M at B . The corresponding rotation is given by

$$M = \frac{2EI}{\sqrt{3} \cdot l} (s_1 + \sqrt{3} \cdot s_2) \theta$$

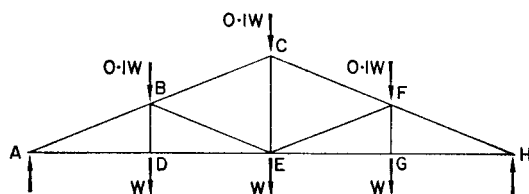
Hence
$$K = \frac{2EI}{\sqrt{3} \cdot l} (s_1 + \sqrt{3} \cdot s_2)$$

$$\frac{K}{K_0} = \frac{s_1 + \sqrt{3} \cdot s_2}{4(1 + \sqrt{3})}$$

A graph of K/K_0 against ρ_1 is also given in Fig. 3.3. As is to be expected it agrees with the previous determinations of the critical load. Note that the critical load $\rho_1 = 2.62$ is greater than for a strut fixed at A and pinned at B ($\rho_1 = 2.045$) because of the restraint afforded by BC . At the critical load all deflexions are indeterminate; and it is wrong to think of just one member buckling since the phenomenon involves the whole frame.

3.5 Critical Loads—Example

Consider the symmetrical truss shown in Fig. 3.5 with member properties as shown in the table below the figure. $P_E = \pi^2 EI/L^2 = \pi^2 k/L$ and is therefore an alternative way of specifying the



Member	P/W	$L(\text{in})$	$P_E(\text{ton})$	$P/P_E W$	
AB	4.443	129.2	38.88	0.114	Strut
BC	2.962	129.2	20.81	0.142	Strut
AD	4.125	120	16.96	0.243	Tie
DE	4.125	120	16.96	0.243	Tie
BD	1000	48	1.51	0.662	Tie
BE	1.481	129.2	7.98	0.185	Strut
CE	2.100	96	3.50	0.600	Tie

FIG. 3.5

stiffness of a member. The example is one treated by Allen⁽²⁴⁾ and the problem is to determine the value of W at the first critical load. For any member say BC

$$\begin{aligned}
 M_{BC} &= sk\theta_B + sck\theta_C \\
 &= \frac{sLP_E}{\pi^2} (\theta_B + c\theta_C)
 \end{aligned}$$

For a particular value of W we know the value of $\rho = P/P_E$ for each member and hence the corresponding values of s and c . For example at $W = 9$ we have

Member	LP_E/π^2	P/P_E	s	c	sLP_E/π^2	$scLP_E/\pi^2$	
AB	510	1.03	2.41	1.03	1230	1270	Strut
AD	206	2.19	6.31	0.25	1300	325	Tie

Therefore

$$M_{AB} = 1230\theta_A + 1270\theta_B$$

$$M_{AD} = 1300\theta_A + 325\theta_D$$

$$M_A = M_{AB} + M_{AD} = 2530\theta_A + 325\theta_D + 1270\theta_B$$

and for the complete truss we have

	θ_A	θ_D	θ_B	θ_E	θ_C	θ_F	θ_G	θ_H
$M_A =$	2534	325	1267	0	0	0	0	0
$M_D =$	325	2670	10	325	0	0	0	0
$M_B =$	1267	10	1936	320	729	0	0	0
$M_E =$	0	325	320	3121	47	320	325	0
$M_C =$	0	0	729	47	1348	729	0	0
$M_F =$	0	0	0	320	729	1936	10	1267
$M_G =$	0	0	0	325	0	10	2670	325
$M_H =$	0	0	0	0	0	1267	325	2534

(3.3)

Note the reciprocal check on the coefficients. The demonstration calculation is done with slide rule accuracy. The slightly different values in the complete table are taken from Allen's paper where more significant figures are carried. Allen uses the notation $U = skV = sck$. The table contains all the possible information about the response of the truss to disturbing moments at the joints. How one proceeds is a matter of choice. Livesley and Chandler⁽¹⁷⁾ for a truss of the same general shape but different member details use the stiffness approach and solve by relaxation⁽²⁵⁾ for θ_B with $M_B = M_F$ and all other moments zero. Then $M_B = K\theta_B$ and a plot of the stiffness K determines the critical load by the value of W for which $K = 0$.

Allen solves by successive elimination of the unknowns from each end with all moments zero except M_E and M_C until he obtains the equations

$$\begin{aligned}M_E &= 2864\theta_E - 336\theta_C \\M_C &= -336\theta_E + 526\theta_C\end{aligned}$$

The behaviour of the truss can thus be considered as that of an equivalent member EC satisfying the above equations. In Allen's notation

$$\begin{aligned}M_E &= U_{EC}\theta_E + V_{EC}\theta_C \\M_C &= V_{CE}\theta_E + U_{CE}\theta_C\end{aligned}$$

He now puts M_C equal to zero and obtains

$$M_E = \left(U_{EC} - \frac{V_{EC}V_{CE}}{U_{CE}} \right) \theta_E$$

He states that the truss is stable if the expression in the brackets is positive, the critical load being given by the vanishing of the expression. In our notation $M_E = K\theta_E$ and thus Allen's method is in effect the stiffness method. He performs the successive elimination of the unknowns on a picture of the truss rather than by the more usual algebraic methods.

To retain all the available information about the truss we will give here the complete solution of the equations (3.3). It was obtained using a digital computer but may be obtained by desk calculations. It is

$10^6\theta$	M_A	M_D	M_B	M_E	M_C	M_F	M_G	M_H
$\theta_A =$	796	-109	-776	125	623	-384	-38	197
$\theta_D =$	-109	395	117	-60	-100	72	12	-38
$\theta_B =$	-776	117	1522	-234	-1220	749	72	-384
$\theta_E =$	125	-60	-234	377	240	-234	-60	125
$\theta_C =$	623	-100	-1200	240	2052	-1220	-100	623
$\theta_F =$	384	72	749	-234	-1220	1522	117	-776
$\theta_G =$	-38	12	72	-60	-100	117	395	-109
$\theta_H =$	197	-38	-384	125	623	-776	-109	796

Similar calculations were performed for $W = 0, 3$ and 10 . These enable the stiffness curves shown in Fig. 3.6 to be drawn. Thus for $W = 9$ and all disturbing moments zero except M_B we have $\theta_B = 1522M_B$ and similar information is available for the other values of W .

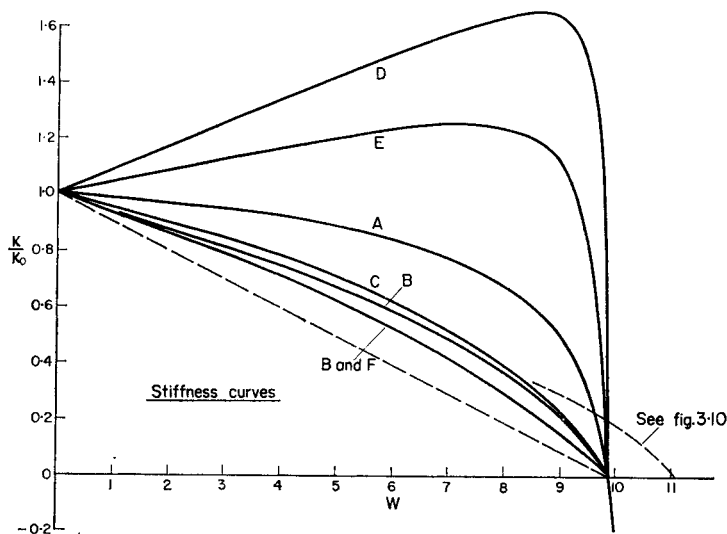


FIG. 3.6

Figure 3.6 illustrates several of the important effects of stability. Notice that the initial slopes of the stiffness curves depend on the type of members intersecting at the joints concerned. Thus for D which is at the intersection of three ties increase of W causes an increase of stiffness. A similar although less marked effect is shown for E which is at the intersection of three ties and two struts and initially the gain in stiffness of the ties is greater than the loss in stiffness of the struts. Joint A is at the intersection of a tie and a strut and initially exhibits little change in stiffness with load. Despite the initial increase in stiffness for D and E all the

curves pass through zero at the critical load which is seen to be given by $W = 9.9$. The buckling of the truss is not then a local phenomenon but all the joints suffer large rotations and the truss as a whole distorts. It is of interest to note that if W could assume negative values there would also be a corresponding critical load on the other side of the origin.

If, as in the Southwell method, we can write

$$\frac{1}{K} = \frac{b_1}{1 - P/P_{C1}} + b_2 \text{ then}$$

$$\left[\frac{K}{K_0} - (1 + \lambda) \right] \left[\frac{P}{P_{C1}} - (1 + \lambda) \right] = \lambda (1 + \lambda)$$

where

$$\lambda = \frac{b_1}{b_2}$$

i.e. the stiffness curves should be rectangular hyperbolae passing through $P = P_{C1}$ at $K = 0$ and having $P/P_{C1} = 1 + \lambda$ as an asymptote. The nearness of the asymptote to $P/P_{C1} = 1$ for the stiffness curves for joints D and E indicate that for these joints $b_2 \gg b_1$ and consequently the effect of the amplification factor $1/(1 - P/P_{C1})$ is swamped for small values of P and these stiffness curves are far from rectangular hyperbolae.

3.6 Combination of Disturbances

At the critical load the truss as a whole distorts and all the joints exhibit large rotations. To excite such a shape for $W = 0$ will require disturbances distributed along the members but it is of interest to investigate how nearly the buckling shape can be excited by disturbing moments applied only at the joints. From Fig. 3.6 it is obvious that the most important disturbing moments are those at B , F and C . From symmetry we would expect the buckling mode to have $\theta_B = \theta_F$ and therefore as a first step

we will investigate the case of all joint moments zero except $M_B = M_F$. Then at $W = 9$

$$10^6 \theta_B = 1522M_B + 749M_F = 2271M_B$$

and as before we can plot K/K_0 for the composite disturbance. This curve is more nearly linear than those for any of the separate joints and is also shown in Fig. 3.6.

Let us now incorporate a disturbing moment $M_C = \lambda M_B = \lambda M_F$. Then at $W = 9$ we have

$$\begin{aligned} 10^6 \theta_B &= 2271M_B - 1220M_C = (2271 - 1220\lambda)M_B \\ 10^6 \theta_C &= -2440M_B + 2052M_C = (-2440 + 2052\lambda)M_B \end{aligned}$$

The work done in applying these disturbing moments

$$\begin{aligned} &= \Sigma \frac{1}{2} M\theta = M_B\theta_B + \frac{1}{2} M_C\theta_C \\ &= 10^{-6} M_B^2 (2271 - 2440\lambda + 1026\lambda^2) \end{aligned}$$

The disturbing moments are defined by the parameter M_B . If we define a corresponding deflexion \mathbb{H} by the requirement that the work done is the same

$$\text{i.e.} \quad \frac{1}{2} M_B \mathbb{H} = \Sigma \frac{1}{2} M\theta$$

$$\text{Then} \quad \frac{1}{2} M_B \mathbb{H} = 10^{-6} M_B^2 (2271 - 2440\lambda + 1026\lambda^2)$$

The stiffness K to the composite disturbance may then be considered as given by $M_B = K\mathbb{H}$ and thus at $W = 9$ we have

$$K = 10^6 (4542 - 4880\lambda + 2052\lambda^2)^{-1}$$

A similar calculation at $W = 0$ gives

$$K_0 = 10^6 (690 - 320\lambda + 469\lambda^2)^{-1}$$

and thus at $W = 9$

$$\frac{K}{K_0} = \frac{690 - 320\lambda + 469\lambda^2}{4542 - 4880\lambda + 2026\lambda^2}$$

For $\lambda = 0$ this agrees with our previous result for $M_B = M_F$ and $M_C = 0$. For large values of λ , K/K_0 approaches the value we have calculated for M_C acting by itself as shown in Fig. 3.6. A graph of K/K_0 against λ is shown in Fig. 3.7. The minimum value is given by λ approximately equal to -0.8 and then

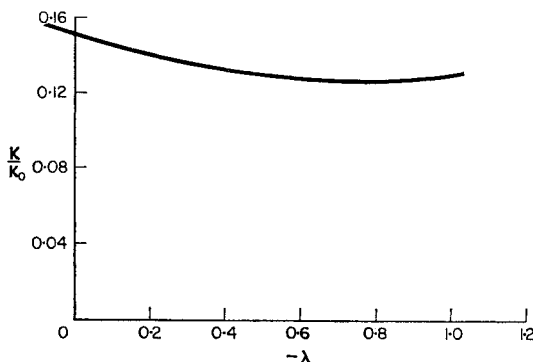


FIG. 3.7

$K/K_0 = 0.127$. For $M_C = 0$ and $M_B = M_F$ we had $K/K_0 = 0.152$. As was to be expected we have obtained a lower stiffness and more nearly excited the buckling mode by including a disturbing moment at C .

To obtain a still lower value of K/K_0 we must use disturbing moments at more joints. Figure 3.8 shows the relative rotations of the joints in terms of θ_B for all moments zero except M_B and Fig. 3.9 shows a sketch of the corresponding buckling shape. The buckling shape at $W = 9.9$ is defined by approximately

$$\theta_A = \theta_H = -0.54 \theta_B$$

$$\theta_D = \theta_G = 0.09 \theta_B$$

$$\theta_F = \theta_B$$

$$\theta_E = -0.23 \theta_B$$

$$\theta_C = -1.30 \theta_B$$

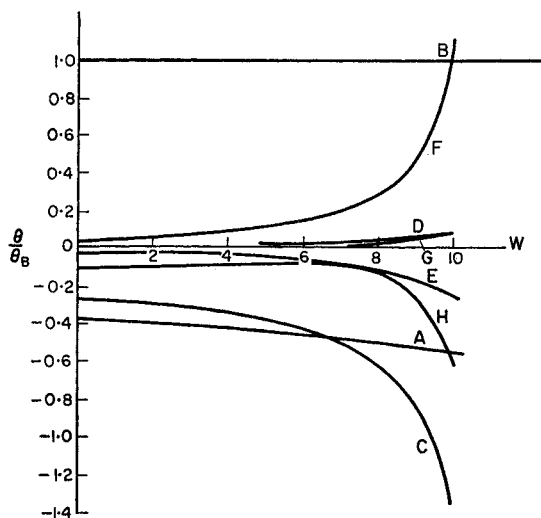


FIG. 3.8

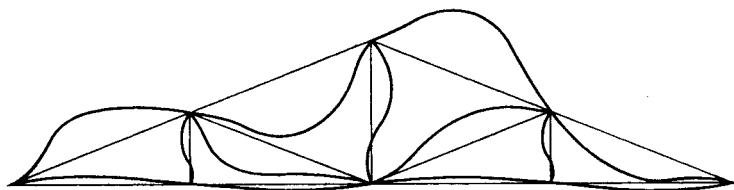


FIG. 3.9

The small values obtained for θ_D and θ_E confirm what we have already deduced from Fig. 3.6 that the rotations of these joints have the smallest components in the buckling mode. Notice that, though we are using an unsymmetrical disturbing moment system, the buckling mode itself exhibits symmetry as is to be expected. The same buckling mode is excited whatever disturbing moment is applied.

We can evaluate the moment pattern corresponding to these values of θ at $W = 0$. It is

$$M_A = M_H = -481 (\theta_B)_0$$

$$M_D = M_G = -151 (\theta_B)_0$$

$$M_B = M_F = 2266 (\theta_B)_0$$

$$M_E = -198 (\theta_B)_0$$

$$M_C = -1936 (\theta_B)_0$$

At $W = 9$ we obtain for this pattern of moments

$$\theta_A = \theta_H = -4.311 (\theta_B)_0 = -0.540 \theta_B$$

$$\theta_D = \theta_G = 0.642 (\theta_B)_0 = 0.081 \theta_B$$

$$\theta_B = \theta_F = 7.975 (\theta_B)_0 = 1.00 \theta_B$$

$$\theta_E = -1.702 (\theta_B)_0 = -0.214 \theta_B$$

$$\theta_C = -10.105 (\theta_B)_0 = -1.27 \theta_B$$

Notice the very small changes in the θ/θ_B ratios. These small changes are due to our assumed rotation pattern at $W = 0$ being only a near approximation to the buckling shape. Treating the complete pattern of moments as a composite disturbance in exactly the same way as we did for M_B , M_F and M_C acting together we obtain $K/K_0 = 0.125$. The same result is also obtained by comparing directly the ratios of θ_A and θ_B at $W = 0$ and 9 as in these cases there is no correction due to the small changes in the rotation pattern.

We have now shown that if we use a disturbing moment pattern which excites the buckling mode at $W = 0$ then this pattern is preserved as W increases. Further the lowest value of K/K_0 that can be obtained by any combination of disturbing moments at the joints is 0.125 at $W = 9$ and this is very little less than can be obtained by applying disturbing moments at B , F and C only. If we had been able to excite the buckling mode exactly by disturbing moments at the joints we would have expected a linear fall off in stiffness with W . As the critical value of W is 9.9 a linear variation in stiffness would give a value of $K/K_0 = 0.100$ at $W = 9.0$.

The difference between this value and the minimum value of K/K_0 that we have obtained must be attributed to the fact that we have not applied disturbing forces along the length of the members but only at the joints.

3.7 Approximate Methods of Calculation of Critical Loads

The reason for seeking approximate methods of calculation is to reduce the time taken in the solution of sets of equations such as equations (3.3). Approximate methods may be divided into two classes:

- (a) those that deal with the whole structure, and
- (b) those that deal with a simplified structure.

In class (a) there are various methods of fitting an equation to the stiffness curve from calculations at specific values. From a knowledge of similar structures one can form an estimate of P/P_E in the most heavily loaded member at collapse (in our case $(P/P_E)_{BE} = 1.83$). Two calculations in this region should allow of linear interpolation, i.e. in our example the calculations at $W = 9$ and $W = 10$.

Calculations for several values of the load parameter permit of the fitting of a rectangular hyperbola to the stiffness curve. Inspection of Fig. 3.6 shows that this is not likely to be successful for such joints as *D* and *E* where the rectangular hyperbola dominated by the critical load only prevails in the near region of the critical load.

Unless special measures are taken, relaxation type solutions do not usually converge in the negative stiffness region. The expansion $(1 - x)^{-1} = 1 + x + x^2 + x^3 + \dots$ is only valid for $x < 1$ although $(1 - x)^{-1}$ exists and is negative for greater values of x . Relaxation solutions can be considered as calculating by a series expansion. For this reason Hoff⁽²⁶⁾ uses convergence of the calculations as a test for stability and this method has been elaborated by Bolton.⁽²⁷⁾

Method (b) using a simplified structure is a more practical one. Our investigations of combined disturbances show that disturbances at joints some distance from B do not have much effect on the response at B . We shall therefore assume that the response at B can be obtained by assuming that all the members one remove from B have no change of slope at the far end when calculating the response at B . The simplified structure thus obtained is shown in Fig. 3.10 and the resulting equations for $W = 9$ are shown below.

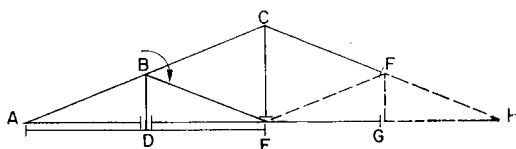


FIG. 3.10

	θ_A	θ_D	θ_B	θ_E	θ_C
$M_A = 0 =$	2534	0	1267	0	0
$M_D = 0 =$	0	2670	10	0	0
$M_B =$	1267	10	1936	320	729
$M_E = 0 =$	0	0	320	3121	0
$M_C = 0 =$	0	0	729	0	1348

(3.4)

The equation for M_A gives θ_A in terms of θ_B and similarly for M_D , M_E and M_C . Substituting in the equation for M_B we obtain $M_B = 876\theta_B$. The estimate of K obtained this way is therefore 876. The accurate value obtained by inversion of the equations (3.3) is $M_B = 658\theta_B$. Part of the $(K/K_0, W)$ relation for the simplified structure is also shown on Fig. 3.6. It corresponds to an approximate estimate of the critical value of $W = 11$ instead of the accurate value of $W = 9.9$. The advantage of this approximate method is that no formal solution of a system of simultaneous equations is required. A better approximation would be obtained by restricting the problem to the five equations (3.4) but filling in the missing coefficients and thus requiring the formal solution

of five simultaneous equations instead of the complete set. This would correspond to putting $\theta_F = \theta_G = \theta_H = 0$ in the real structure and thus introducing restraints at these points. It would therefore still give an over-estimate of the critical load.

3.8 Effect of Rigid Gussets

In Chapter 2 we have shown how the stiffness s and carry-over factor c are modified by the presence of rigid gussets to \bar{s} and \bar{c} and have shown how to calculate these modified values. Therefore there is no difficulty in principle in determining the critical load of a truss with gusset plates, but the calculations are

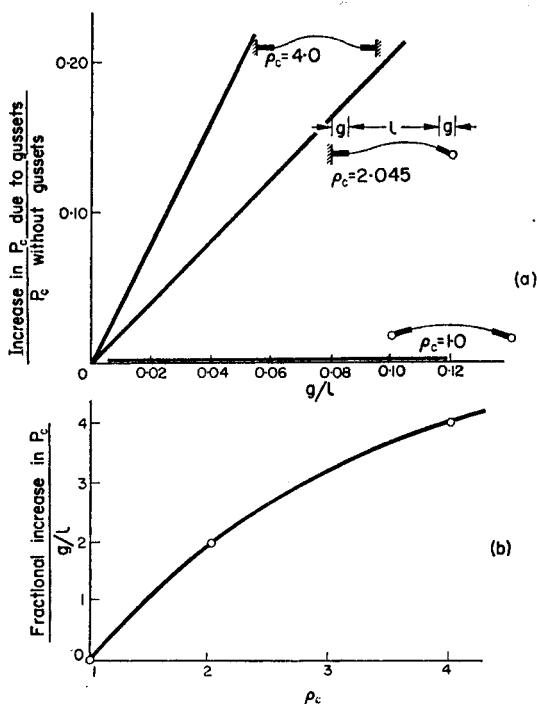


FIG. 3.11

rather longer than if there were no gusset plates. It is therefore useful to have an idea of the extent to which critical loads are likely to be increased by gusset plates and this can be obtained by reference to three simple cases for an isolated member. In Fig. 3.11 the critical load of a member with symmetrical gusset plates at either end is compared with the critical load of a prismatic member of the same overall length. There is almost no difference between the two cases for the pin-ended strut. This is because the gussets are in the region of low bending moment and thus have little effect on the stiffness. The other two cases give an almost linear increase due to g/l in the range considered. Plotting the rate of increase divided by g/l against the critical load for the three cases shown we obtain the relationship shown in Fig. 3.11(b). In default of complete calculations it is suggested that this graph can be used to estimate the increase in critical loads due to gusset plates.

Examples

3.1 Find the lowest critical load of the structure shown in Fig. 3.12 for the three cases given below. The members are straight

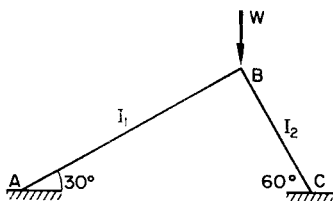


FIG. 3.12

and of constant cross-section, their moments of inertia being shown on the figure. A and C are fixed ends and B is a rigid joint.

Case I I_2 is small compared with I_1 ,

Case II $I_1 = \sqrt{3} I_2$,

Case III I_1 is small compared with I_2 .

(Manchester, Honours B.Sc. Tech., Part II 1953.)

3.2 An equilateral rigid-jointed triangular plane framework is tested in the arrangement shown in Fig. 3.13. The loads are applied through pins at A , B and C . Indicate how the critical

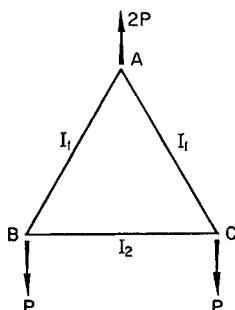


FIG. 3.13

load of the frame can be obtained and sketch the buckling mode. Determine limits for the critical value of P compared with the Euler Load of the strut BC .

(Manchester, Honours B.Sc. Tech., Part II 1955.)

3.3 The rigid-jointed Warren girder shown in Fig. 3.14 is subjected to a compression along the bottom chord. All the triangles are equilateral and all the members are of the same cross-section.

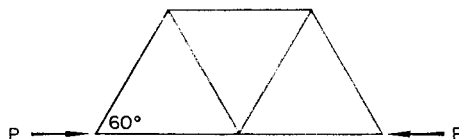


FIG. 3.14

Determine the stiffness of the central joint against rotation when the compressive load is equal to the Euler load of an individual member. (At $P = P_E$, $s = 2.467$, $c = 1.0$.)

(Manchester, Honours B.Sc. Tech., Part II 1959.)

3.4 The cantilever bracket (Fig. 3.15) is made from a uniform prismatic member. It is encastered at A and C and rigidly jointed at B . Show that if buckling out of the plane of ABC is

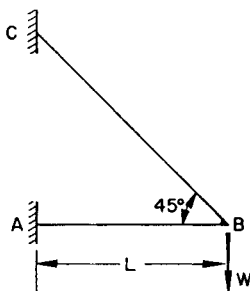


FIG. 3.15

prevented and plasticity effects are negligible, then the rotation of B is given by

$$\frac{W}{AE} \cdot \frac{s_1(1 + c_1)(1 + 2\sqrt{2}) + s_2(1 + c_2) \left(\frac{1 + \sqrt{2}}{\sqrt{2}} \right)}{s_1 + \frac{s_2}{\sqrt{2}}}$$

where s_1 and c_1 are the stiffness and carry-over factors for AB , and s_2 and c_2 are the stiffness and carry-over factors for BC . Hence determine the critical value of W .

(Manchester, Honours B.Sc. Tech., Part II 1963).

(Answers to the above questions may be found on page 154).

Rigid-Jointed Frames

4.1 Introduction

In a triangulated frame, any set of loads, provided all loads act at joints, could be supported in equilibrium by a system of internal forces acting as axial loads in the members without any bending action. Non-triangulated frames will support certain load systems also in this way, but only if the load systems are suitable. Examples are given in Fig. 4.1. The behaviour of frames so loaded is similar to that of triangulated frames statically determinate in their primary stresses, buckling modes being theoretically possible at a series of critical loads. The essential difference from triangulated structures is the incidence of sway modes involving the translation of one end of a member relative to the other (Fig. 2.1 (e)). The calculation of critical loads of this type is the first subject dealt with in this chapter. Just as for a pin-ended strut, deformations due to imperfections or disturbing forces are magnified as the first critical load is approached.

Suppose that, in a frame subjected to proportional loading, the elastic critical deflexion modes are represented by y_1, y_2, \dots with critical load factors $\lambda_{C1}, \lambda_{C2}, \dots$. Let the deformations y_0 due to initial imperfections or disturbing forces, measured at zero axial load level ($\lambda = 0$) be expressed in terms of the elastic critical modes, viz.

$$y_0 = a_1 y_1 + a_2 y_2 + \dots$$

where a_1, a_2, \dots are constants. Then it has been shown^(21,22,23) that, in the range of small deflexions, and provided the structure

is such that axial loads increase in proportion to the external load parameter, the deflexions at any load factor λ become

$$y = \frac{a_1 y_1}{1 - \frac{\lambda}{\lambda_{C1}}} + \frac{a_2 y_2}{1 - \frac{\lambda}{\lambda_{C1}}} + \dots$$

While, therefore, no distinct bifurcation of equilibrium states occurs at the lowest critical load factor λ_{C1} , and the structure is

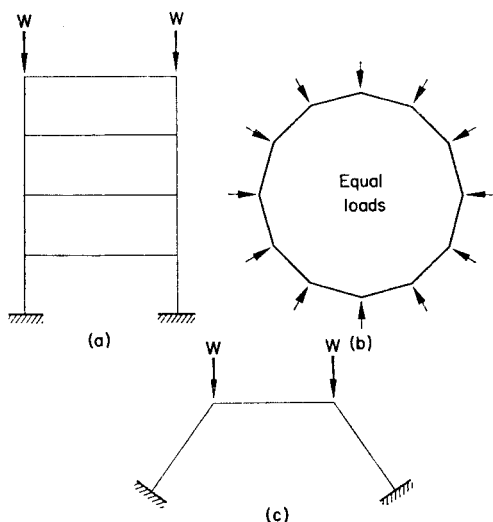


FIG. 4.1

stable at all loads $\lambda < \lambda_{C1}$, the lowest critical load factor is important since the deflexions increase more and more rapidly as it is approached.

A frame which sustains the applied loads entirely in axial compression or tension is structurally the most efficient, but it is not possible so to support any arbitrary combination of joint loads acting on a rigid frame, and bending is necessarily involved.

Examples of joint loads producing bending action are shown in Fig. 4.2. Further, any structure (either triangulated or rigid frame) which carries transverse loads within the length of any member (Fig. 4.3) must contain primary bending moments. In this class of problem, the critical load concept has no direct significance, since as the load parameter increases, the relative

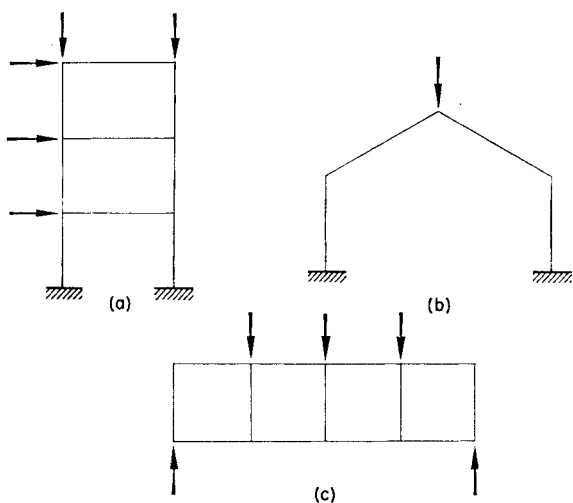


FIG. 4.2

bending stiffnesses of the members alter, and therefore the bending moment pattern, and hence in turn the axial load pattern, also alter. The axial loads do not increase in proportion with the load parameter, and the ideas of analysing an initial deflexion in terms of the buckling modes and each component being magnified by its own factor are no longer applicable. Nevertheless, such structures may become unstable in that at a particular value of the load parameter they may cease to have any stiffness to a disturbing force, for small deflexion theory, and thus exhibit large deflexions. It is proposed to call such loads buckling loads

and to reserve the name "critical loads" for the phenomena exhibited by structures of the types shown in Fig. 4.1.

Buckling loads are more difficult to calculate than critical loads as there is an interdependence between bending moments and axial loads which requires an iterative method of calculation to

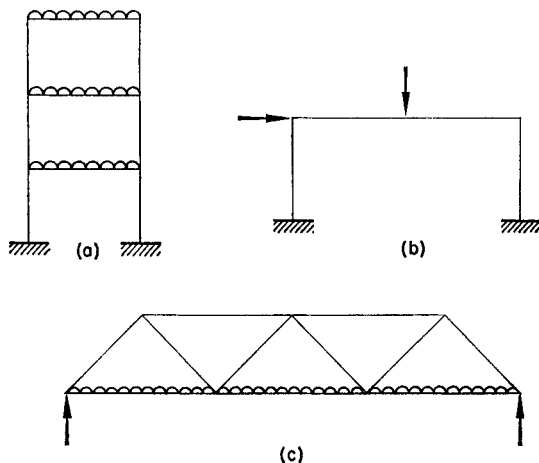
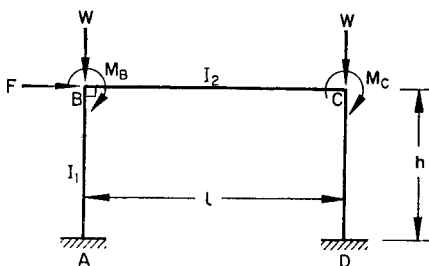


FIG. 4.3

be used. Furthermore ideas of the Southwell plot and about the shape of stiffness curves to which we have become accustomed require modification. A simple example of buckling loads of this type is discussed later in the chapter, but attention is first given to frames loaded after the manner of those in Fig. 4.1.

4.2 Simple Portal

Consider the simple portal shown in Fig. 4.4 where all the loads are applied at the joints and M_B , M_C and F are small disturbing forces. If there are no inaccuracies in manufacture, etc., there will be no bending moments in the members and no axial force in



$$k_1 = \frac{I_1}{h}$$

$$k_2 = \frac{I_2}{l}$$

FIG. 4.4

BC. The operations table for rotations of *B* and *C* and a sway is

	<i>A</i>	<i>B</i>	<i>C</i>	<i>D</i>	<i>FI</i>		
Rot. <i>B</i>	$csk_1\theta_B$	$sk_1\theta_B$	$4k_2\theta_B$	$2k_2\theta_C$	0	0	$-s(1+c)k_1\theta_B$
Rot. <i>C</i>	0	0	$2k_2\theta_C$	$4k_2\theta_C$	$sk_1\theta_C$	$csk_1\theta_C$	$-s(1+c)k_1\theta_C$
Sway	$-s(1+c)k_1\frac{\delta}{h}$	0	0	$-s(1+c)k_1\frac{\delta}{h}$	$-s(1+c)k_1\frac{\delta}{h}$	$\frac{4s(1+c)k_1}{m}\frac{\delta}{h}$	
	$-s(1+c)k_1\frac{\delta}{h}$			$-s(1+c)k_1\frac{\delta}{h}$			

and the equations of equilibrium are therefore

$$\left. \begin{aligned} M_B &= (sk_1 + 4k_2)\theta_B + 2k_2\theta_C - s(1+c)k_1\frac{\delta}{h} \\ M_C &= 2k_2\theta_B + (sk_1 + 4k_2)\theta_C - s(1+c)k_1\frac{\delta}{h} \\ FI &= -s(1+c)k_1\theta_B - s(1+c)k_1\theta_C + \frac{4s(1+c)}{m}k_1\frac{\delta}{h} \end{aligned} \right\} \quad (4.1)$$

provided M_B , M_C and F are such small disturbing forces that they do not sensibly change the value of P/P_E in the members.

These equations (4.1) correspond to the similar equations we found for triangulated frames except that for trusses only joint equations are required and here we have two joint equations and a shear equation.

As for trusses we could determine and draw the stiffness curves for the response to the individual disturbing forces. We should expect all these curves to pass through zero at the lowest critical load. Because of the symmetry of the structure and loading it is more convenient here to use composite disturbances.

Thus a particular solution of equations (4.1) is given by $\theta_C = -\theta_B$, $\delta = 0$ if

$$\begin{aligned}M_B &= (sk_1 + 2k_2) \theta_B \\M_C &= -(sk_1 + 2k_2) \theta_B \\FI &= 0\end{aligned}$$

which we can write as $M = K\theta$

where

$$K = sk_1 + 2k_2$$

and

$$\frac{K}{K_0} = \frac{s + \frac{2k_2}{k_1}}{4 + 2\frac{k_2}{k_1}}$$

Another solution of equations (4.1) is

$$\theta_B = \theta_C, \quad \frac{\delta}{h} = \frac{m}{2} \theta_B$$

if
$$M_C = M_B = (sk_1 + 6k_2)\theta_B - \frac{m}{2}s(1+c)k_1\theta_B$$

$$FI = 0$$

or in the notation of Chapter 2

$$M_C = M_B = (nk_1 + 6k_2) \theta_B$$

i.e. $M = K\theta$

where $K = nk_1 + 6k_2$

and
$$\frac{K}{K_0} = \frac{n + \frac{6k_2}{k_1}}{1 + \frac{6k_2}{k_1}}$$

A third solution of equations (4.1) is given by

$$\theta_B = \theta_C = \frac{s(1+c)}{s+6k_2/k_1} \frac{\delta}{h}$$

where $M_B = M_C = 0$

and
$$Fl = 2s(1+c)k_1 \frac{\delta}{h} \left[\frac{2}{m} - \frac{s(1+c)}{s+6k_2/k_1} \right]$$

i.e. $Fl = K \frac{\delta}{h}$

where
$$K = 2s(1+c)k_1 \left[\frac{2}{m} - \frac{s(1+c)}{s+6k_2/k_1} \right]$$

and
$$\frac{K}{K_0} = \frac{s(1+c) \left[\frac{2}{m} - \frac{s(1+c)}{s+6k_2/k_1} \right]}{6 \left[2 - \frac{6}{4+6k_2/k_1} \right]}$$

Graphs of these three non-dimensional stiffness curves are shown in Fig. 4.5 for $k_2/k_1 = 1.0$.

They seem normal stiffness curves, the first indicates a critical load at $P_C/P_E = 2.56$ and the other two at $P_C/P_E = 0.76$.

We stated that the stiffness curve for any composite disturbance should pass through zero at the lowest critical load and it is important to understand how the symmetrical system of disturbing moments has failed to indicate the lower of the critical loads.

In Chapter 3 we gave a general expression for the stiffness curves in the form

$$\frac{1}{K} = \frac{b_1}{1 - P/P_{C1}} + \frac{b_2}{1 - P/P_{C2}} + \dots$$

and pointed out that providing a disturbing force excites any component of the first buckling mode (i.e. providing b_1 exists, however small) then K vanished when $P = P_{C1}$.

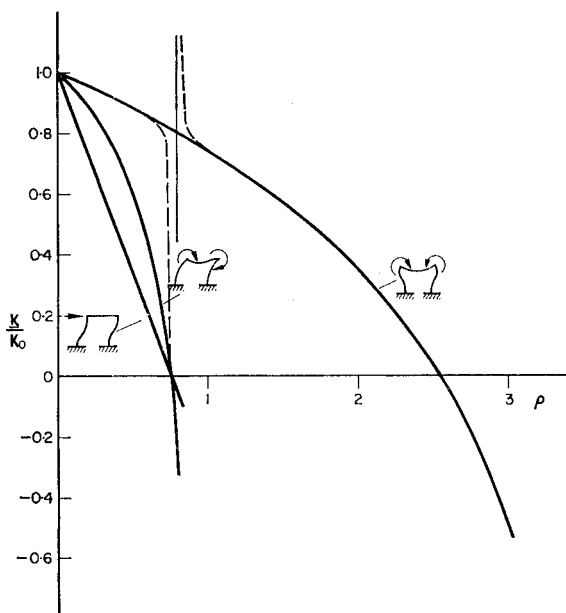


FIG. 4.5

The lower of the two critical loads indicated by Fig. 4.5 is a sway mode and as the first disturbing system of moments does not contain any sway component it fails to reveal the sway critical mode. In practice if there were any unsymmetrical imperfection of the structure or the loading system then this would

be magnified indefinitely at the lower critical mode and an experimental stiffness curve would look like the one dotted.

The fact that the first disturbing system misses the lower critical load is then a mathematical curiosity and is of no practical

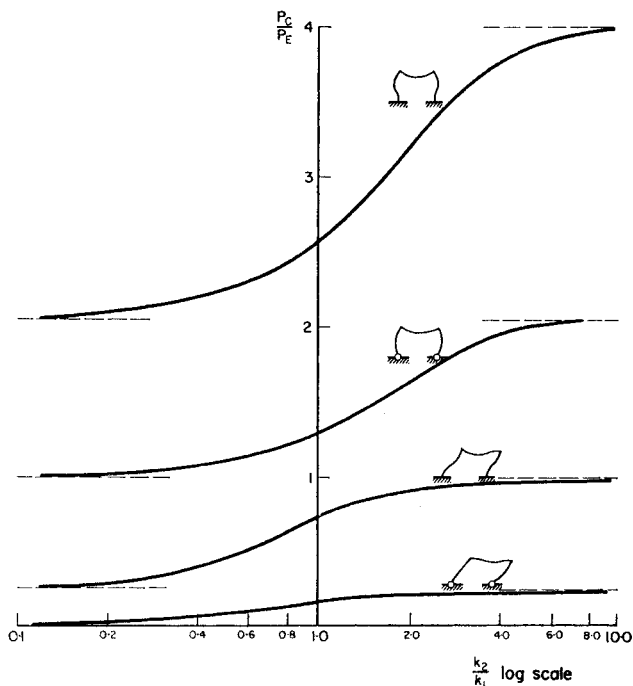


FIG. 4.6

significance. As the structure would have a negative stiffness to sway disturbances above the lower critical load it would be unstable and the load could not be increased past the critical load without being provided with a lateral restraint to prevent sideways displacements developing. In practice this may be provided by bracing systems in the plane of the beams and the higher critical

load (symmetrical case) has then a practical significance. The four standard cases for single-storey portals are shown in Fig. 4.6.

4.3 Multi-storey Single-bay Portals

The sway and no sway critical loads of multi-storey portals as shown in Fig. 4.7 are easily obtained.

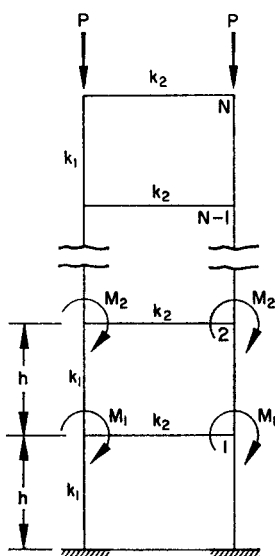


FIG. 4.7

Thus, for the sway case we have in succession

$$M_1 = (2nk_1 + 6k_2)\theta_1 - ok_1\theta_2$$

$$M_2 = -ok_1\theta_1 + (2nk_1 + 6k_2)\theta_2 - ok_1\theta_3$$

$$M_{N-1} = -ok_1\theta_{N-2} + (2nk_1 + 6k_2)\theta_{N-1} - ok_1\theta_N$$

$$M_N = -ok_1\theta_{N-1} + (nk_1 + 6k_2)\theta_N$$

At the critical load $M_1 = M_2 = M_N = 0$ and writing $X = (2nk_1 + 6k_2)/ok_1$

we have

$$0 = X\theta_1 - \theta_2$$

$$0 = -\theta_1 + X\theta_2 - \theta_3$$

$$0 = -\theta_2 + X\theta_3 - \theta_4$$

$$0 = -\theta_{N-2} + X\theta_{N-1} - \theta_N$$

$$0 = -\theta_{N-1} + (X - n/o)\theta_N$$

i.e.

$$\theta_2 = X\theta_1$$

$$\theta_3 = (-1 + X^2)\theta_1$$

$$\theta_4 = -X\theta_1 + (-1 + X^2)X\theta_1$$

$$= +X(-2 + X^2)\theta_1 \text{ and so on}$$

If the portal is, for example, four stories high we also have the last equation

$$0 = -\theta_3 + (X - n/o)\theta_4$$

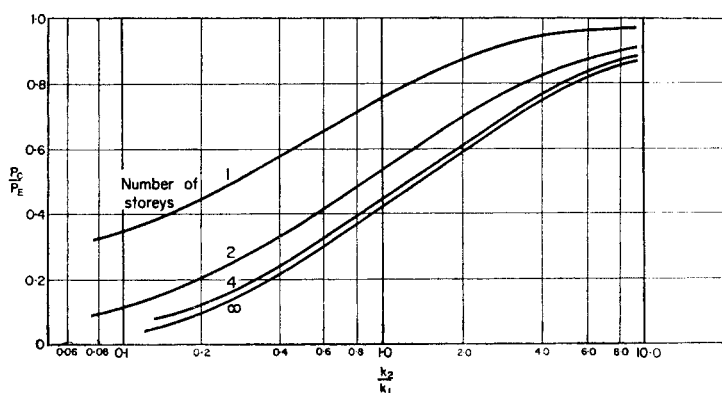


FIG. 4.8

and so $0 = (1 - X^2) \theta_1 - X(2 - X^2)(X - n/o) \theta_1$

$$\text{i.e.} \quad X(X^2 - 2)(X - n/o) = X^2 - 1 \quad (4.2)$$

Equation (4.2) is easily solved. For any particular value of X it gives the corresponding value of n/o and therefore of n and o separately. k_2/k_1 is then obtained from the expression for X .

The resulting P_C/P_E curves are shown in Fig. 4.8; also shown are results for various numbers of stories.⁽¹⁸⁾

The corresponding no sway critical loads are even simpler to obtain and are left as an exercise for the reader.

4.4 Multi-bay Multi-storey Portals

The sway deflexion characteristics of a single-bay portal can be used to obtain the similar characteristics of a particular family of multi-bay portals.

A series of identical portals under identical loads will have the same deflexions. Adjacent columns can therefore be superimposed and fastened together without causing any redistribution of stresses. All the portals shown in Fig. 4.9 will therefore have the same sway deflexion characteristics and in particular the same sway critical loads.

For all these portals the equivalent single-bay portal may be obtained by the application of the following rules:

$$\begin{aligned} \Sigma \text{ column stiffness of single bay} &= \Sigma \text{ column stiffness of multi-bay} \\ \Sigma \text{ column loads of single bay} &= \Sigma \text{ column loads of multi-bay} \\ \text{beam stiffness} &= \Sigma \text{ beam stiffness.} \end{aligned}$$

Now consider the application of these rules to form an equivalent single-bay portal for a multi-bay portal which is not formed in accordance with this "Principle of Multiples"⁽²⁸⁾ and in the first place suppose that stability effects are negligible.

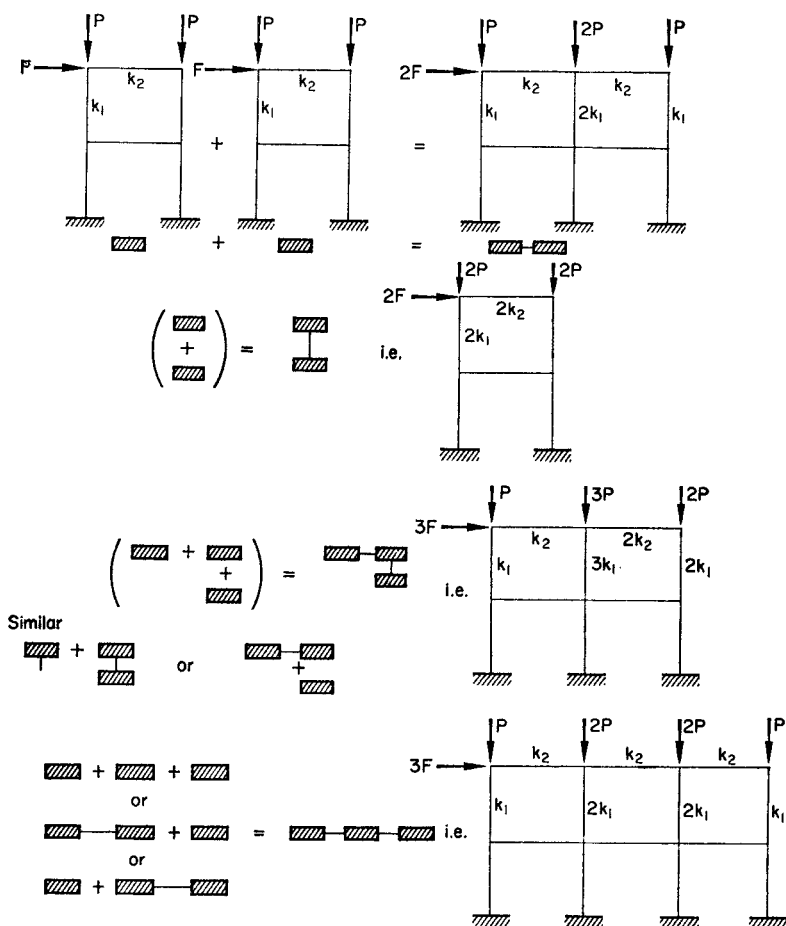


FIG. 4.9

The deflexions of the equivalent single-bay portal may be calculated and if these are imposed as a composite disturbance on the real frame then the accompanying bending moments can be calculated. This is sharing the bending moments of the single-bay frame amongst the members of the real frame in proportion

to their stiffnesses. As the real frame is not proportioned in accordance with the Principle of Multiples individual joints will not necessarily be in equilibrium, but the bending moments as a whole will satisfy the shear equations and at any floor the sum of all the beam and column moments will be zero.

The deflexions of the equivalent single-bay frame therefore give a solution of the real frame loaded with the right shear forces and sets of self-equilibrating moments at each floor level. By St. Venant's principle a set of self-equilibrating moments can be expected only to cause a local perturbation and not to have an appreciable effect on the overall sway of a structure. For purposes of determining sway deflexion, although not for determining moments in individual members, a multi-bay frame can therefore be replaced by an equivalent single-bay frame.

If we use such a frame for stability calculations we make the further assumption that it is sufficiently accurate to use a mean value of P/P_E at any storey given by $(P/P_E)_{\text{mean}} = \Sigma P / \Sigma P_E$ for all the columns instead of the values for each individual column. It has been shown⁽²⁹⁾ that these methods can be used to predict the sway critical loads of multi-bay frames with considerable accuracy.

These methods represent about the limit of what is at present feasible by hand calculations. For more complicated structures recourse must be had to computer methods, but no new physical principles are involved.

4.5 Frames in which Members Carry Primary Bending Moments

Having dealt with loads capable of being transmitted through the structure by axial loads only (Fig. 4.1), we now turn our attention to frames in which bending action predominates (Figs. 4.2 and 4.3). We take as an example the symmetrical, uniform-section portal frame shown in Fig. 4.10(a), and assume that sway is prevented.

The only possible displacements are equal and opposite rotations of B and C . Suppose equal and opposite bending moments

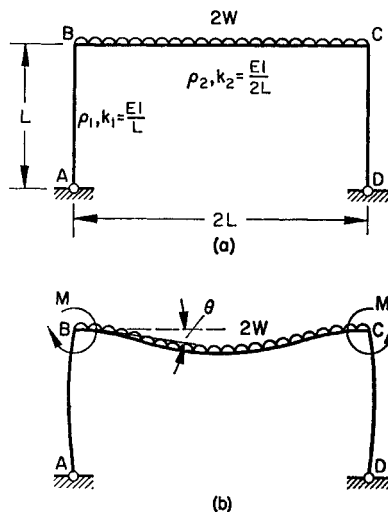


FIG. 4.10

M are applied at these joints, as shown in Fig. 4.10(b). Introducing the fixed-end moments in the beam due to the uniformly distributed load $2W$ (see Chapter 2), the operations table becomes:

	A		B		C		D	
F.E.M.	—	—	$-f_2 \left(\frac{WL}{3} \right)$	$f_2 \left(\frac{WL}{3} \right)$	—	—	—	—
Rotate B and C	0	$s_1'' k_1 \theta$	$s_2 k_2 \theta$	$-s_2 c_2 k_2 \theta$	$-s_2 k_2 \theta$	$s_2 c_2 k_2 \theta$	$-s_1'' k_1 \theta$	0

Since $k_1 = 2k_2$, the equations of equilibrium for the joints B and C are both given by

$$M = \left[2s_1'' + s_2(1 - c_2) \right] k_2 \theta - f_2 \left(\frac{WL}{3} \right). \quad (4.3)$$

The horizontal thrust at A and D is $s_1'' k_1 \theta / L$, whence

$$\rho_2 = \frac{4}{\pi^2} \cdot s_1'' \theta. \quad (4.4)$$

Since the load in each column is W ,

$$\rho_1 = \frac{1}{\pi^2} \cdot \frac{WL}{k_1} \quad (4.5)$$

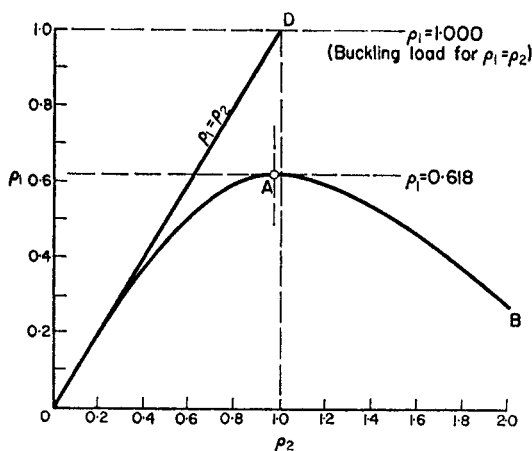


FIG. 4.11

If there are no external moments acting at B and C , so that $M = 0$, ρ_1 and ρ_2 are related by the equation

$$\frac{4}{3} f_2 \rho_1 = \left[1 + \frac{s_2(1 - c_2)}{2s_1''} \right] \rho_2 \quad (4.6)$$

obtained by eliminating W and θ from equations (4.3), (4.4) and (4.5). The numerical solution of equation (4.6) by iteration leads to the relationship between ρ_1 and ρ_2 depicted by OAB in Fig. 4.11. It is found that ρ_1 reaches a maximum value of

0.618 when $\rho_2 = 0.972$, so that $\rho_1 = 0.618$ or $W = 0.618\pi^2(EI/L^2)$ represents the buckling load. The variation of the rotation θ with ρ_1 is given by curve OAB in Fig. 4.12.

According to linear elastic theory (i.e. ignoring the effect of axial loads on flexure), the axial load in the beam would be $1/4$

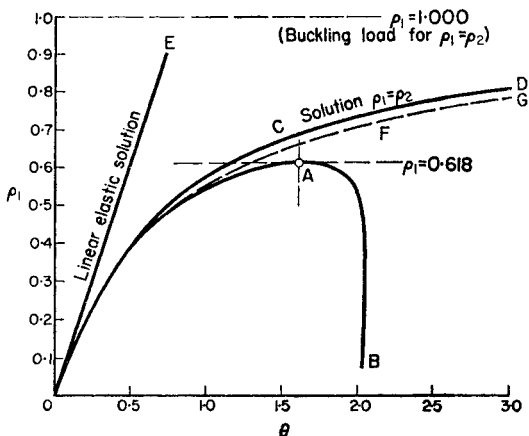


FIG. 4.12

that in each column, whence $\rho_1 = \rho_2$ (OD in Fig. 4.11). With this assumption, and putting $M = 0$ in equation (4.3), it would follow that

$$\theta = \frac{2}{3} \pi^2 \frac{f\rho_1}{s(1-c)(3+2c)} \quad (4.7)$$

where the stability functions s , c and f correspond to $\rho = \rho_1$. This results in the curve OCD in Fig. 4.12, the rotations θ becoming infinite when $c = 1$ or $\rho_1 = 1$, which therefore represents the buckling load for the assumption $\rho_1 = \rho_2$. The stiffness of the structure, at a given value of W , with respect to small applied bending moments dM at B and C , assuming $\rho_1 = \rho_2$,

may be obtained by differentiating equation (4.3) with respect to θ . Hence

$$\frac{dM}{d\theta} = [2s_1'' + s_2(1 - c_2)]k_2 \quad (4.8)$$

in which s_1'' , s_2 and c_2 are all stability functions corresponding to $\rho_1 = \rho_2 = WL/\pi^2 k_1$. The variation of $dM/d\theta$ with ρ_1 is represented by ABC in Fig. 4.13, and as would be expected, $dM/d\theta$ becomes zero when $\rho_1 = 1$.

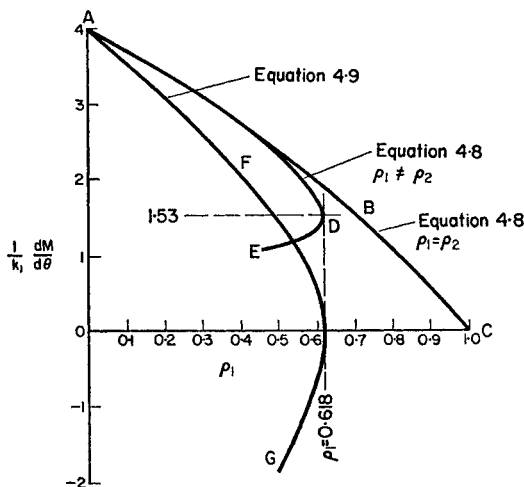


FIG. 4.13

It might seem reasonable to assume that the stiffness of the frame, allowing for the variation of ρ_2 with ρ_1 , could be obtained from equation (4.8) by substituting the appropriate values of s_1'' , s_2 and c_2 . However, when this is done, the curve obtained is ADE in Fig. 4.13. When ρ_1 reaches the buckling value of 0.618, equation (4.8) gives $dM/d\theta = 1.53k_1$. This apparently contradicts the concept of zero stiffness as a property of a structure at its buckling load. The anomaly is resolved by differentiating

equation (4.3), but allowing in the differentiation for the dependence of ρ_2 on θ at stationary ρ_1 . Denoting $ds/d\rho$ by \dot{s} , $dc/d\rho$ by \dot{c} and $df/d\rho$ by \dot{f} , and using $k_1 = 2k_2$ and $d\rho_2/d\theta = 4s_1''/\pi^2$ from equation (4.4), it follows that:

$$\begin{aligned} \frac{dM}{d\theta} = & \left[2s_1'' + s_2(1 - c_2) \right] K_2 \\ & + \frac{4}{\pi^2} s_1'' \left[\dot{s}_2(1 - c_2) - s_2\dot{c}_2 \right] \theta k_2 - \frac{8}{3}\rho_1 s_1'' \dot{f}_2 k_2. \quad (4.9) \end{aligned}$$

The above modified stiffness is plotted as curve *AFG* in Fig. 4.13 and it will be seen that the stiffness becomes zero when $\rho_1 = 0.618$. It may be noted that the effect of including the differentials of the stability functions (curve *AFG* compared with *ADE*) is much greater than the effect of allowing only for the variation of ρ_2 with ρ_1 (curve *ADE* compared with curve *ABC*).

The presence of the additional terms in equation (4.9) (compared with equation (4.8)) implies that the stiffness of a frame carrying loads which produce primary bending moments is not identical with that of a frame supporting the appropriate axial loads only. The discrepancy in stiffness only becomes appreciable, however, when deformations become large. Thus, when $\theta = 0.02$ radian, the discrepancy is about 1 percent, when $\theta = 0.1$ radian it is about 5 percent, and when $\theta = 0.5$ radian it is about 30 percent. The effect of terms involving the differentials of the stability functions or buckling loads has also been discussed by Le-Wu-Lu.⁽³⁰⁾

We have included this dissertation in order that our results should show mathematical consistency. The mathematics used, however, have long ceased to represent the behaviour of the frame before these effects become appreciable. We have been using equations valid for small deflexions only in the region of large deflexions where the effects of change of geometry and bowing would have to be introduced before a mathematical analysis was valid.

Despite the above limitations, the elastic critical load retains its significance in the magnification factor $1/(1 - W/W_c)$ used to

estimate the effects of axial loads on deformations. According to linear elastic theory, the rotation θ for the joints B and C (Fig. 4.10(a)) is $\theta = WL^2/12EI = \pi^2 I_1/12$ giving the straight line OE in Fig. 4.12. Applying the magnification factor $1/(1 - W/W_C)$ where W_C is obtained from the $\rho_1 = \rho_2$ solution (i.e. $I_1 = 1.000$ or $W_C = \pi^2 EI/L^2$), the corrected load-rotation relation is the dotted curve OFG in Fig. 4.12, agreeing almost exactly with the correct solution OAB up to $I_1 = 0.5$ and $\theta = 0.8$.

The practical conclusion is that for frames where bending stresses form a large component of the total stresses then stability effects will be small, and the concept of elastic buckling loads will not be applicable. Where it is necessary to investigate stability effects it will be sufficient to do so using the axial load pattern obtained from a linear elastic analysis.

It is shown in Chapter 5 that nominal elastic critical loads also have significance in the estimation of elastic-plastic failure loads.

The above analysis of the frame in Fig. 4.10(a) has been carried out on the assumption that buckling in a sway mode is prevented. An approximation to the sway buckling load (neglecting stability effects in the beam) may be obtained from Fig. 4.6, and gives $\rho_1 = 0.15$. A more complete analysis reveals that the finite deformations induced by the loads before sway buckling occurs modify the sway buckling load slightly, due to the presence of terms involving the differentials of the stability functions. This type of problem has been investigated extensively by Chwalla,⁽³¹⁾ Chilver⁽³²⁾ and Horne.⁽³³⁾ Again, such effects appear to have little practical significance.

In multi-storey frames, although all loads may be applied as beam loads or horizontal sway loads, instability effects increase in importance with increase in number of storeys, because of the build-up of axial loads in the lower column lengths. When such frames are free to sway, the buckling load differs little from the critical load obtained by dividing the beam loads equally between the columns, and the effect of stability on deflexions is discussed very accurately by assuming the linear elastic sway deflexions to

be multiplied simply by the amplification factor $1/(1 - \lambda/\lambda_c)$. In multi-storey frames restrained against sway, stability functions may have to be employed to obtain reasonable estimates of elastic stresses, since the elastic critical loads may not be more than a few times the working load. It is found unnecessary to take into account the effect on stiffness of the small axial loads induced in the beams by bending action.

Examples

4.1 A rectangular portal frame $ABCD$ has two vertical stanchions AB and CD of height L rigidly joined to a horizontal beam BC of length $2L/3$. All members are of uniform flexural rigidity. The stanchion feet A and D are encastred to a rigid base. Equal vertical loads are applied at B and C . Show that the stiffness of the frame in respect of sway disturbance is zero when

$$m_1 s_1 (1 + c_1) - 2s_1 = 18,$$

where s_1 , c_1 , m_1 are stability functions for the stanchions.

(Cambridge Mech. Sci. Tripos Part II 1962.)

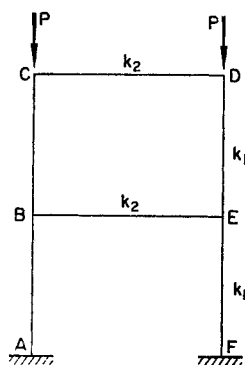


FIG. 4.14

4.2 Show that the critical loads of the symmetrical single-bay rigid frame shown in Fig. 4.14 with side sway prevented are given by the equation

$$\left(\frac{2}{s} \frac{k_2}{k_1} + 1\right) \left(\frac{k_2}{sk_1} + 1\right) = \frac{c^2}{2}.$$

(Manchester, Honours B.Sc. Tech., Part II 1954.)

4.3 Show that the sway critical load of the portal shown in Fig. 4.15 is given by the equation

$$s + 3 \frac{k_2}{k_1} = \frac{ms(1+c)}{4-m(1+c)}.$$

B is a rigid joint and *C* is a pin. *A* and *D* are fixed ends.

(Manchester, Honours B.Sc. Tech., Part II 1957.)

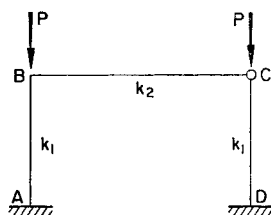


FIG. 4.15

4.4 Show that the sway critical load of the symmetrical single-bay rigid frame shown in Fig. 4.14 is given by the equation:

$$o^2 = \left\{n + 6 \frac{k_2}{k_1}\right\} \left\{2n + 6 \frac{k_2}{k_1}\right\}$$

where *n*, *o* are no-shear stability functions and *k*₂, *k*₁ the stiffness of the beam and column members. Draw an approximate graph

showing how you would estimate the sway critical load to vary with the ratio of k_2 to k_1 and in particular determine the limit when k_2/k_1 approaches zero.

(Manchester, Honours B.Sc. Tech., Part II 1960.)

4.5 Figure 4.16 shows a column, of constant cross-section of second moment of area equal to I_1 , having pinned ends, which is restrained against buckling by being pinned at its mid-point to a

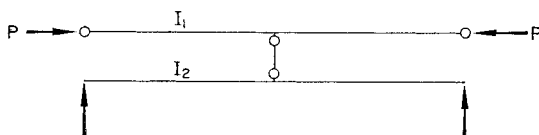


FIG. 4.16

uniform simply supported beam of the same span as the column and moment of inertia I_2 . Show that for all values of I_2/I_1 greater than 3.28 the column will buckle at a load corresponding to the Euler value for its half length.

Note. At $P = P_E$, $s = 2.467$, $c = 1.0$, $m = \infty$.

(Manchester, Honours B.Sc. Tech., Part II 1961.)

4.6 Investigate the stability in the plane of the structure indicated in Fig. 4.17 for which $k_2 = 2k_1$, and determine the critical load in terms of P/P_E , where P_E is the Euler load of a pin-ended strut of stiffness k_1 and height h . Tables of stability functions are provided. The members are rigidly jointed at A and B . All other joints are pinned.

(Manchester, Honours B.Sc. Tech., Part II 1962.)

4.7 The end A of a member AB , length l and flexural rigidity EI , is held by other members which together provide a restraining moment of $Q_A\theta_A$ when end A is rotated through an angle θ_A . End B is restrained against rotation by a member of rotational

stiffness qk where $k = EI/l$. The member AB carries an axial load, and is subjected at end B to a “no-shear” rotation during which equilibrium is maintained at end A . Show that, for a joint rotation of θ_B at end B , the total moment applied at that joint is $Q_B\theta_B$ where

$$\frac{Q_B}{nk} = \left(1 + \frac{q}{n}\right) - \frac{\left(\frac{o}{n}\right)^2}{1 + Q_A/nk}$$

where o and n are stability functions for member AB .

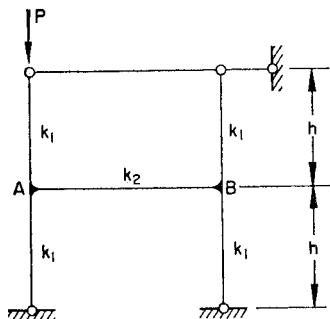


FIG. 4.17

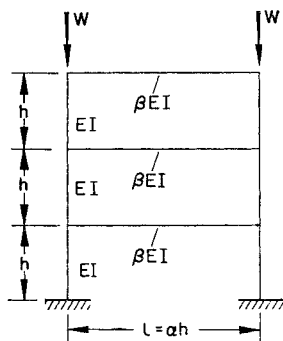


FIG. 4.18

The three-storey frame in Fig. 4.18 has uniform columns of flexural rigidity EI and beams of flexural rigidity βEI . The feet of the columns are fixed in position and direction, and the columns each sustain a uniform axial load P . Using the above result or otherwise, show that the frame becomes unstable in a sidesway mode when

$$\frac{o}{n} = \frac{2(3\beta + \alpha n)}{\alpha n} \sqrt{\frac{(6\beta + \alpha n)}{3(4\beta + \alpha n)}}$$

where n and o are stability functions corresponding to $\rho = Ph^2/\pi^2 EI$.

4.8 Figure 4.19 shows a compression testing machine consisting of four circular equal members AA' , BB' , etc., each of length l and flexural rigidity EI , fixed into rigid end blocks. When testing a short pin-ended specimen EF of length a , show that the machine will become unstable when the compressive load in EF is given by

$$\frac{s(1+c)}{\rho m} + \frac{\pi^2 l}{2a} = 0$$

where s , c and m are stability functions corresponding to $\rho = -Pl^2/4\pi^2 EI$.

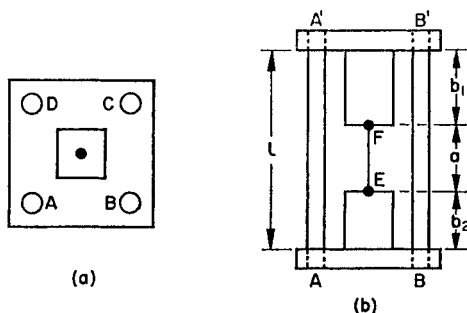


FIG. 4.19

4.9 A compression testing machine consists of two circular equal members AA' and BB' , each of length l and flexural rigidity EI , fixed into rigid end blocks. An elevation of the machine would appear as in Fig. 4.19. Show that the testing machine would, when used to test the pin-ended specimen EF , become unstable by buckling out of the plane $AA'B'B$ when the compressive load in EF was given by

$$\left\{ s - \frac{P}{2k} \frac{b_1(a+b_1)}{a} \right\} \left\{ s - \frac{P}{2k} \frac{b_2(a+b_2)}{a} \right\} - \left\{ sc - \frac{P}{2k} \frac{b_1 b_2}{a} \right\}^2 = 0$$

Elastic-Plastic Behaviour

5.1 Introduction

When considering elastic stability, the stiffness of each member of a structure affects the buckling load, and it is incorrect (except when the members are pin-jointed) to speak of the buckling load of an individual member. The same is true in the elastic-plastic range, but in many cases final failure may in fact take place in

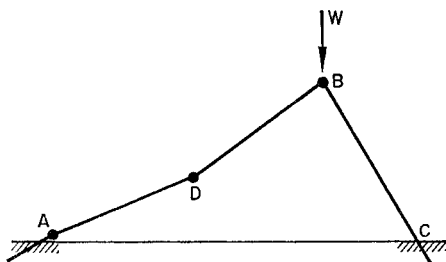


FIG. 5.1

one member only, and it is then easier to think of the problem primarily in terms of the behaviour of that particular member. Thus in the simple structure in Fig. 3.1, ultimate failure might involve the deformation of member AB as a mechanism with plastic hinges at A , B and at some section near the mid-point of AB , as shown in Fig. 5.1. After considerable deformation, a fourth hinge would form at C , but this would be well after the attainment of the peak load, and it is the stages leading up to the formation of plastic hinges at A , B and D that have to be studied

in order to predict the failure load. It should be noted that the behaviour of the "critical" member AB is throughout affected by the behaviour of member BC . Hence, failure is to be discussed in terms of the influence of the remainder of the structure on the failure of the "critical" member—leaving aside for the moment the problem of how the "critical" member is to be identified.

The above approach to elastic-plastic buckling is applicable wherever the "critical" member could sustain the applied load by an axial compressive load only. The bending moments that

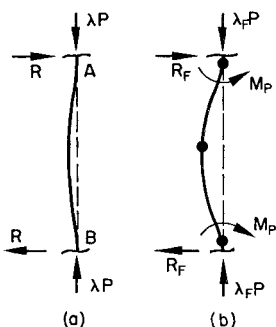


FIG. 5.2

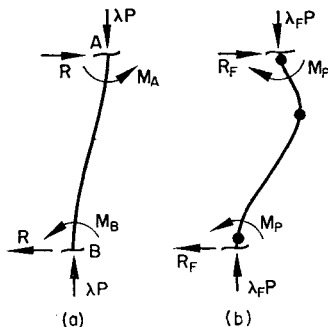


FIG. 5.3

actually arise in the "critical" members are due either to imperfections, axial deformations, lateral loads ("beam" loads) applied to adjacent members, or to combinations of these factors. The three individual causes are illustrated in Figs. 5.2, 5.3 and 5.4 respectively.

Imperfections (Fig. 5.2) are always present in some degree, due to lack of straightness or lack of fit or both, and may be important in their effect on the failure loads of compression members in triangulated structures, or of columns in multi-storey frames restrained against sway. Ultimately a mechanism will form as shown, with hinges at both ends and near the centre of length. If the surrounding members are weaker than the failing member, then hinges may form in these adjacent members.

Axial deformations are important in triangulated frames, in which they induce joint translations with accompanying double curvature bending as shown in Fig. 5.3(a). Ultimate failure involves the deformation of the member to one side of the longitudinal centre line, and if in Fig. 5.3(a) $M_A > M_B$, failure will occur as in Fig. 5.3(b).

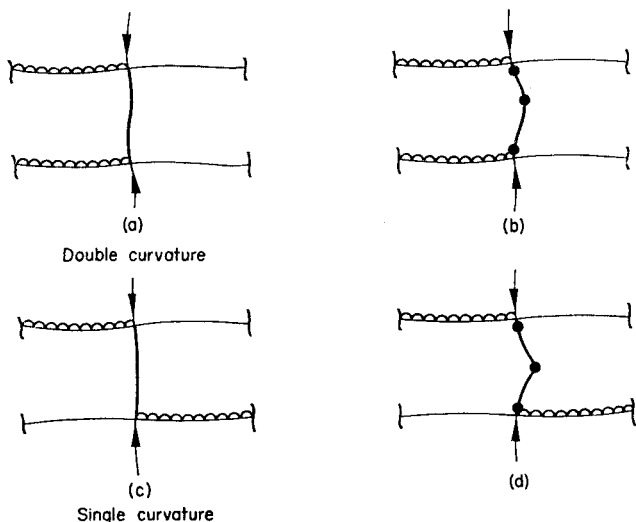


FIG. 5.4

Beam loads have an important effect on the columns of multi-storey frames restrained against sway. In the elastic range, differing arrangements of beam loading cause double or single curvature flexure in the columns, as shown in Figs. 5.4(a) and (c) respectively, but ultimate failure is similar in mode (Figs. 5.4(b) and (d)).

Although, in all the above cases, the final failure mode is much the same, this does not mean that it is at all easy to obtain a reasonable estimate of the maximum axial loads sustained by the members before the final plastic hinge mechanism forms. At the peak load the member is in an intermediate condition, being

neither elastic nor having a fully developed plastic hinge mechanism, and a laborious step-by-step elastic-plastic analysis is necessary to obtain a theoretical failure load. Few such analyses have been made, but a study of the behaviour of columns in building frames has revealed interesting general results of a qualitative nature, and these will be described. Some progress has been made in empirical methods, and these will also be dealt with.

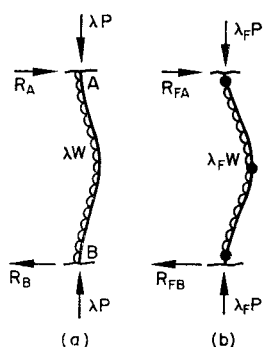


FIG. 5.5

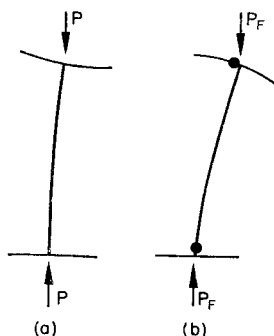


FIG. 5.6

Although the final failure of the compression members in Figs. 5.2 to 5.4 involves bending, the primary loading is axial, and so the members may all be described as “compression loaded”. An entirely different type of member may be described as “lateral loaded”. The simplest example would be a member which itself carried lateral load in addition to axial load, see Fig. 5.5. However, all the members in the frame in Fig. 4.2 may also be referred to as “lateral loaded” in that their bending resistance is a primary factor in the total rigidity of the structure with respect to the applied loads. The ultimate behaviour of such a member may be represented diagrammatically as in Fig. 5.6, but it is here not at all useful to refer to the “failure” of the member, since the bending moment distribution and the incidence of plastic hinges depends primarily on the behaviour of the structure as a

whole. There is another important difference between “compression loaded” and “lateral loaded” members. In the former, since the bending moments are secondary, their distribution may change radically, not only (as has been seen in Chapter 3) in the elastic range, but also in the plastic range. In laterally loaded members, on the other hand, the bending moment distributions, while varying in detail, tend to remain recognisably similar, even during plastic deformation, since they are dictated by overall equations of equilibrium.

We first discuss structures in which elastic-plastic stability is controlled by the behaviour of compression loaded members, and subsequently we discuss structures that are lateral loaded.

5.2 The Elastic-Plastic Behaviour of Compression-loaded Members

In the course of a lengthy experimental investigation into columns bent by beam loads into double and single curvature (Fig. 5.4(a) and (c))^(33, 34) a theoretical study was made of the spread of plasticity in the columns as the axial loads were increased to failure. The experimental test frames for single and double curvature are shown in Figs. 5.7(a) and (b) respectively. The beams were of high tensile steel, of width 0.75 in. and depth 1.25 in., so that plastic deformation was confined to the mild steel columns, some of which were of rectangular cross-section and some of *I*-section. The full beam loads were first applied, and further direct axial load was then added to the top of the column until complete failure occurred. The calculated sequence of behaviour for one of the rectangular section columns (width 1.25 in., depth 0.375 in.) bent in single curvature about its minor axis is shown in Fig. 5.8. The calculations have been performed on the assumption that the material has an idealised elastic-pure plastic stress-strain relation, with an upper yield stress of 22.9 ton/in², a lower yield stress of 20.3 ton/in², and a modulus of elasticity of 13,000 ton/in². The load deflexion curve (for central lateral deflexion of the column) is given by *OEABCD* in Fig. 5.9, while the changes with axial load of the end and central bending

moments in the column are shown in Fig. 5.10. Yield first occurred at the centre of the concave face of the column at an axial load of 3.98 ton (Fig. 5.8(a) and points *A* in Figs. 5.9 and 5.10). As the axial load increased (the beam loads remaining constant), the end

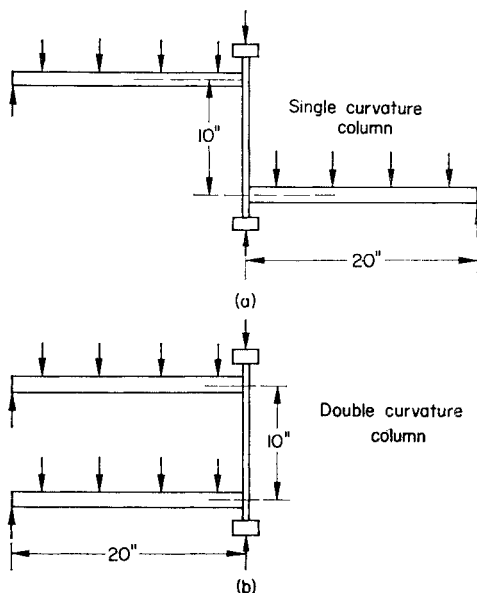


FIG. 5.7

moments decreased, eventually changing sign, while the central moment increased, causing plastic zones, first in compression on the concave face, and then in tension on the convex face. The reversed bending moment at the ends also caused first compressive yielding and then tensile yielding. At the peak load of 6.82 ton (Fig. 5.8(c) and points *C* in Figs. 5.9 and 5.10), no yielding had occurred in tension either at the ends or the centre, and a "plastic hinge" was nowhere fully operative, although it is evident that the degree of plasticity near the centre would seriously

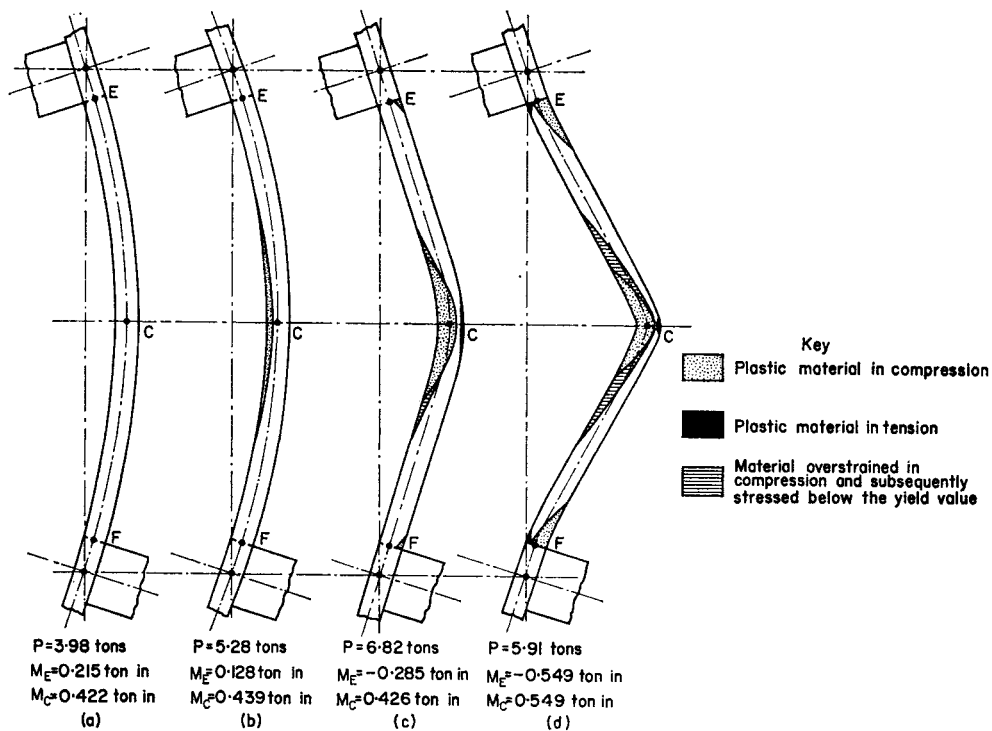


FIG. 5.8

reduce the rigidity of the column. Since the plastic zones which show increasing plastic flow have no rigidity, the peak load of 6.82 ton must be identical with the critical load of a structure consisting of the beams and a column of varying section, the cross-section of this column being the original section less these

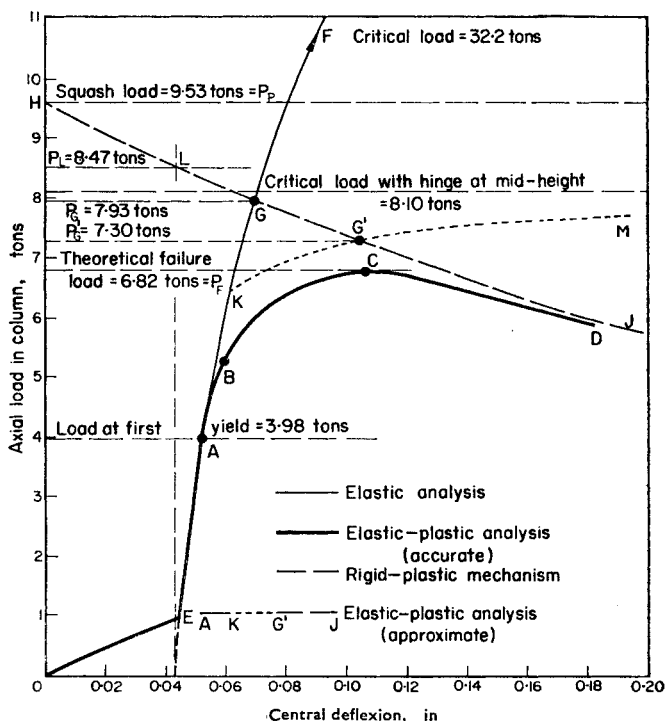


FIG. 5.9

plastic zones. It will be seen from Fig. 5.8(c) that the cross-section of this reduced column at mid-height is very small, whereas the ends of the column are almost fully elastic. It would therefore be expected that a rough approximation to this critical load would be obtained by assuming a structural hinge at mid-height in the column, as shown in Fig. 5.11. In fact, the critical

load of this "reduced structure" is found to be 8.1 ton, compared with 32.2 ton for the fully elastic structure. This explains why the column fails at the stage at which full plasticity is approached at mid-height.

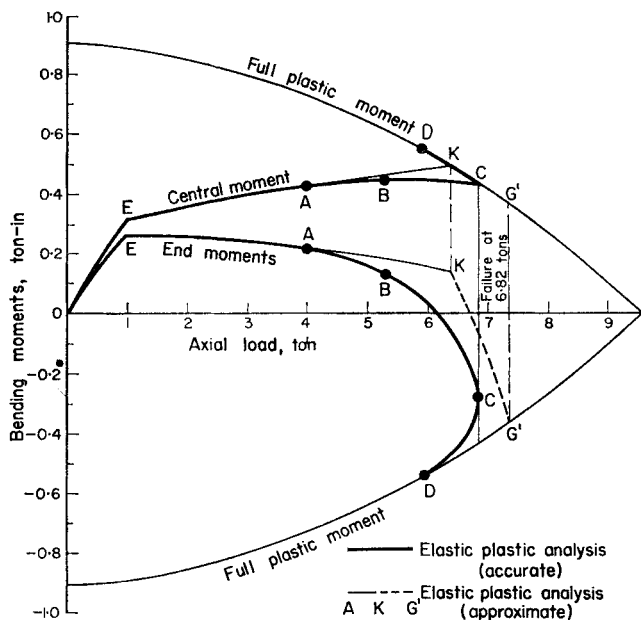


FIG. 5.10

The theoretical failure load of 6.82 ton agrees very well with the experimental failure load for this frame of 6.67 ton. An exact elastic-plastic analysis of this nature, although instructive, is however tedious, and it is desirable to investigate how closely approximate methods will predict the result.⁽³⁵⁾ The elastic response of the frame for the given load sequence, derived from s and c functions, is represented by $OEAF$ in Fig. 5.9. The rigid-plastic response is obtained from the plastic hinge mechanism

in Fig. 5.12, and this leads to the mechanism line HJ in Fig. 5.9. The calculation of HJ is similar to that for a pin-ended member, Figs. 1.18 and 1.19. Equations (1.33) and (1.34) apply, and taking moments about one end for half the column, $Py_c = 2M_P'$ where y_c is the central deflexion (Fig. 5.12). Hence

$$y_c = \frac{d}{2} \left\{ \frac{bd\sigma_y}{P} - \frac{P}{bd\sigma_y} \right\} \quad (5.1)$$

where $b \times d$ is the cross-section of the member and σ_y is the yield stress.

Without performing the labour of an "exact" elastic-plastic analysis, a rough estimate of the failure load will be given by G , the intersection of the elastic curve $OEAF$ with the mechanism

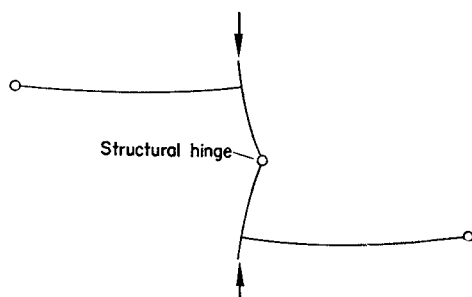


FIG. 5.11

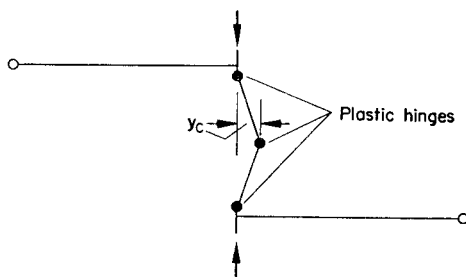


FIG. 5.12

line HJ (Fig. 5.9). This gives a load $P_G = 7.93$ ton, 19 percent above the experimental value, and not a particularly close estimate.

The end and central moments vary, according to the elastic solution, as shown by the thinner continuous curves in Fig. 5.10, and full plastic moment is in fact reached at mid-height when the axial load is 6.40 ton, represented by points K in Figs. 5.9 and 5.10. Assuming that plasticity is confined to the plastic hinge, a more accurate elastic-plastic analysis may be obtained beyond point K with the help of stability functions by applying these to the two halves of the column above and below the hinge. The deflexions then increase according to the dotted curve KM in Fig. 5.9, and if no further hinges formed, would tend to indefinitely large values as the critical load for a column with a central hinge (i.e. 8.10 ton) was approached. In fact, full plastic moment is reached at the ends at an axial load of 7.3 ton, corresponding to points G' in Figs. 5.9 and 5.10. Thereafter the theoretical load-deflexion curve follows the mechanism line $G'J$. The approximate elastic-plastic load-deflexion curve $OEKG'J$ thus furnishes a high estimate of the failure load, but the analysis of a number of columns shows that the overestimate is a consistent one of about 10 percent compared with experimental values. In a similar series of tests with columns of 1.25×0.25 in. cross-section (i.e. 50 percent more slender than the above) the point corresponding to K in Fig. 5.9 is found to lie above the reduced critical load for a column with a central hinge, so that G' lies below K , and the load at K then becomes the best estimate of failure. Again, this estimate is found to be about 10 percent above the experimental value.

5.3 The Estimation of Failure Loads of Compression-loaded Members

Although the above discussion has been with reference to a compression loaded member disturbed by bending moments induced by lateral loads in adjacent members, essentially similar phenomena are observed when the disturbing moments are due

to initial imperfections or lack of fit, or changes in the axial lengths of members.

A complete plastic zone analysis for a rigid-jointed triangle, in which the bending moments are those due to axial extension and contraction only, has been given by Foulkes.⁽³⁶⁾ Murray⁽³⁷⁾ tested a number of triangulated structures, and calculated loads P_G corresponding to point G in Fig. 5.9. Murray assumed that bending was induced in the members by imperfections only, and ignored the effects of changes in length; he found that failure loads lay between 77 and 98 percent of P_G . Since in practice disturbing moments arise from a number of causes, each of which may be important, it is readily seen that any attempt to perform a theoretical analysis is bound to be difficult, and for practical purposes, recourse must be had to empirical methods justified by experimental data.

The most useful general method hitherto suggested is the Rankine load P_R already described in Chapter 1 in relation to pin-ended members (equation (1.39))⁽⁹⁾. If λ_C is the elastic critical load factor for a structure containing a member which reaches its "squash load" (area of cross-section times yield stress) at a load factor of λ_P , then what appears to be a satisfactory approximation to the failure load is given by the Rankine load factor λ_R where

$$\frac{1}{\lambda_R} = \frac{1}{\lambda_C} + \frac{1}{\lambda_P}. \quad (5.2)$$

The compression member chosen is that having the lowest squash load factor for the given pattern of loads. For the column illustrated in Figs. 5.7(a) and 5.8 to 5.10, the axial loads in the column are:

Elastic critical, 32.2 ton

Squash load, 9.53 ton

$$\text{Hence Rankine load } P_R = \frac{32.2 \times 9.53}{32.2 + 9.53} = 7.35 \text{ ton,}$$

which is 10.2 percent above the experimental failure load.

When the rigid-plastic load is thus interpreted (i.e. simply as the squash load in the compression member), no influence of beam loading appears. If the collapse load of a compression member in a truss is estimated from equation (5.2), the failure load will always be increased if the restraint offered by an adjacent member is increased, since λ_C then increases while λ_P remains unchanged. Neal and Mansell⁽³⁸⁾ have shown, however, that increasing the restraint on a compression member may reduce the failure load. Merchant⁽³⁵⁾ has proposed the use of a modified rigid-plastic load in place of the squash load, so that allowance is made for the deformations imposed on the compression member by adjacent members that remain elastic. The deformation is the elastic deformation calculated without reference to stability effects. Applying this to the aforementioned frame in the Cambridge series (Fig. 5.7(a)), the rigid-plastic load is taken at point L on the mechanism line HJ (Fig. 5.9) corresponding to the elastic central deflexion at full beam load but zero axial load. This gives a load $P_L = 8.74$ ton, and substituting this in the Rankine formula, the estimated failure load becomes

$$P_R = \frac{32 \times 8.47}{32 + 8.47} = 6.71 \text{ ton.}$$

This is in excellent agreement with the observed failure load of 6.67 ton.

The correlation between experimental failure loads and Rankine loads for single and double curvature columns of 1.25×0.375 in. cross-section in the Cambridge tests⁽³⁴⁾ is summarised in Tables 5.1 and 5.2.

For the single curvature frames, the Rankine loads are calculated using both the squash load P_P and Merchant's load P_L as the rigid-plastic failure load. It is seen that the Merchant loads give greatly improved correlation for the more heavily loaded single curvature columns. The Rankine loads for the less heavily loaded single curvature columns and all the double curvature columns are conservative estimates of the actual failure loads.

TABLE 5.1. COLUMNS BENT IN SINGLE CURVATURE

Frame No.	Beam Load	Axial Load at Failure P_F	Rigid-Plastic Loads P_P	Elastic Critical Load P_C	Rankine Load	$\frac{P_F}{P_R}$ $\frac{P_F}{P_R'}$
					$P_R = \frac{P_P P_C}{P_P + P_C}$ $P_R' = \frac{P_L P_C}{P_L + P_C}$	
	(ton)	(ton)	(ton)	(ton)	(ton)	
2/48	0	7.76	8.34 8.34	32.2	6.62 6.62	1.17 1.17
2/47	0.5	7.67	8.34 8.10	32.2	6.62 6.47	1.16 1.19
2/15	1.48	6.86	9.53 8.75	32.2	7.35 6.87	0.93 1.00
2/16	1.99	6.67	9.53 8.47	32.2	7.35 6.71	0.91 0.99
2/17	2.49	6.25	9.53 8.13	32.2	7.35 6.50	0.85 0.96
2/46	2.50	5.58	8.34 7.19	32.2	6.62 5.88	0.84 0.95
2/18	2.99	6.17	9.53 7.98	32.2	7.35 6.38	0.84 0.97

TABLE 5.2. COLUMNS BENT IN DOUBLE CURVATURE

Frame No.	Beam Load	Axial Load at Failure P_F	Squash Load P_P	Elastic Critical Load P_C	Rankine Load	$\frac{P_F}{P_R}$
					$P_R = \frac{P_P P_C}{P_P + P_C}$	
	(ton)	(ton)	(ton)	(ton)	(ton)	
1/17	0	7.87	8.53	32.2	6.63	1.19
1/5	1.00	8.03	8.90	32.2	6.98	1.15
1/13	1.50	7.61	8.53	32.2	6.63	1.15
1/15	2.00	7.63	8.53	32.2	6.63	1.15
1/10	2.50	7.32	8.90	32.2	6.98	1.05

In view of the sensitivity of failure loads in columns to initial imperfections, the general level of agreement is satisfactory.

The result of applying the Rankine load concept to derive the failure loads of model triangulated frames is shown in Fig. 5.13.⁽³⁹⁾ The results are plotted non-dimensionally, with P_P/P_C horizontally and P_F/P_C vertically. The ratio P_F/P_C is a measure

of slenderness, while P_R/P_P shows the extent to which the failure load falls below the squash load. Only two of the fourteen results shown fall below the Rankine load, which thus provides an acceptable lower bound.

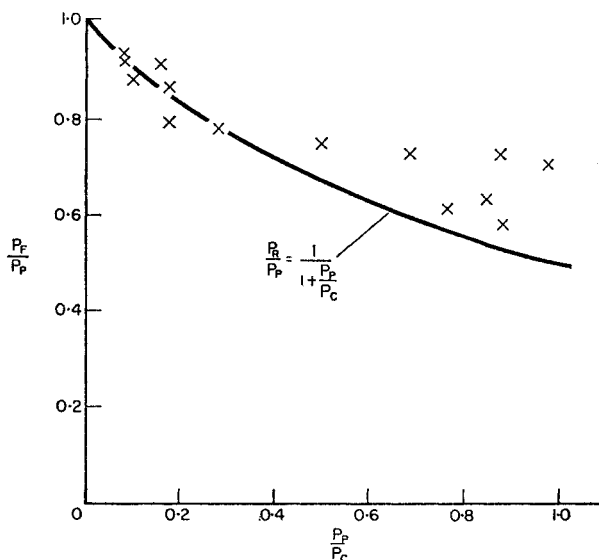


FIG. 5.13

In view of the many factors that affect the actual failure load of a compression loaded member (lateral loads on adjacent members, imperfections, lack of fit and accompanying internal stresses, internal stresses due to methods of fabrication, and axial deformations in the structure), it is unlikely that the Rankine load can be much improved upon as a general method of assessing failure loads.

In a triangulated frame which contains more than the minimum number of members required to render it simply stiff as a pin-jointed frame, the load carried by a compression member may decrease without this causing a decrease in the loading level on the

truss. The behaviour then becomes quite involved, and as has been shown by Davies and Neal^(40,41), dynamic jumps may occur. The treatment of such frames is beyond the scope of this volume.

5.4 The Elastic-Plastic Failure of Lateral Loaded Frames Behaviour of a Two-storey Frame

The subject is best introduced by taking a specific example, and the theoretical results will be given for the two-storey, single-bay frame illustrated in Figs. 5.14 and 5.15.⁽¹⁰⁾ The dimensions of the frame and the applied loads are shown in Fig.

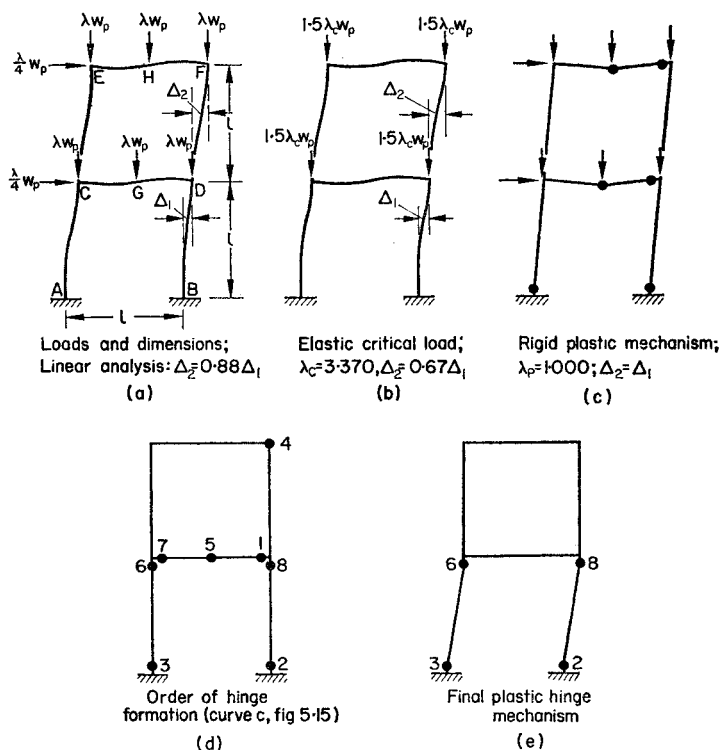


FIG. 5.14

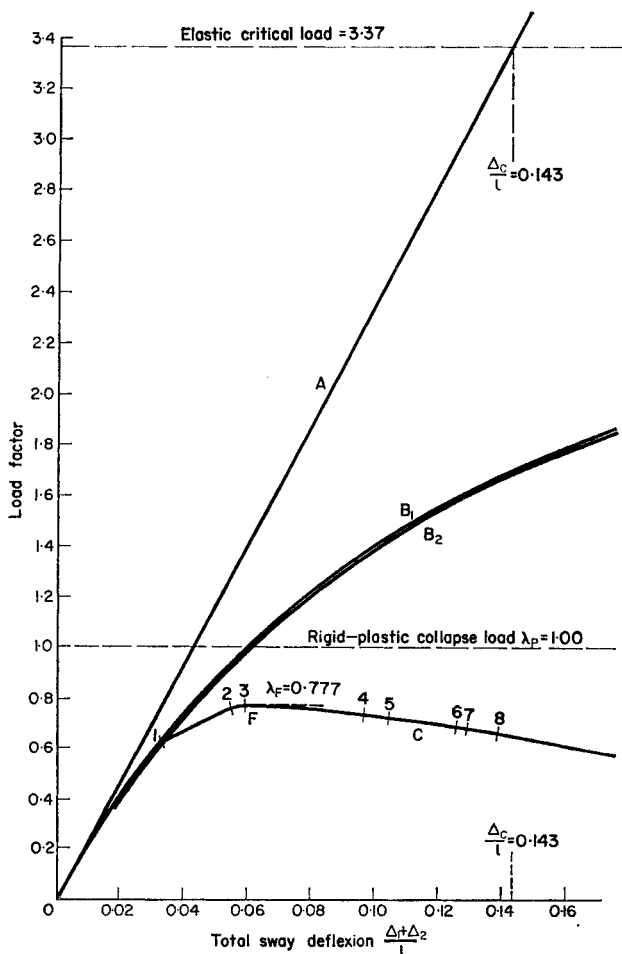


FIG. 5.15

5.14(a), the loads λW_P being such that rigid-plastic collapse of the frame occurs when $\lambda = 1.00$. All members are of the same uniform symmetrical I-section with the web in the plane of the frame. It is assumed that the area of the web is negligible compared with that of the flanges, so that the cross-section has unit

shape factor and all members remain fully elastic except at the plastic hinge positions. (This assumption greatly simplifies the analysis and leads to imperceptible error in problems of this type.) The depth between the flanges is $2r$ where, therefore, r is the radius of gyration for bending in the plane of the web. All members are of the same length l where $l/r = 100$. The modulus of elasticity is $E = 30 \times 10^6$ lb/in², and the yield stress (at which indefinite plastic deformation can occur) is 36×10^3 lb/in². The variation of full plastic moment with axial load is small in a frame of this slenderness, and is therefore neglected.

Figure 5.14(a) shows the deformation of the structure according to a linear elastic analysis, that is, ignoring the effect of axial loads on the stiffnesses of the members. The ratio of upper to lower storey sway Δ_2/Δ_1 is 0.88. When the total sway ($\Delta_1 + \Delta_2$) is plotted against the load factor λ , the straight line A (Fig. 5.15) is obtained. Under axial loads only (Fig. 5.14(b)), the first elastic critical load is obtained at $\lambda_C = 3.37$, the ratio Δ_2/Δ_1 being 0.67. Under the full loading, allowing for instability effects, the elastic analysis gives curve B_1 in Fig. 5.15. Curve B_2 is an approximation to the elastic response obtained from the linear analysis (straight line A) by multiplying the total sway deflexion at any given load factor λ by $1/(1 - \lambda/\lambda_C)$. This is equivalent to assuming that the modes of deformation in Fig. 5.14(a) and (b) are identical, and that only the first terms in equations (1.23) and (1.24) have non-zero coefficients. It will be seen that the difference between the modes has negligible effect.

The rigid-plastic collapse mechanism (giving $\lambda_P = 1.00$ and $\Delta_2/\Delta_1 = 1.00$) is shown in Fig. 5.14(c). Curve C in Fig. 5.15 is the elastic-plastic load-deflexion curve, the order of hinge formation being as shown in Fig. 5.14(d). The peak load occurs on the formation of the third hinge at point F in Fig. 5.15, giving $\lambda_F = 0.777$. Hinge 5 (at the centre of the lower beam) ceases to be operative when hinge 6 forms, while hinges 1, 4 and 7 also cease when hinge 8 forms. The final plastic collapse mechanism is thus with hinges in the lower storey only, as shown in

Fig. 5.14(e), and thus differs significantly from the rigid-plastic mechanism, Fig. 5.14(c).

It is of some interest to trace the decline in the stability of the structure with the progressive formation of plastic hinges. This may be achieved by reference to the "reduced critical loads", obtained by assuming structural hinges at these sections. Results are given in Table 5.3, which also shows the loads at which the plastic hinges form in the loading sequence.

TABLE 5.3

Positions of Hinges (Fig. 5.14(d))	Load Factor at which New Hinge Forms	Reduced Elastic Critical Load Factor
Elastic	—	3.37
1	0.613	2.02
1, 2	0.768	1.52
1, 2, 3	0.777	0.54
1, 2, 3, 4	0.745	0.48

With the formation of the third hinge at $\lambda_P = 0.777$, the reduced critical load falls to $\lambda = 0.54$ so that the frame is unstable and the load has to be decreased at higher deflexions to maintain equilibrium. Similar results have been obtained by Wood for two four-storey frames.⁽⁴²⁾

5.5 The Elastic-Plastic Failure of Lateral Loaded Frames The Rankine Load as an Approximation to Failure Load

The Rankine load again appears to be a sufficiently reliable lower bound on failure loads. In this application λ_P in equation (5.2) is to be interpreted as the rigid-plastic failure load factor

of the structure, and may be obtained by any of a number of established methods.^(34,43) The elastic critical load factor λ_G refers to a distribution of axial loads in which there is some freedom of choice, but it is found that the actual distribution selected has little effect on the final result. When considering multi-storey frames, it is sufficient to ignore axial loads in the beams and

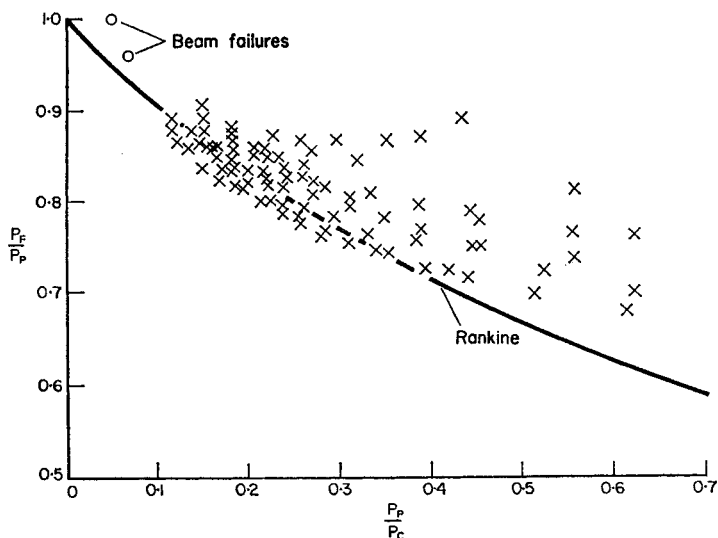


FIG. 5.16

the effect of horizontal loads generally, and to divide beam loads equally between columns. In pitched roof portal frames, it is permissible either to take the distribution of axial loads obtained as the result of a linear elastic analysis, or to assume axial loads proportional to those obtained at rigid-plastic collapse.

Salem⁽⁴⁴⁾ has compared Rankine loads with theoretical failure loads for a large number of single and two-storey frames, and his results are summarised in Fig. 5.16. The Rankine load is a close estimate of the failure load when the general forms of the first elastic critical mode and of the rigid plastic failure mechanism are

similar, as, for example, in the case of the two-storey frame analysed above (Rankine load factor $\lambda_R = 1.00 \times 3.37/(1.00 + 3.37) = 0.772$, failure load factor $\lambda_F = 0.777$). When the side load on a frame is small, so that rigid-plastic failure is confined to a beam, the Rankine load may fall well below the failure load. These features are illustrated by the plotted points in Fig. 5.16.

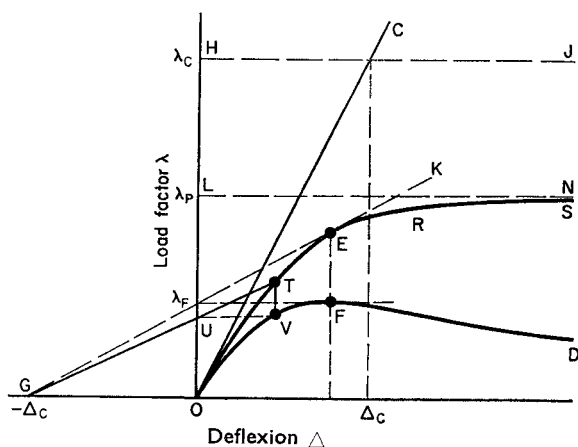


FIG. 5.17

It has been shown⁽¹⁰⁾ that there is some theoretical justification for the Rankine load when the rigid-plastic mechanism and first elastic critical mode are similar in form. Initial imperfections and lack of fit have, for such frames, negligible effect on failure loads, and need not therefore be considered in the argument.

In Fig. 5.17, in which the vertical scale is that of load factor and the horizontal scale is for a typical deflection, HJ represents the elastic critical load level for a structure, and LN the rigid-plastic collapse load level. The elastic load-deflection relation ignoring instability and change of geometry is the straight line OC . Similarly, it would be possible to calculate an elastic-plastic load-deflection curve ORS which also ignored instability effects and change of geometry. This theoretical curve would

either meet, or become asymptotic to, the line LN . If the rigid-plastic failure mechanism and the elastic critical mode are closely similar, the following construction may be used to derive the true elastic-plastic response curve OFD from the curve ORS .

Let Δ_C be the deflexion obtained on the linear elastic line OC at load factor λ_C . From point G at a deflexion $-\Delta_C$ on the horizontal axis draw GT to any point T on ORS , intersecting the vertical axis at U . Then point V , where TV and UV are vertical and horizontal respectively, is on the true elastic-plastic load-deflexion curve OFD . The more the rigid-plastic mechanism and the elastic critical modes differ the more will the derived curve fall below the true curve. An estimate of the failure load factor is obtained by drawing the tangent GE to the curve ORS , and this estimate must be conservative.

The Rankine load may now be derived by taking, as an approximation to the curve OES , the two straight lines OEN in Fig. 5.18. From similar triangles GUO , GEE' ,

$$\frac{\lambda_P}{\lambda_F} = \frac{\Delta_E + \Delta_C}{\Delta_C}$$

and from similar triangles OEE' , OCC' ,

$$\frac{\lambda_C}{\lambda_P} = \frac{\Delta_C}{\Delta_E}.$$

Eliminating Δ_C/Δ_E , it follows that

$$\frac{1}{\lambda_F} = \frac{1}{\lambda_C} + \frac{1}{\lambda_P},$$

i.e. λ_F so derived is the Rankine load.

Since OEN in Fig. 5.18 is always an upper bound to ORS in Fig. 5.17, a consistent tendency for the Rankine load to over-estimate the failure load is here superimposed on the tendency inherent in the construction of Fig. 5.17 to lead, due to differences between the rigid-plastic mechanism and the elastic critical mode,

to an underestimate. It is the cancellation of these contradictory effects that causes the Rankine load to be a close estimate of failure except when the elastic critical mode and the rigid-plastic mechanism are completely different in form.

It should be remembered that actual failure loads depend on internal stresses and cannot, therefore, be expected to be invariants for nominally identical frames. Refined detailed analysis can

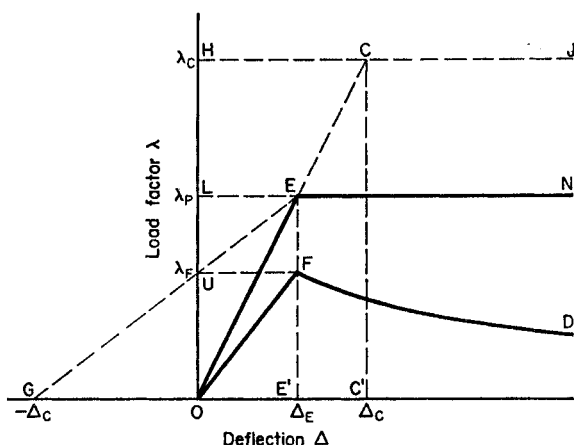


FIG. 5.18

therefore hardly be justified and the test of formulae should be empirical. Unfortunately, complete frame tests are rare and most of those done have been performed at model scale.

Design codes dealing with stability effects are at present (1964) largely out of date and indeed some are at present undergoing revision. It is not the aim of this book to explain or comment on particular codes but rather to give a perspective of the phenomena involved in the behaviour of frames. It is hoped that it will be found useful for this purpose.

As a further comment it is worth emphasising the low sway critical loads of portal frames. It is certainly desirable to provide

sway stiffness to tall buildings by shear walls or such devices and tall skeletal buildings should not be erected without a proper understanding of the phenomena described in this chapter.

5.6 Ultimate Loads of Structures in Strain-hardening Material

The use of the tangent modulus concept to obtain estimates of ultimate loads for pin-ended compression members has already been mentioned in Chapter 1. It was emphasised there that, because of the importance of imperfections, this is essentially an empirical procedure, but that it has been found highly successful for a number of materials. The application of the same concept to structures containing compression loaded and tensile loaded members involves trial calculations at increasingly high load levels until the critical load, calculated using the tangent moduli of the individual members, drops to the level of the applied load. This is a straightforward if tedious process, but is the only general method at present available. Little progress has been made in calculating the failure loads of structures in strain-hardening material when lateral loading predominates.

Examples

5.1 The uniform rectangular portal frame $ABCD$ shown in Fig. 5.19 is subjected to axial loads W in the columns and a shear load of $0.2 W$. With W equal to 4000 lb, 10,000 lb, and 20,000 lb the elastic lateral deflexions Δ at B would be 1.378 in., 4.5 in. and 18.3 in. respectively. The frame is made of a 2 in. \times 2 in. solid rectangular section throughout with an E -value of 30×10^6 lb/in² and a yield stress of 30×10^3 lb/in².

Plot the elastic stability line for the structure in terms of W against Δ showing the elastic critical load. Also plot a plastic collapse line on the assumption of a rigid-plastic behaviour of the material, taking into account the change of equilibrium of the collapse mechanism with finite deflexions. Ignore the reduction

of plastic moment due to end load and assume negligible axial load in the beam.

Using an empirical formula calculate the maximum value of W which the structure will carry and sketch in a probable line to describe its real behaviour.

(Manchester, Honours Engineering, Faculty of Science Part II 1962.)

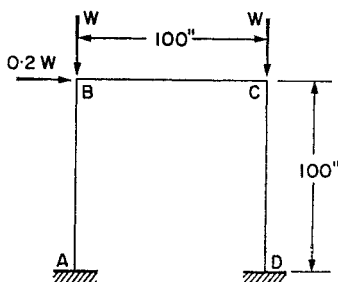


FIG. 5.19

5.2 A member of length L is contained in a triangulated plane frame. Linear elastic analysis shows that, when the frame is subjected to working loads applied at nodal points only, secondary moments cause terminal bending stresses in the member of σ_1 and σ_2 where, when σ_1 and σ_2 are of like sign, the terminal moments act in like sense. If the extreme fibre distance is c and the modulus of elasticity is E , show that the central lateral deflexion of the member at load factor λ is $\lambda(\sigma_1 - \sigma_2)L^2/16 Ec$.

The member has an additional central deflexion of $a_1 = \eta r^2/c$ where r is the radius of gyration and η is the imperfection coefficient (see Section 1.14). The full plastic moment under a mean axial stress $\lambda\sigma$ may be expressed in the form

$$M_P = \sigma_y S_2 \left(1 - \frac{\lambda\sigma}{\sigma_y} \right) \left(S_3 + \frac{\lambda\sigma}{\sigma_y} \right)$$

where σ_y is the yield stress and S_2 and S_3 are constants. The stress σ is the mean axial stress in the member at working loads. Show

that, with a central deflexion of $\{a_1 + \lambda(\sigma_1 - \sigma_2)L^2/16 Ec\}$, rigid-plastic failure occurs with plastic hinges at both ends and at the centre at a load factor λ_P given by the solution of the quadratic equation

$$\left(\frac{\lambda_P \sigma}{\sigma_y}\right)^2 \left\{1 + \frac{\pi^2}{32} \frac{\sigma_y(\sigma_1 - \sigma_2)}{\sigma \sigma_E} \frac{Ar^2}{cS_2}\right\} - \left(\frac{\lambda_P \sigma}{\sigma_y}\right) \left\{1 - S_3 - \frac{\eta Ar^2}{2cS_2}\right\} - S_3 = 0$$

where σ_E is the mean axial stress corresponding to the Euler buckling load for the member treated as a pin-ended strut, and A is the area of cross-section.

For such a member, $A = 5.88 \text{ in}^2$, $r = 1.20 \text{ in.}$, $c = 2.63 \text{ in.}$, $L = 150 \text{ in.}$, $\eta = 0.003 L/r$, $S_2 = 10.45 \text{ in}^3$, $S_3 = 0.383$, $\sigma = 4.5 \text{ ton/in}^2$, $\sigma_1 = 3.5 \text{ ton/in}^2$, $\sigma_2 = 0$, $E = 13,000 \text{ ton/in}^2$, $\sigma_y = 16 \text{ ton/in}^2$. At the elastic critical load of the truss, the stress in the member is $2.14\sigma_E$. If failure of the truss occurs due to elastic-plastic failure of the member, use the rigid-plastic failure load as derived above together with the elastic critical load, to obtain an estimate of the load factor at failure.

(Answers to the above questions may be found on page 154.)

Answers to Examples

Chapter 1

- 1.3 9.45 ton/in^2 .
1.6 $10^4 \times 2.227 < \sigma_F < 10^4 \times 2.326 \text{ lb/in}^2$.
 $10^4 \times 1.965 \text{ lb/in}^2$.

Chapter 3

- 3.1 $W = \frac{32}{\sqrt{3}} \pi^2 \frac{EI_2}{L^2}$, $W = \frac{2.045 \times 8}{3} \pi^2 \frac{EI_1}{L^2}$, $W = \frac{32}{3} \pi^2 \frac{EI_1}{L^2}$.
3.2 $\sqrt{3} P_E < P < 4\sqrt{3} P_E$.
3.3 $10.8 EI/L$.
3.4 $W_C = 3.22 \pi^2 EI/L^2$.

Chapter 4

- 4.4 $P/P_E \rightarrow 1/16$ as $k_2/k_1 \rightarrow 0$.
4.6 $P/P_E = 0.492$

Chapter 5

- 5.1 Intersection of elastic line and plastic mechanism line at
 $W = 8800 \text{ lb}$.
Elastic critical load = 29,200 lb.
Rankine load = 8500 lb.
5.2 $\lambda_P = 3.10$, $\lambda_C = 3.89$, $\lambda_F = 1.73$.

Bibliography

1. SOUTHWELL, R. V. *Theory of Elasticity*. Oxford University Press, 1941.
2. BLEICH, F. *Buckling Strength of Metal Structures*. McGraw-Hill, 1952.
3. HORNE, M. R. (1956). The Elastic-Plastic Theory of Compression Members, *J. Mech. Phys. Solids*, **4**, 104.
4. ELLIS, J. (1958). Plastic Behaviour of Compression Members, *J. Mech. Phys. Solids*, **6**, 282.
5. MERCHANT, W. (1949). The Buckling of Pin-ended Struts under Axial Load, *Structural Engineer*, **27**, 363.
6. ROBERTSON, A. (1925). *The Strength of Struts*. Inst. Civ. Engrs. Selected Engineering Paper No. 28.
7. OSGOOD, W. R. (1946). Column Formulas, *Trans. Amer. Soc. Civ. Engrs.* **111**, 165.
8. RANKINE, W. J. M. *Useful Rules and Tables*. London, 1866.
9. MERCHANT, W. (1954). The Failure Load of Rigidly Jointed Frameworks as Influenced by Stability, *Structural Engineer*, **32**, 185.
10. HORNE, M. R. (1963). Elastic-Plastic Failure Loads of Plane Frames, *Proc. Roy. Soc. A* **274**, 343.
11. ENGESSER, F. (1895). *Schweizerische Bauzeitung*, **26**, 24.
12. SHANLEY, F. R. (1947). Inelastic Column Theory, *J. Aer. Sci.* **14**, 261.
13. BULL, F. B. and SVED, G. *Moment Distribution Analysis*. Pergamon Press (1964).
14. BERRY, A. (1916). The Calculation of Stresses in Aeroplane Spars, *Trans. Roy. Aer. Soc.*, No. 1.
15. JAMES, B. W. (1935). *Principal Effects of Axial Load by Moment Distribution Analysis of Rigid Structures*. National Advisory Committee for Aeronautics, Technical Note No. 534.
16. LUNDQUIST, E. E. and KROLL, W. D. *Extended Tables of Stiffness and Carryover Factors for Structural Members Under Axial Load*. National Advisory Committee for Aeronautics, Wartime Report L-255 (A.R.R. 4B 24).
17. LIVESLEY, R. K. and CHANDLER, D. B. *Stability Functions for Structural Frameworks*. Manchester University Press, 1956.
18. MERCHANT, W. (1955). Critical Loads of Tall Building Frames, *Structural Engineer*, **33**, 85.
19. LIVESLEY, R. K. *Matrix Methods in Structural Analysis*. Pergamon Press, 1964.
20. BRITVEC, S. J. Ph.D. Thesis, Cambridge 1960.
21. MERCHANT, W. (1956). *A Connection between Rayleigh's Method and Stiffness Methods of Determining Critical Loads*. International Congress of Applied Mechanics, Brussels.

22. ARIARATNAM, S. T. (1961). The Southwell Method for Predicting Critical Loads of Elastic Structures, *Quart. J. Mech. App. Maths.*, **14**.
23. HORNE, M. R. (1962). The Effect of Finite Deformations in the Elastic Stability of Plane Frames, *Proc. Roy. Soc. A* **266**, 47.
24. ALLEN, H. G. (1955). The Estimation of the Critical Load of a Braced Framework, *Proc. Roy. Soc. A* **231**, 25.
25. SOUTHWELL, R. V. *Relaxation Methods in Engineering Science*. Oxford University Press, 1940.
26. HOFF, N. J., BOLEY, B. A., NARDO, S. V. and KAUFMAN, S. (1950). Buckling of Rigid-Jointed Plane Trusses, *Trans. Amer. Soc. Civ. Engrs.* **116**, 958.
27. BOLTON, A. (1955). A Quick Approximation to the Critical Loads of Rigidly Jointed Trusses, *Structural Engineer* **33**, 90.
28. LIGHTFOOT, E. (1956). The Analysis of Wind Loading of Rigid Jointed Multi-storey Building Frames, *Civil Engineering*, **51**, 757, 887.
29. BOWLES, R. E. and MERCHANT, W. (1958). Critical Loads of Tall Building Frames Pt. IV, *Structural Engineer* **36**, 187.
30. LU, LE WU. (1963). Stability of Frames Under Primary Bending Moments, *Proc. Amer. Soc. Civ. Engrs. Structural Div.* **89**, 35.
31. CHWALLA, E. (1938). Die Stabilität lotrecht belasteter Rechteckrahmen, *Der Bauingenieur* **19**, 69.
32. CHILVER, A. H. (1956). Buckling of a Simple Portal Frame, *J. Phys. Mech. Solids*, **5**, 18.
33. BAKER, J. F., HORNE, M. R. and RODERICK, J. W. (1949). The Behaviour of Continuous Stanchions, *Proc. Roy. Soc. A* **198**, 493.
34. BAKER, J. F., HORNE, M. R. and HEYMAN, J. *The Steel Skeleton*, Vol. II. C.U.P. 1956.
35. MERCHANT, W. (1956). Frame Instability in the Plastic Range, *British Welding Journal*, **3**, 366.
36. FOULKES, J. Ph.D. Thesis, Cambridge University 1953. See also Horne, *Structural Engineer*, **34**, 294 (1956).
37. MURRAY, J. *Proc. Inst. Civ. Engrs. Part III*, **5**, 213 (1956) and *Proc. Inst. Civ. Engrs.*, **10** 503 (1958).
38. NEAL, B. G. and MANSELL, D. S. (1963). The Effect of Restraint upon the Collapse Loads of Mild Steel Trusses, *Int. J. Mech. Sci.* **5**, 87.
39. MERCHANT, W., RASHID, C. A., BOLTON, A., and SALEM, A. (1958). *The Behaviour of Unclad Frames*. Proc. Fiftieth Anniv. Conf., Inst. Struct. Engrs.
40. DAVIES, G. and NEAL, B. G. (1959). The Dynamical Behaviour of a Strut in a Truss Framework, *Proc. Roy. Soc. A*, **A253**, 542.
41. DAVIES, G. and NEAL, B. G. (1963). An Experimental Examination of the Dynamical Behaviour of a Strut in a Rigidly Jointed Truss Framework. *Proc. Roy. Soc. A*, **A274**, 225.
42. WOOD, R. H. (1957). The Stability of Tall Buildings, *Proc. Inst. Civ. Engrs.* **11**, 69.
43. NEAL, B. G. *The Plastic Methods of Structural Analysis*. Chapman and Hall, 1956.
44. SALEM, A. Ph.D. Thesis, Manchester 1958.

Tables of Stability Functions

TABLE A1 STABILITY

ρ	s	c	s''	sc
0.00	4.0000	0.5000	3.0000	2.0000
	—132	25	—198	33
0.01	3.9868	0.5025	2.9802	2.0033
	—132	25	—199	33
0.02	3.9736	0.5050	2.9603	2.0066
	—132	25	—200	34
0.03	3.9604	0.5075	2.9403	2.0100
	—133	26	—202	33
0.04	3.9471	0.5101	2.9201	2.0133
	—133	26	—202	34
0.05	3.9338	0.5127	2.8999	2.0167
	—134	26	—204	34
0.06	3.9204	0.5153	2.8795	2.0201
	—134	26	—205	34
0.07	3.9070	0.5179	2.8590	2.0235
	—134	27	—206	35
0.08	3.8936	0.5206	2.8384	2.0270
	—134	27	—207	34
0.09	3.8802	0.5233	2.8177	2.0304
	—135	27	—209	35
0.10	3.8667	0.5260	2.7968	2.0339
	—136	28	—210	35
0.11	3.8531	0.5288	2.7758	2.0374
	—135	28	—211	36
0.12	3.8396	0.5316	2.7547	2.0410
	—136	28	—213	35
0.13	3.8260	0.5344	2.7334	2.0445
	—137	28	—214	36
0.14	3.8123	0.5372	2.7120	2.0481
	—136	29	—215	36
0.15	3.7987	0.5401	2.6905	2.0517
	—138	29	—217	36
0.16	3.7849	0.5430	2.6688	2.0553
	—137	30	—218	37
0.17	3.7712	0.5460	2.6470	2.0590
	—138	30	—219	36
0.18	3.7574	0.5490	2.6251	2.0626
	—138	30	—221	37
0.19	3.7436	0.5520	2.6030	2.0663
	—139	30	—222	38
0.20	3.7297	0.5550	2.5808	2.0701
	—139	31	—224	37
0.21	3.7158	0.5581	2.5584	2.0738
	—139	31	—225	38
0.22	3.7019	0.5612	2.5359	2.0776
	—140	32	—227	37
0.23	3.6879	0.5644	2.5132	2.0813
	—140	32	—228	39
0.24	3.6739	0.5676	2.4904	2.0852

FUNCTIONS $\rho = 0$ to 1.00

$s(1 + c)$	f	m	n	o	ρ
6.0000	1.0000	1.0000	1.0000	1.0000	0.00
—99	16	83	—331	166	
5.9901	1.0016	1.0083	0.9669	1.0166	0.01
—99	17	85	—336	171	
5.9802	1.0033	1.0168	0.9333	1.0337	0.02
—99	17	86	—340	174	
5.9703	1.0050	1.0254	0.8993	1.0511	0.03
—99	16	89	—345	179	
5.9604	1.0066	1.0343	0.8648	1.0690	0.04
—99	17	90	—350	182	
5.9505	1.0083	1.0433	0.8298	1.0872	0.05
—100	17	92	—355	188	
5.9405	1.0100	1.0525	0.7943	1.1060	0.06
—99	17	93	—359	192	
5.9306	1.0117	1.0618	0.7584	1.1252	0.07
—100	17	96	—366	196	
5.9206	1.0134	1.0714	0.7218	1.1448	0.08
—100	17	98	—370	202	
5.9106	1.0151	1.0812	0.6848	1.1650	0.09
—100	17	101	—377	206	
5.9006	1.0168	1.0913	0.6471	1.1856	0.10
—100	18	102	—382	212	
5.8906	1.0186	1.1015	0.6089	1.2068	0.11
—101	17	105	—388	217	
5.8805	1.0203	1.1120	0.5701	1.2285	0.12
—100	18	107	—395	223	
5.8705	1.0221	1.1227	0.5306	1.2508	0.13
—101	17	109	—401	229	
5.8604	1.0238	1.1336	0.4905	1.2737	0.14
—100	18	113	—407	235	
5.8504	1.0256	1.1449	0.4498	1.2972	0.15
—101	17	114	—415	241	
5.8403	1.0273	1.1563	0.4083	1.3213	0.16
—101	18	118	—422	248	
5.8302	1.0291	1.1681	0.3661	1.3461	0.17
—102	18	120	—428	254	
5.8200	1.0309	1.1801	0.3233	1.3715	0.18
—101	18	123	—437	261	
5.8099	1.0327	1.1924	0.2796	1.3976	0.19
—101	18	127	—445	269	
5.7998	1.0345	1.2051	0.2351	1.4245	0.20
—102	18	129	—452	276	
5.7896	1.0363	1.2180	0.1899	1.4521	0.21
—102	19	133	—461	284	
5.7794	1.0382	1.2313	0.1438	1.4805	0.22
—102	18	136	—470	293	
5.7692	1.0400	1.2449	0.0968	1.5098	0.23
—102	18	140	—479	300	
5.7590	1.0418	1.2589	0.0489	1.5398	0.24

TABLE A1 (continued overleaf)

TABLE A1 (continued)

p	s	c	s''	sc
0.24	3.6739	0.5676	2.4904	2.0852
	—141	32	—230	38
0.25	3.6598	0.5708	2.4674	2.0890
	—141	33	—231	39
0.26	3.6457	0.5741	2.4443	2.0929
	—141	33	—233	39
0.27	3.6316	0.5774	2.4210	2.0968
	—142	33	—235	39
0.28	3.6174	0.5807	2.3975	2.1007
	—143	34	—237	39
0.29	3.6031	0.5841	2.3738	2.1046
	—142	34	—238	40
0.30	3.5889	0.5875	2.3500	2.1086
	—143	35	—239	40
0.31	3.5746	0.5910	2.3261	2.1126
	—144	35	—242	40
0.32	3.5602	0.5945	2.3019	2.1166
	—144	36	—243	40
0.33	3.5458	0.5981	2.2776	2.1206
	—144	36	—245	41
0.34	3.5314	0.6017	2.2531	2.1247
	—145	36	—247	41
0.35	3.5169	0.6053	2.2284	2.1288
	—145	37	—249	41
0.36	3.5024	0.6090	2.2035	2.1329
	—146	37	—251	42
0.37	3.4878	0.6127	2.1784	2.1371
	—146	38	—252	41
0.38	3.4732	0.6165	2.1532	2.1412
	—146	38	—255	42
0.39	3.4586	0.6203	2.1277	2.1454
	—147	39	—256	43
0.40	3.4439	0.6242	2.1021	2.1497
	—147	39	—259	42
0.41	3.4292	0.6281	2.0762	2.1539
	—148	40	—260	43
0.42	3.4144	0.6321	2.0502	2.1582
	—149	40	—263	44
0.43	3.3995	0.6361	2.0239	2.1626
	—148	41	—265	43
0.44	3.3847	0.6402	1.9974	2.1669
	—149	41	—267	44
0.45	3.3698	0.6443	1.9707	2.1713
	—150	42	—269	44
0.46	3.3548	0.6485	1.9438	2.1757
	—150	43	—272	44
0.47	3.3398	0.6528	1.9166	2.1801
	—151	43	—273	45
0.48	3.3247	0.6571	1.8893	2.1846

$s(1 + c)$	f	m	n	o	p
5-7590	1-0418	1-2589	0-0489	1-5398	0-24
—102	19	143	—489	310	
5-7488	1-0437	1-2732	0-0000	1-5708	0-25
—103	19	148	—498	319	
5-7385	1-0456	1-2880	—0-0498	1-6027	0-26
—102	18	151	—509	328	
5-7283	1-0474	1-3031	—0-1007	1-6355	0-27
—103	19	155	—520	339	
5-7180	1-0493	1-3186	—0-1527	1-6694	0-28
—103	19	160	—530	349	
5-7077	1-0512	1-3346	—0-2057	1-7043	0-29
—103	19	165	—542	359	
5-6974	1-0531	1-3511	—0-2599	1-7402	0-30
—103	19	169	—554	372	
5-6871	1-0550	1-3680	—0-3153	1-7774	0-31
—103	19	174	—567	383	
5-6768	1-0569	1-3854	—0-3720	1-8157	0-32
—104	20	179	—580	395	
5-6664	1-0589	1-4033	—0-4300	1-8552	0-33
—103	19	185	—594	409	
5-6561	1-0608	1-4218	—0-4894	1-8961	0-34
—104	20	190	—608	422	
5-6457	1-0628	1-4408	—0-5502	1-9383	0-35
—104	19	196	—623	437	
5-6353	1-0647	1-4604	—0-6125	1-9820	0-36
—104	20	202	—638	451	
5-6249	1-0667	1-4806	—0-6763	2-0271	0-37
—104	20	209	—655	467	
5-6145	1-0687	1-5015	—0-7418	2-0738	0-38
—105	20	216	—672	484	
5-6040	1-0707	1-5231	—0-8090	2-1222	0-39
—104	20	222	—691	501	
5-5936	1-0727	1-5453	—0-8781	2-1723	0-40
—105	20	231	—709	519	
5-5831	1-0747	1-5684	—0-9490	2-2242	0-41
—105	20	238	—729	539	
5-5726	1-0767	1-5922	—1-0219	2-2781	0-42
—105	20	246	—750	558	
5-5621	1-0787	1-6168	—1-0969	2-3339	0-43
—105	21	255	—772	580	
5-5516	1-0808	1-6423	—1-1741	2-3919	0-44
—106	20	265	—796	603	
5-5410	1-0828	1-6688	—1-2537	2-4522	0-45
—105	21	274	—820	626	
5-5305	1-0849	1-6962	—1-3357	2-5148	0-46
—106	21	285	—845	651	
5-5199	1-0870	1-7247	—1-4202	2-5799	0-47
—106	21	295	—874	678	
5-5093	0-0891	1-7542	—1-5076	2-6477	0-48

TABLE A1 (continued overleaf)

TABLE A1 (continued)

p	s	c	s''	sc
0.48	3.3247	0.6571	1.8893	2.1846
	—151	43	—276	45
0.49	3.3096	0.6614	1.8617	2.1891
	—151	45	—279	45
0.50	3.2945	0.6659	1.8338	2.1936
	—152	45	—281	46
0.51	3.2793	0.6704	1.8057	2.1982
	—153	45	—283	46
0.52	3.2640	0.6749	1.7774	2.2028
	—153	46	—286	46
0.53	3.2487	0.6795	1.7488	2.2074
	—153	46	—288	47
0.54	3.2334	0.6841	1.7200	2.2121
	—154	48	—291	47
0.55	3.2180	0.6889	1.6909	2.2168
	—155	48	—294	47
0.56	3.2025	0.6937	1.6615	2.2215
	—155	49	—296	48
0.57	3.1870	0.6986	1.6319	2.2263
	—155	49	—299	48
0.58	3.1715	0.7035	1.6020	2.2311
	—156	50	—302	48
0.59	3.1559	0.7085	1.5718	2.2359
	—156	51	—304	48
0.60	3.1403	0.7136	1.5414	2.2407
	—157	51	—308	49
0.61	3.1246	0.7187	1.5106	2.2456
	—158	52	—311	50
0.62	3.1088	0.7239	1.4795	2.2506
	—158	53	—313	49
0.63	3.0930	0.7292	1.4482	2.2555
	—159	54	—317	50
0.64	3.0771	0.7346	1.4165	2.2605
	—159	55	—320	51
0.65	3.0612	0.7401	1.3845	2.2656
	—159	55	—323	50
0.66	3.0453	0.7456	1.3522	2.2706
	—160	57	—326	51
0.67	3.0293	0.7513	1.3196	2.2757
	—161	57	—330	52
0.68	3.0132	0.7570	1.2866	2.2809
	—161	58	—333	52
0.69	2.9971	0.7628	1.2533	2.2861
	—162	59	—336	52
0.70	2.9809	0.7687	1.2197	2.2913
	—163	59	—341	53
0.71	2.9646	0.7746	1.1856	2.2966
	—163	61	—344	53
0.72	2.9483	0.7807	1.1512	2.3019

$s(1 + c)$	f	m	n	o	ρ
5.5093	0.0891	1.7542	-1.5076	2.6477	0.48
-106	21	307	-902	706	
5.4987	1.0912	1.7849	-1.5978	2.7183	0.49
-106	21	321	-932	737	
5.4881	1.0933	1.817	-1.691	2.792	0.50
-106	21	33	-97	77	
5.4775	1.0954	1.850	-1.788	2.869	0.51
-107	21	35	-100	80	
5.4668	1.0975	1.885	-1.888	2.949	0.52
-106	22	36	-103	83	
5.4562	1.0997	1.921	-1.991	3.032	0.53
-107	21	37	-108	88	
5.4455	1.1018	1.958	-2.099	3.120	0.54
-107	22	40	-111	92	
5.4348	1.1040	1.998	-2.210	3.212	0.55
-108	22	41	-116	96	
5.4240	1.1062	2.039	-2.326	3.308	0.56
-107	22	43	-121	100	
5.4133	1.1084	2.082	-2.447	3.408	0.57
-107	22	45	-126	106	
5.4026	1.1106	2.127	-2.573	3.514	0.58
-108	22	47	-132	111	
5.3918	1.1128	2.174	-2.705	3.625	0.59
-108	22	49	-137	116	
5.3810	1.1150	2.223	-2.842	3.741	0.60
-108	23	53	-144	123	
5.3702	1.1173	2.276	-2.986	3.864	0.61
-108	22	55	-105	130	
5.3594	1.1195	2.331	-3.136	3.994	0.62
-109	23	58	-158	137	
5.3485	1.1218	2.388	-3.294	4.131	0.63
-108	23	61	-165	145	
5.3377	1.1241	2.449	-3.459	4.276	0.64
-109	23	65	-175	153	
5.3268	1.1264	2.514	-3.634	4.429	0.65
-109	23	68	-183	163	
5.3159	1.1287	2.582	-3.817	4.592	0.66
-109	23	72	-194	173	
5.3050	1.1310	2.654	-4.011	4.765	0.67
-109	23	77	-205	183	
5.2941	1.1333	2.731	-4.216	4.948	0.68
-110	24	82	-218	197	
5.2831	1.1357	2.813	-4.434	5.145	0.69
-109	23	87	-230	209	
5.2722	1.1380	2.900	-4.664	5.354	0.70
-110	24	94	-246	224	
5.2612	1.1404	2.994	-4.910	5.578	0.71
-110	24	100	-262	241	
5.2502	1.1428	3.094	-5.172	5.819	0.72

TABLE A1 (continued overleaf)

TABLE A1 (continued)

p	s	c	s''	sc
0.72	2.9483 -163	0.7807 62	1.1512 -347	2.3019 53
0.73	2.9320 -164	0.7869 63	1.1165 -351	2.3072 54
0.74	2.9156 -165	0.7932 63	1.0814 -356	2.3126 54
0.75	2.8991 -165	0.7995 65	1.0458 -359	2.3180 54
0.76	2.8826 -166	0.8060 66	1.0099 -363	2.3234 55
0.77	2.8660 -166	0.8126 67	0.9736 -368	2.3289 56
0.78	2.8494 -167	0.8193 68	0.9368 -371	2.3345 55
0.79	2.8327 -168	0.8261 69	0.8997 -376	2.3400 56
0.80	2.8159 -168	0.8330 70	0.8621 -381	2.3456 57
0.81	2.7991 -169	0.8400 72	0.8240 -385	2.3513 57
0.82	2.7822 -169	0.8472 72	0.7855 -390	2.3570 57
0.83	2.7653 -170	0.8544 74	0.7465 -394	2.3627 58
0.84	2.7483 -171	0.8618 75	0.7071 -400	2.3685 58
0.85	2.7312 -171	0.8693 77	0.6671 -404	2.3743 59
0.86	2.7141 -172	0.8770 78	0.6267 -410	2.3802 59
0.87	2.6969 -172	0.8848 79	0.5857 -415	2.3861 60
0.88	2.6797 -173	0.8927 81	0.5442 -420	2.3921 60
0.89	2.6624 -174	0.9008 82	0.5022 -426	2.3981 61
0.90	2.6450 -175	0.9090 83	0.4596 -431	2.4042 61
0.91	2.6275 -175	0.9173 85	0.4165 -438	2.4103 61
0.92	2.6100 -176	0.9258 87	0.3727 -443	2.4164 62
0.93	2.5924 -176	0.9345 88	0.3284 -449	2.4226 63
0.94	2.5748 -178	0.9433 90	0.2835 -456	2.4289 63
0.95	2.5570 -178	0.9523 92	0.2379 -462	2.4352 63
0.96	2.5392	0.9615	0.1917	2.4415

$s(1+c)$	f	m	n	o	p
5.2502	1.1428	3.094	-5.172	5.819	0.72
-110	24	107	-281	259	
5.2392	1.1452	3.201	-5.453	6.078	0.73
-110	24	115	-301	279	
5.2282	1.1476	3.316	-5.754	6.357	0.74
-111	25	125	-324	302	
5.2171	1.1501	3.441	-6.078	6.659	0.75
-111	24	136	-349	327	
5.2060	1.1525	3.577	-6.427	6.986	0.76
-111	25	147	-379	357	
5.1949	1.1550	3.724	-6.806	7.343	0.77
-111	24	160	-411	389	
5.1838	1.1574	3.884	-7.217	7.732	0.78
-111	25	176	-450	427	
5.1727	1.1599	4.060	-7.667	8.159	0.79
-111	25	193	-492	471	
5.1616	1.1624	4.253	-8.159	8.630	0.80
-112	26	213	-534	520	
5.1504	1.1650	4.466	-8.702	9.150	0.81
-112	25	237	-601	578	
5.1392	1.1675	4.703	-9.303	9.728	0.82
-112	25	265	-670	648	
5.1280	1.1700	4.968	-9.973	10.376	0.83
-112	26	298	-752	729	
5.1168	1.1726	5.266	-10.725	11.105	0.84
-112	26	338	-850	827	
5.1056	1.1752	5.604	-11.575	11.932	0.85
-113	26	386	-969	946	
5.0943	1.1778	5.990	-12.544	12.878	0.86
-112	26	446	-1.116	1.093	
5.0831	1.1804	6.436	-13.660	13.971	0.87
-113	26	520	-1.299	1.276	
5.0718	1.1830	6.956	-14.959	15.247	0.88
-113	27	614	-1.532	1.508	
5.0605	1.1857	7.570	-16.491	16.755	0.89
-114	26	737	-1.835	1.812	
5.0491	1.1883	8.307	-18.326	18.567	0.90
-113	27	—	—	—	
5.0378	1.1910	9.208	-20.57	20.78	0.91
-114	27	—	—	—	
5.0264	1.1937	10.334	-23.36	23.55	0.92
-114	27	—	—	—	
5.0150	1.1964	11.781	-26.95	27.12	0.93
-114	27	—	—	—	
5.0036	1.1991	13.711	-31.73	31.87	0.94
-114	28	—	—	—	
4.9922	1.2019	16.413	-38.41	38.53	0.95
-114	27	—	—	—	
4.9808	1.2046	20.47	-48.43	48.53	0.96

TABLE A1 (continued overleaf)

TABLE A1 (continued)

p	s	c	s''	sc
0.96	2.5392 -178	0.9615 94	0.1917 -469	2.4415 64
0.97	2.5214 -179	0.9709 95	0.1448 -476	2.4479 65
0.98	2.5035 -180	0.9804 97	0.0972 -482	2.4544 65
0.99	2.4855 -181	0.9901 99	0.0490 -490	2.4609 65
1.00	2.4674	1.0000	0.0000	2.4674

TABLE A2 STABILITY

p	s	c	s''	sc
1.00	2.467 -184	1.000 111	0.000 -534	2.467 69
1.10	2.283 -193	1.111 138	-0.534 -635	2.536 74
1.20	2.090 -201	1.249 175	-1.169 -775	2.610 81
1.30	1.889 -211	1.424 232	-1.944 -978	2.691 88
1.40	1.678 -221	1.656 317	-2.922 -1293	2.779 96
1.50	1.457 -233	1.973 462	-4.215 -1817	2.875 105
1.60	1.224 -246	2.435 731	-6.032 -2793	2.980 116
1.70	0.978 -261	3.166 —	-8.825 —	3.096 128
1.80	0.717 -278	4.497 —	-13.783 —	3.224 143
1.90	0.439 -296	7.661 —	-25.352 —	3.367 158
2.00	0.143 -319	(24.68) —	(-86.86) —	3.525 177
2.10	-0.176	(-21.07)	(77.83)	37.02

$s(1+c)$	f	m	n	o	ρ
4.9808 —115	1.2046 28	20.47 —	—48.43 —	48.53 —	0.96
4.9693 —115	1.2074 28	27.22 —	—65.11 —	65.19 —	0.97
4.9578 —115	1.2102 28	40.73 —	—98.47 —	98.51 —	0.98
4.9463 —115	1.2130 28	81.26 —	—198.48 —	198.51 —	0.99
4.9348	1.2158	∞	∞	∞	1.00

FUNCTIONS $\rho = 1.00$ to 4.00

$s(1+c)$	f	m	n	o	ρ
4.935 —117	1.216 29	∞ —	∞ —	∞ —	1.00
4.818 —118	1.245 32	—7.902 —	21.32 —	—21.57 —	1.10
4.700 —120	1.277 33	—3.847 —	11.13 —	—11.65 —	1.20
4.580 —123	1.310 36	—2.495 —	7.60 —	—8.40 —	1.30
4.457 —125	1.346 39	—1.818 —	5.73 —	—6.83 —	1.40
4.332 —128	1.385 42	—1.411 272	4.51 —89	—5.93 56	1.50
4.204 —130	1.427 46	—1.139 195	3.62 —72	—5.37 35	1.60
4.074 —133	1.473 49	—0.944 146	2.90 —61	—5.02 22	1.70
3.941 —135	1.522 54	—0.798 115	2.29 —55	—4.80 13	1.80
3.806 —138	1.576 60	—0.683 92	1.74 —51	—4.67 6	1.90
3.668 —142	1.636 66	—0.591 75	1.23 —50	—4.61 4	2.00
3.526	1.702	—0.516	0.73	—4.61	2.10

TABLE A2 (continued overleaf)

TABLE A2 (continued)

ρ	s	c	s''	sc
2.10	-0.176	(-21.07)	(77.83)	3.702
	-343	—	—	199
2.20	-0.519	-7.511	28.781	3.901
	-374	—	—	226
2.30	-0.893	-4.623	18.185	4.127
	-408	—	—	256
2.40	-1.301	-3.370	13.472	4.383
	-449	697	-2718	295
2.50	-1.750	-2.673	10.754	4.678
	-499	442	-1806	340
2.60	-2.249	-2.231	8.948	5.018
	-560	303	-1317	397
2.70	-2.809	-1.928	7.631	5.415
	-636	220	-1025	469
2.80	-3.445	-1.708	6.606	5.884
	-731	165	-839	560
2.90	-4.176	-1.543	5.767	6.444
	-856	127	-714	680
3.00	-5.032	-1.416	5.053	7.124
	-1020	100	-629	838
3.10	-6.052	-1.316	4.424	7.962
	-1245	80	-568	1059
3.20	-7.297	-1.236	3.856	9.021
	-1566	63	-527	1374
3.30	-8.863	-1.173	3.329	10.395
	-2045	51	-497	1847
3.40	-10.908	-1.122	2.832	12.242
	-2811	40	-479	2607
3.50	-13.719	-1.082	2.353	14.849
	—	31	-467	—
3.60	-17.87	-1.051	1.886	18.79
	—	23	-463	—
3.70	-24.68	-1.028	1.423	25.39
	—	16	-465	—
3.80	-38.17	-1.012	0.958	38.65
	—	9	-473	—
3.90	-78.34	-1.003	0.485	78.58
	—	3	-485	—
4.00	— ∞	-1.000	0.000	∞

$s(1 + c)$	f	m	n	o	p
3.526	1.702	-0.516	0.73	-4.61	2.10
-144	72	64	-48	-6	
3.382	1.774	-0.452	0.25	-4.67	2.20
-148	81	54	-50	-10	
3.234	1.855	-0.398	-0.25	-4.77	2.30
-151	91	46	-51	-16	
3.083	1.946	-0.352	-0.76	-4.93	2.40
-155	103	41	-53	-20	
2.928	2.049	-0.311	-1.29	-5.13	2.50
-159	118	36	-58	-27	
2.769	2.167	-0.275	-1.87	-5.40	2.60
-163	135	32	-62	-33	
2.606	2.302	-0.243	-2.49	-5.73	2.70
-167	158	29	-69	-42	
2.439	2.460	-0.214	-3.18	-6.15	2.80
-171	186	26	-78	-51	
2.268	2.646	-0.188	-3.96	-6.66	2.90
-176	223	23	-90	-64	
2.092	2.869	-0.165	-4.86	-7.30	3.00
-181	272	22	-106	-80	
1.911	3.141	-0.143	-5.92	-8.10	3.10
-187	339	20	-127	-103	
1.724	3.480	-0.123	-7.19	-9.13	3.20
-192	436	19	-159	-135	
1.532	3.916	-0.104	-8.78	-10.48	3.30
-198	581	18	-207	-182	
1.334	4.497	-0.086	-10.85	-12.30	3.40
-204	813	16	-283	-259	
1.130	5.31	-0.070	-13.68	-14.89	3.50
-211	—	15	—	—	
0.919	6.53	-0.055	-17.84	-18.81	3.60
-218	—	15	—	—	
0.701	8.56	-0.040	-24.67	-25.40	3.70
-225	—	14	—	—	
0.476	12.61	-0.026	-38.17	-38.66	3.80
-234	—	13	—	—	
0.242	24.77	-0.013	-78.33	-78.58	3.90
-242	—	13	—	—	
0	∞	0	$-\infty$	$-\infty$	4.00

TABLE A3 RECIPROCAL

ρ	$\frac{1}{c}$	$\frac{1}{s''}$	
0.80			
0.90			
1.00	1.0000		
1.10	0.9002		
1.20	0.8008		
1.30	0.7020		
1.40	0.6040	-0.3422	
1.50	0.5068	-0.2372	1050
1.60	0.4107	-0.1658	714
1.70	0.3158	-0.1133	525
1.80	0.2224	-0.0726	407
1.90	0.1305	-0.0394	332
2.00	0.0405	-0.0115	279
2.10	-0.0475	0.0128	243
2.20	-0.1331	0.0347	219
2.30	-0.2163	0.0550	203
2.40	-0.2967	0.0742	192
2.50	-0.3741	0.0930	188

STABILITY FUNCTIONS

		$\frac{1}{m}$	$\frac{1}{n}$	$\frac{1}{o}$	ρ
		0.2351	-0.1226	0.1159	0.80
		-1147	680	-620	
		0.1204	-0.0546	0.0539	0.90
		-1204	546	-539	
		0.0000	0.0000	0.0000	1.00
		-1266	469	-464	
		-0.1266	0.0469	-0.0464	1.10
		-1333	429	-394	
		-0.2599	0.0898	-0.0858	1.20
		-1410	418	-332	
		-0.4009	0.1316	-0.1190	1.30
		-1493	430	-274	
		-0.5502	0.1746	-0.1464	1.40
		-1587	470	-222	
		-0.7089	0.2216	-0.1686	1.50
		-1692	548	-175	
		-0.8781	0.2764	-0.1861	1.60
		-1811	683	-131	
		-1.0592	0.3447	-0.1992	1.70
		-1945	922	-93	
		-1.2537	0.4369	-0.2085	1.80
					1.90
					2.00
					2.10
					2.20
					2.30
					2.40
					2.50

TABLE A4 STABILITY FUNCTIONS FOR

p	s	c	s''	sc
-0.00	4.0000	0.5000	3.0000	2.0000
	1299	-235	1921	-319
-0.10	4.1299	0.4765	3.1921	1.9681
	1268	-212	1822	-301
-0.20	4.2567	0.4553	3.3743	1.9380
	1237	-193	1736	-284
-0.30	4.3804	0.4360	3.5479	1.9096
	1209	-177	1658	-267
-0.40	4.5013	0.4183	3.7137	1.8829
	1181	-162	1588	-254
-0.50	4.6194	0.4021	3.8725	1.8575
	1157	-149	1526	-239
-0.60	4.7351	0.3872	4.0251	1.8336
	1132	-137	1469	-227
-0.70	4.8483	0.3735	4.1720	1.8109
	1110	-127	1417	-216
-0.80	4.9593	0.3608	4.3137	1.7893
	1088	-118	1370	-204
-0.90	5.0681	0.3490	4.4507	1.7689
	1067	-109	1327	-195
-1.00	5.1748	0.3381	4.5834	1.7494
	1047	-102	1287	-185
-1.10	5.2795	0.3279	4.7121	1.7309
	1029	-96	1249	-176
-1.20	5.3824	0.3183	4.8370	1.7133
	1011	-89	1216	-167
-1.30	5.4835	0.3094	4.9586	1.6965
	993	-84	1184	-160
-1.40	5.5828	0.3010	5.0770	1.6805
	978	-79	1154	-153
-1.50	5.6806	0.2931	5.1924	1.6652
	961	-74	1127	-146
-1.60	5.7767	0.2857	5.3051	1.6506
	947	-70	1101	-140
-1.70	5.8714	0.2787	5.4152	1.6366
	931	-66	1076	-134
-1.80	5.9645	0.2721	5.5228	1.6232
	919	-62	1053	-128
-1.90	6.0564	0.2659	5.6281	1.6104
	904	-59	1032	-122
-2.00	6.1468	0.2600	5.7313	1.5982
	892	-56	1011	-118
-2.10	6.2360	0.2544	5.8324	1.5864
	879	-53	992	-113
-2.20	6.3239	0.2491	5.9316	1.5751
	868	-51	974	-108
-2.30	6.4107	0.2440	6.0290	1.5643
	856	-48	956	-104
-2.40	6.4963	0.2392	6.1246	1.5539
	845	-46	940	-101
-2.50	6.5808	0.2346	6.2186	1.5438

NEGATIVE ρ VALUES 0 to -2.5

$s(1 + c)$	f	m	n	o	ρ
6.0000	1.0000	1.0000	1.000	1.0000	-0.00
980	-161	-749	309	-1473	
6.0980	0.9839	0.9251	1.309	0.8527	-0.10
967	-153	-625	276	-1190	
6.1947	0.9686	0.8626	1.585	0.7337	-0.20
953	-147	-531	250	-975	
6.2900	0.9539	0.8095	1.835	0.6362	-0.30
941	-141	-457	228	-809	
6.3841	0.9398	0.7638	2.063	0.5553	-0.40
929	-134	-397	211	-677	
6.4770	0.9264	0.7241	2.274	0.4876	-0.50
917	-130	-348	197	-573	
6.5687	0.9134	0.6893	2.471	0.4303	-0.60
905	-124	-309	185	-488	
6.6592	0.9010	0.6584	2.656	0.3815	-0.70
894	-119	-275	174	-419	
6.7486	0.8891	0.6309	2.830	0.3396	-0.80
883	-115	-247	166	-362	
6.8369	0.8776	0.6062	2.996	0.3034	-0.90
873	-111	-223	157	-314	
6.9242	0.8665	0.5839	3.153	0.2720	-1.00
863	-106	-203	151	-274	
7.0105	0.8559	0.5636	3.304	0.2446	-1.10
852	-103	-185	144	-240	
7.0957	0.8456	0.5451	3.448	0.2206	-1.20
843	-99	-170	140	-211	
7.1800	0.8357	0.5281	3.588	0.1995	-1.30
833	-96	-156	134	-187	
7.2633	0.8261	0.5125	3.722	0.1808	-1.40
825	-93	-144	129	-166	
7.3458	0.8168	0.4981	3.851	0.1642	-1.50
815	-90	-134	126	-147	
7.4273	0.8078	0.4847	3.977	0.1495	-1.60
807	-87	-124	121	-132	
7.5080	0.7991	0.4723	4.098	0.1363	-1.70
798	-84	-116	119	-117	
7.5878	0.7907	0.4607	4.217	0.1246	-1.80
790	-81	-108	115	-106	
7.6668	0.7826	0.4499	4.332	0.1140	-1.90
782	-79	-102	112	-95	
7.7450	0.7747	0.4397	4.444	0.1045	-2.00
774	-77	-96	110	-85	
7.8224	0.7670	0.4301	4.554	0.0960	-2.10
767	-74	-89	107	-77	
7.8991	0.7596	0.4212	4.661	0.0883	-2.20
759	-72	-85	104	-70	
7.9750	0.7524	0.4127	4.765	0.0813	-2.30
751	-71	-80	102	-64	
8.0501	0.7453	0.4047	4.867	0.0749	-2.40
745	-68	-76	101	-57	
8.1246	0.7385	0.3971	4.968	0.0692	-2.50

TABLE A5 STABILITY FUNCTIONS FOR

ρ	s	c	s''	sc
-0.0	4.000 1175	0.5000 -1619	3.000 1583	2.0000 -2506
-1.0	5.175 972	0.3381 -781	4.583 1148	1.7494 -1512
-2.0	6.147 841	0.2600 -455	5.731 935	1.5982 -991
-3.0	6.988 749	0.2145 -297	6.666 806	1.4991 -691
-4.0	7.737 680	0.1848 -209	7.472 719	1.4300 -504
-5.0	8.417 627	0.1639 -156	8.191 654	1.3796 -383
-6.0	9.044 583	0.1483 -121	8.845 604	1.3413 -300
-7.0	9.627 548	0.1362 -97	9.449 564	1.3113 -241
-8.0	10.175 519	0.1265 -80	10.013 530	1.2872 -198
-9.0	10.694 492	0.1185 -67	10.543 504	1.2674 -166
-10.0	11.186 471	0.1118 -57	11.047 479	1.2508 -140
-11.0	11.657 451	0.1061 -50	11.526 458	1.2368 -122
-12.0	12.108 434	0.1011 -43	11.984 440	1.2246 -105
-13.0	12.542 418	0.0968 -38	12.424 424	1.2141 -93
-14.0	12.960 404	0.0930 -35	12.848 409	1.2048 -82
-15.0	13.364 392	0.0895 -31	13.257 396	1.1966 -74
-16.0	13.756 380	0.0864 -27	13.653 384	1.1892 -67
-17.0	14.136 369	0.0837 -26	14.037 373	1.1825 -60
-18.0	14.505 360	0.0811 -23	14.410 363	1.1765 -55
-19.0	14.865 351	0.0788 -22	14.773 353	1.1710 -50
-20.0	15.216	0.0766	15.126	1.1660

Greater negative values of ρ . The following approximations

$$s = \frac{\alpha(2\alpha - 1)}{\alpha - 1}, \quad s'' = s(1 - c^2) = \frac{4\alpha^2}{2\alpha - 1},$$

$$c = \frac{1}{2\alpha - 1}, \quad sc = \frac{\alpha}{\alpha - 1},$$

NEGATIVE ρ VALUES 0 to -20

$s(1 + c)$	f	m	n	o	ρ
6.000	1.0000	1.0000	1.000	1.0000	0.0
924	-1335	-4161	2.153	-7280	
6.924	0.8665	0.5839	3.153	0.2720	-1.0
821	-918	-1442	1.291	-1675	
7.745	0.7747	0.4397	4.444	0.1045	-2.0
742	-677	-753	998	-574	
8.487	0.7070	0.3644	5.442	0.0471	-3.0
680	-525	-473	841	-236	
9.167	0.6545	0.3171	6.283	0.0235	-4.0
629	-420	-329	742	-110	
9.796	0.6125	0.2842	7.025	0.0125	-5.0
589	-347	-245	670	-55	
10.385	0.5778	0.2597	7.695	0.0070	-6.0
554	-293	-192	617	-29	
10.939	0.5485	0.2405	8.312	0.0041	-7.0
524	-251	-155	574	-16	
11.463	0.5234	0.2250	8.886	0.0025	-8.0
498	-218	-128	539	-10	
11.961	0.5016	0.2122	9.425	0.0015	-9.0
476	-192	-109	510	-5	
12.437	0.4824	0.2013	9.935	0.0010	-10.0
457	-171	-94	485	-4	
12.894	0.4653	0.1919	10.420	0.0006	-11.0
438	-153	-81	463	-2	
13.332	0.4500	0.1838	10.883	0.0004	-12.0
424	-138	-72	444	-1	
13.756	0.4362	0.1766	11.327	0.0003	-13.0
409	-126	-65	428	-1	
14.165	0.4236	0.1701	11.755	0.0002	-14.0
396	-115	-57	412	-1	
14.561	0.4121	0.1644	12.167	0.0001	-15.0
384	-106	-52	399	0	
14.945	0.4015	0.1592	12.566	0.0001	-16.0
373	-98	-48	387	0	
15.318	0.3917	0.1544	12.953	0.0001	-17.0
364	-91	-43	376	-1	
15.682	0.3826	0.1501	13.329	0.0000	-18.0
354	-84	-40	365	0	
16.036	0.3742	0.1461	13.694	0.0000	-19.0
346	-79	-37	356	0	
16.382	0.3663	0.1424	14.050	0.0000	-20.0

are sufficiently accurate—Let $\alpha = \frac{\pi}{2} \sqrt{(-\rho)}$.

$$s(1 + c) = \frac{2\alpha^2}{\alpha - 1}, \quad m = \frac{1}{\alpha}, \quad o = \text{zero}.$$

$$f = \frac{3(\alpha - 1)}{\alpha^2}, \quad n = 2\alpha.$$

Index

- Allen, H. G. 87, 89
 Amplification factor
 in rigid frames 109, 121, 145
 in struts 19
 in triangulated frames 84
 Ariaratnam, S. T. 85, 102
 Baker, J. F. 132
 Berry, A. 51
 Bifurcation of equilibrium
 in frames 103
 in struts 13, 40, 42
 Bleich, F. 15, 20, 75
 Bolton, A. 27, 141
 Bracing 110
 British Standard 449 (1958) 34
 Britvec, S. J. 78
 Buckling loads, definition 104
 Bull, F. B. 48
 Carry-over factor 48
 Chandler, D. B. viii, 51, 70, 88
 Chilver, A. H. 121
 Chwalla, E. 121
 Compression loaded members 131
 Critical loads
 experimental determination 21
 pin-jointed trusses 78
 reduced 135, 146
 rigid frames 105
 rigid-jointed trusses 82
 strut 8
 Critical member 129
 Critical modes
 rigid frames 109
 rigid-jointed trusses 94
 strut 8
 Davies, G. 143
 Davies, M. J. viii
 Deformations, large
 in portal frames 120
 in struts 10
 Disturbing forces 85
 combinations of 91, 107
 Double curvature bending, in
 columns 130, 132
 Double modulus load 37
 Dynamic jump 143
 Eccentric loading of strut 29, 33, 43
 Effective length of strut 8
 Elastic critical loads, *see* Critical loads
 Elastic critical modes, *see* Critical modes
 Elastica 10
 Elastic-plastic behaviour
 columns 132
 rigid frames 143
 rigid-jointed triangulated frames 141
 struts 26
 Ellis, J. 29
 End conditions in strut 8
 Engesser, F. 41
 Equilibrium, stable and unstable 14
 Euler load 7
 Experimental determination of
 critical load 21
 Factor of safety 44
 Failure load, elastic
 portal frame 117
 strut 5
 Failure load, elastic-plastic
 columns 132
 rigid frames 143
 rigid-jointed triangulated frames 141

- Fixed-end moments 50
 - concentrated load 65
 - uniformly distributed load 63
- Flexural shortening 12
- Foulkes, J. 139
- Fourier series, use in strut 16
- Four-moment equation 75
- Gardner, N. J. viii
- Generalised displacements 62
- Gusset plates
 - effect on critical loads 98
 - effect on stability functions 67
- Heyman, J. 132
- Hinges, plastic 30, 128, 135, 143
- Hoff, N. J. 96
- Imperfections
 - effect on elastic-plastic failure loads 129, 139, 148
 - in portal frames 109
 - in struts 21, 28, 33, 43
 - in triangulated frames 83
- Inelastic behaviour, *see* Elastic-plastic behaviour
- Internal stresses 83, 150
- James, B. W. 51
- Kroll, W. D. 51
- Lack of fit 83, 148
- Lack of straightness 21
- Lateral loaded members, in rigid frames 129
- Lateral loads, in struts 15, 36, 63
- Le-Wu-Lu 120
- Linear analysis 1
- Livesley, R. K. vii, 51, 70, 73, 88
- Load factor 44
- Lundquist, E. E. 51
- Magnification factor
 - in rigid frames 109, 121, 145
 - in struts 19
 - in triangulated frames 84
- Mansell, D. S. 140
- Moment distribution 48
- Moment of resistance, plastic 31
- Moments, fixed-ended 50
 - concentrated load 65
 - uniformly distributed load 63
- Murray, J. 139
- Neal, B. G. 140, 143, 147
- No-shear functions 58
- Non-linearity of deflexions 2
- Non-uniform members 20
- Operations, general tables of 60, 62
- Orthogonal relations 20
- Perry-Robertson formula for struts 33
- Pitched roof portal frames 147
- Plastic hinges 30, 128, 135, 143
- Plastic moment of resistance 31
- Plastic zones
 - in columns 133
 - in struts 29
 - in triangulated frames 139
- Portals
 - multi-storey, multi-bay 113
 - multi-storey, single bay 111
 - single-storey, single bay 105, 115
- Potential energy 14
- Primary deflexions in struts 17
- Primary moments, effect on stability 115
- Primary moments in struts 15
- Proof stress 44
- Rankine load
 - in columns 139
 - in lateral loaded struts 37
 - in rigid frames 146
 - in struts 35
 - in triangulated frames 141
- Rankine, W. J. M. 35
- Rashid, C. A. 141
- Reduced critical loads 135, 146
- Reduced modulus 39
- Reduced structure 136
- Relaxation 88

- Rigid-plastic behaviour
 - in columns 136
 - in rigid frames 143
 - in struts 30, 36
- Robertson, A. 33
- Roderick, J. W. 132
- Safety factor 44
- Salem, A. 141, 147
- Secant formula for struts 33
- Secondary stresses 79
- Shanley, F. R. 42
- Shear centre 72
- Shear deformation, effect on critical loads 14
- Shear walls 150
- Shortening, axial, due to flexure 12
- Single curvature bending, in columns 130
- Slope-deflexion equations
 - no axial load 50
 - with axial load 51
- Southwell plot 22, 85, 105
- Southwell, R. V. 10, 22, 88
- Squash load 28, 139
- Stability functions 48 ff
 - s and c 52
 - s'' 55
 - $s(1 + c)$, m 56
 - n , o 58
 - tables 157
 - with gusset plates 67
- Stiffness
 - member under terminal couples 5
 - negative 7, 110
 - rotational 48
 - translational 50
- Strain hardening 24, 151
- Stress factor 44
- Superposition 49
- Sved, G. 48
- Sway functions 56
- Tangent modulus 25, 38
 - load of frames 151
 - load of strut 43
- Unloading, of inelastic material 25
- Wood, R. H. 146